GIOVANA CLARICE POGGERE

QUANTIFICATION AND CHARACTERIZATION OF PEDOGENETIC MAGHEMITE AND DIGITAL SOIL MAPPING USING MAGNETIC MEASUREMENTS

LAVRAS-MG
2018

GIOVANA CLARICE POGGERE

QUANTIFICATION AND CHARACTERIZATION OF PEDOGENETIC MAGHEMITE AND DIGITAL SOIL MAPPING USING MAGNETIC MEASUREMENTS

Tese apresentada à Universidade Federal de Lavras, como parte das exigências do Programa de Pós-Graduação em Ciência do Solo, área de concentração Recursos Ambientais e Uso da Terra, para a obtenção do título de Doutor.

Prof. Dr. Nilton Curi
Orientador

LAVRAS-MG
2018

Ficha catalográfica elaborada pelo Sistema de Geração de Ficha Catalográfica da Biblioteca Universitária da UFLA, com dados informados pelo(a) próprio(a) autor(a).

Poggere, Giovana Clarice.
Quantification and characterization of pedogenetic maghemite and digital soil mapping using magnetic measurements / Giovana Clarice Poggere. - 2018.
114 p. : il.

Orientador(a): Nilton Curi.
.
Tese (doutorado) - Universidade Federal de Lavras, 2018.
Bibliografia.

1. Solos tropicais. 2. Magnetismo. 3. Mapeamento de solos. I. Curi, Nilton. . II. Título.

GIOVANA CLARICE POGGERE

QUANTIFICATION AND CHARACTERIZATION OF PEDOGENETIC MAGHEMITE AND DIGITAL SOIL MAPPING USING MAGNETIC MEASUREMENTS

Tese apresentada à Universidade Federal de Lavras, como parte das exigências do Programa de Pós-Graduação em Ciência do Solo, área de concentração Recursos Ambientais e Uso da Terra, para a obtenção do título de Doutor.

APROVADA em 28 de março de 2018.

Dr. Vidal Barrón	UCO
Dr. Alberto Vasconcellos Inda	UFRGS
Dr. João José de Sá e Melo Marques	UFLA
Dra. Michele D. Menezes	UFLA

Prof. Dr. Nilton Curi
Orientador

LAVRAS-MG
2018

AGRADECIMENTOS

Em primeiro lugar a Deus, pelo dom da vida.

À Universidade Federal de Lavras, especialmente ao Departamento de Ciência do Solo, pela oportunidade para a realização deste trabalho.

À Coordenação de Aperfeiçoamento de Pessoal de Nível Superior (CAPES) pela concessão da bolsa de estudos; ao Conselho Nacional de Desenvolvimento Científico e Tecnológico (CNPq) e Fundação de Amparo à Pesquisa do Estado de Minas Gerais (FAPEMIG) pelo fomento para a realização do estudo.

Ao professor Nilton Curi pela orientação e pela amizade fraterna. Os ensinamentos que aprendi com o senhor vão muito além do conhecimento científico, e os levarei por toda vida.

Ao professor Alberto Vasconcellos Inda pela amizade e por toda ajuda no decorrer do trabalho.

Ao professor Nestor Kämpf pelas valiosas sugestões para melhoria do trabalho e por todo conhecimento compartilhado.

Ao professor Vidal Barrón e aos colegas da Universidad de Córdoba por me receberem tão bem durante o período sanduíche, pela valiosa contribuição no trabalho da tese e na minha formação.

Aos professores do Departamento de Ciência do Solo da UFLA pelos ensinamentos compartilhados durante o meu doutorado.

À professora Ângela Brito do Departamento de física da UFLA pela ajuda fundamental nas análises magnéticas e na interpretação dos dados correspondentes.

Aos técnicos e laboratoristas especialmente à Geila, João Gualberto, Carlinhos, Lívia, Bethânia, Dirce, Dulce, Regina, Riqueline, Maria Alice e José Roberto, por toda ajuda e orientação na execução das análises.

Ás meninas Alessandra, Denise, Elizabeth, Lidiane e Fátima pela alegria compartilhada.

Aos amigos, especialmente, Aline, Cláudia, Damyani, Diego Ediu, Elidiane, Eliete, Fábio Arnaldo Fábio Bispo Fernanda, Gabriela Henrique, José Ferreira, Lorena, Maíra, Mariana, Marcelo, Pedro, Raquel, Sara e Sérgio por toda ajuda e pelos bons momentos compartilhados.

Aos meus pais João e Amália, aos meus irmãos Rosemari, Rosane, Edilson, César, Sandra, Adelar e Julia, e aos meus sobrinhos, por todo amor, exemplo, ajuda e compreensão.

Ao Julierme pela companhia, carinho e incentivo incondicionais.

MUITO OBRIGADA.

RESUMO

A maghemita (Mh) é mineral ferrimagnético e por isso, pode ser utilizada como estratificador ambiental. Este estudo objetivou comparar diferentes métodos para quantificação de Mh em solos, caracterizar a Mh de solos desenvolvidos sobre diferentes materiais de origem, e avaliar a eficiência de sensores próximos (magnetômetro e fluorescência portátil de raios-X - pXRF) como suporte ao mapeamento digital de Latossolos em área com material de origem variável. Na primeira parte do estudo, a quantificação de Mh foi realizada a partir de quatro métodos: (1) área das reflexões obtidas por difratometria de raios-X (DRX) (método padrão); (2) refinamento Rietveld; (3) dissolução seletiva com H_2SO_4 e; (4) com base na suscetibilidade magnética (χ). A caracterização da Mh foi realizada a partir das curvas de histerese e dos parâmetros cristalográficos. Os métodos baseados na dissolução com H_2SO_4 superestimaram o conteúdo de Mh em relação ao método padrão (DRX), já os teores de Mh por χ e refinamento Rietveld foram mais próximos aos obtidos por DRX. Independentemente do material de origem, as partículas de Mh apresentam simples domínio, entretanto podem adquirir características de multidomínio devido à substituição isomórfica e à agregação com hematita. Na segunda parte do estudo, 39 solos foram classificados, amostrados e analisados por pXRF e χ. Para cada local foram obtidos os valores dos modelos digitais de terreno (MDT). Através dos "*boxplots*" foram identificadas as melhores variáveis para distinguir as classes de solo, que foram mapeadas usando lógica *fuzzy*. O modelo de regressão linear múltipla foi usado para predizer o conteúdo de areia e argila e os MDTs, os elementos químicos obtidos por pXRF e a χ foram utilizados como variáveis preditivas. Os MDTs não foram capazes de distinguir a maioria dos Latossolos, enquanto os dados de χ juntamente com SiO_2 e Fe avaliados por pXRF, auxiliaram na predição das classes de solo. Para o teor de areia e argila, as variáveis obtidas com pXRF mostraram maior capacidade de predição do que os adquiridos com MDT e χ, demonstrando seu o potencial como suporte ao mapeamento digital de solos.

Palavras-chave: Magnetismo. Óxidos de Fe. Fluorescência de raios-X portátil. Magnetômetro. Solos tropicais.

ABSTRACT

Maghemite (Mh) is a ferrimagnetic mineral, so it can be used as an environmental tracer. This study aimed to compare the various methods for quantification of Mh in soils, as well as to characterize Mh of soils developed on different parent materials; and to evaluate the efficiency of proximal sensors (magnetometer and portable X-ray fluorescence - pXRF) as support for the digital mapping in the separation of Oxisols in an area with variable geology. In the first part of the study, the quantification of Mh was performed from four methods: (1) area of the reflections obtained by X-ray diffraction (XRD) (standard method); (2) Rietveld refinement; (3) selective dissolution with H_2 SO_4 and; (4) based on magnetic susceptibility (χ). The characterization of pedogenic Mh was performed from hysteresis sloops and crystallographic parameters. The dissolution-based methods with H_2SO_4 overestimated the Mh content over the standard method based on XRD, whereas Mh values estimated by χ and Rietveld refinement were closer to those obtained by the standard method. Independently of the material of origin, the particles of Mh have simple domain, however they can acquire multidomain characteristics due to the isomorphic substitution and the hematite aggregation. In the second part of the study, 39 soils profiles were classified and analyzed by pXRF and magnetometer (χ). For each sampling site, the values of the digital terrain models (DTMs) were also obtained. Through the visual analysis, the boxplots were used to identify the best variables to distinguish the soil classes, which were further mapped using fuzzy logic and later validated. The multiple linear model were used to predict the sand and clay content. The DTMs, the elements obtained by pXRF and the χ were used as predictive variables. The DTMs were not able to distinguish most of the Oxisols in the study area, while the magnetic susceptibility data, together with SiO_2 and Fe evaluated by pXRF, aided in the prediction of soil classes. To estimate the sand and clay content, the variables obtained with pXRF showed greater predictability than those obtained with DTM and χ, demonstrating the potential of such proximal sensor as support for digital soil mapping.

Keywords: Magnetism. Fe-Oxides. Portable X-ray Fluorescence. Magnetometer. Tropical soils.

SUMÁRIO

1. INTRODUÇÃO

Nos ambientes tropicais, a mineralogia do solo reflete as condições de intenso intemperismo-lixiviação a que estes solos foram submetidos e, por isso, podem apresentar substanciais teores de óxidos de Fe, entre outros minerais secundários, que desempenham papel fundamental no comportamento físico, químico e físico-químico dos solos.

A maghemita é um óxido de Fe secundário, podendo ocorrer em todo o perfil do solo, ou em concreções e nódulos localizados. A principal via de formação é a partir da oxidação da magnetita litogênica ou diretamente do material de origem (CURI; FRANZMEIER, 1984; KÄMPF; CURI, 2000). Embora se conheça a ocorrência da maghemita em solos brasileiros, existe uma grande lacuna no que diz respeito à sua formação pedogênica, mesmo sendo este mineral bastante comum em solos dos trópicos e subtrópicos (COSTA et al., 1999; KÄMPF; CURI, 2000; CARVALHO FILHO et al., 2015).

Uma das principais características que a maghemita confere aos solos é a suscetibilidade magnética. Para que um material ou mineral apresente suscetibilidade magnética, é necessária uma resposta magnética quando se aplica um campo magnético externo. De acordo com Thompson; Oldfield (1986), os diferentes minerais podem ser classificados quanto ao seu caráter magnético como ferrimagnéticos: minerais que exibem forte caráter magnético; antiferromagnéticos: minerais que apresentam momento magnético nulo ou zero; paramagnéticos: minerais que apresentam pequena magnetização e; diamagnéticos: minerais que não apresentam momento magnético.

A quantificação dos óxidos de Fe é tradicionalmente feita a partir de procedimentos físico-químicos, através da difração de raios-X (DRX) e análise química do teor de Fe, extraído por de ditionito-citrato-bicarbonato de sódio (DCB) (CURI; FRANZMEIER, 1987; COSTA et al., 1999; CARVALHO FILHO et al., 2015), ou a partir de procedimentos físicos, através de técnicas de espectroscopia de refletância difusa (BARRÓN; TORRENT, 1986; TORRENT; BARRÓN, 2008; MARQUES Jr et al., 2014; BAHIA et al., 2015). Para maghemita, no entanto, as áreas das reflexões da DRX às vezes são difíceis de determinar, uma vez que este mineral geralmente ocorre em quantidades menores na fração de argila e sua reflexão mais intensa coincide com a reflexão da hematita. Assim, outros métodos para sua quantificação são utilizados como a dissolução seletiva de maghemita com H_2SO_4, proposto inicialmente por Schwertmann; Fetcher (1984) e adaptado por Costa et al. (1999) (INDA et al., 2013; CAMARGO et al., 2014); com base nos valores de susceptibilidade magnética (RESENDE et al., 1988; COSTA, 1999; CAMÊLO et al., 2017); e a partir do refinamento Rietveld em dados DRX (NONAKA et al., 2017). No entanto, não existe consenso sobre qual o método mais adequado a ser utilizado, o que pode dificultar a interpretação e comparação dos dados devido à resultados controversos.

Já a suscetibilidade magnética do solo pode ser facilmente determinada com uso de magnetômetro portátil e, juntamente com outras medidas baseadas em sensores próximos, vêm sendo empregada como marcador ambiental para identificar diferenças no material de origem de solos (SILVA et al., 2010; DJERRAB et al., 2013; CURI et al., 2018), na diferenciação de solos mal drenados e regimes hidrológicos em várzeas

(GRIMLEY et al., 2008; VODYANITSKII et al., 2009; LU et al., 2012) e em estudos relacionados ao monitoramento da poluição urbana (MEENA et al., 2011; LOURENÇO et al., 2012; CERVI; COSTA; SOUZA Jr, 2014), pedogênese (LONG et al., 2015; CAMARGO et al., 2016), fertilidade e mapeamento de solos (MARQUES Jr. et al., 2014; SIQUEIRA et al., 2016), erosão (ROWNTREE et al., 2017), entre outras vertentes. A tendência em utilizar esses sensores próximos em substituição ou complemento a métodos tradicionalmente utilizados deve-se, principalmente, a fatores relacionados à economia de tempo e recursos, o que possibilita analisar um grande número de amostras e realizar estudos mais abrangentes (RIBEIRO et al., 2017).

Assim, os objetivos deste estudo foram comparar os diferentes métodos para quantificação de maghemita em solos, bem como caracterizar a maghemita de solos desenvolvidos sobre diferentes materiais de origem; e avaliar a eficiência de sensores próximos (magnetômetro e pXRF) e dos modelos digitais de terrenos (MDTs) como suporte ao mapeamento digital na separação de Latossolos em área com geologia variável.

2. REFERENCIAL TEÓRICO

2.1. Fundamentos de magnetismo e medidas magnéticas

Na escala atômica, os campos magnéticos surgem pela movimentação dos elétrons, a partir da sua rotação orbital e pelo giro em

seu próprio eixo. No entanto, para melhor entendermos estes conceitos é necessária a distinção dos números quânticos.

Os números quânticos referem-se aos conteúdos de energias dos elétrons. Cada elétron de um átomo apresenta quatro números quânticos, que são: principal (n), secundário ou azimutal (l), magnético (m ou m_l) e *spin* (s ou m_s). O número quântico principal (n) representa o nível de energia em que os elétrons estão localizados na camada da eletrosfera. As camadas da eletrosfera são identificadas por letras (K, L, M, N, O, P, Q), sendo que para cada camada é atribuído um valor (de 1 a 7, respectivamente) (Figura 1).

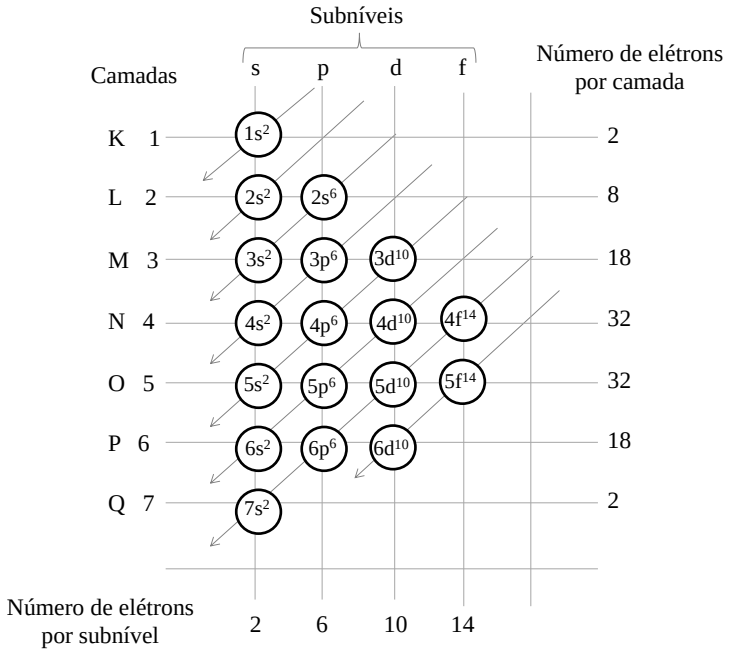

Figura 1. Distribuição eletrônica dos íons evidenciando as camadas de valência, os subníveis energéticos e o número de elétrons por camada e por subnível.

O número quântico secundário (l) corresponde aos subníveis das camadas. Para cada camada existem quatro subníveis de energias (s, p, d, f), sendo que cada subnível suporta um número máximo de elétrons (2, 6, 10, 14 elétrons, respectivamente) (Figura 1).

O número quântico magnético (m ou m_l) indica o número de orientações dos orbitais no espaço. Os seus valores variam, dependendo do orbital (Figura 2). O orbital do subnível *s*, por exemplo, possui forma esférica e por isso só há uma orientação possível, de forma que o número quântico magnético será igual a zero. Já o subnível *p* pode apresentar três orientações espaciais, e por isso três números magnéticos são possíveis, -1, 0, +1.

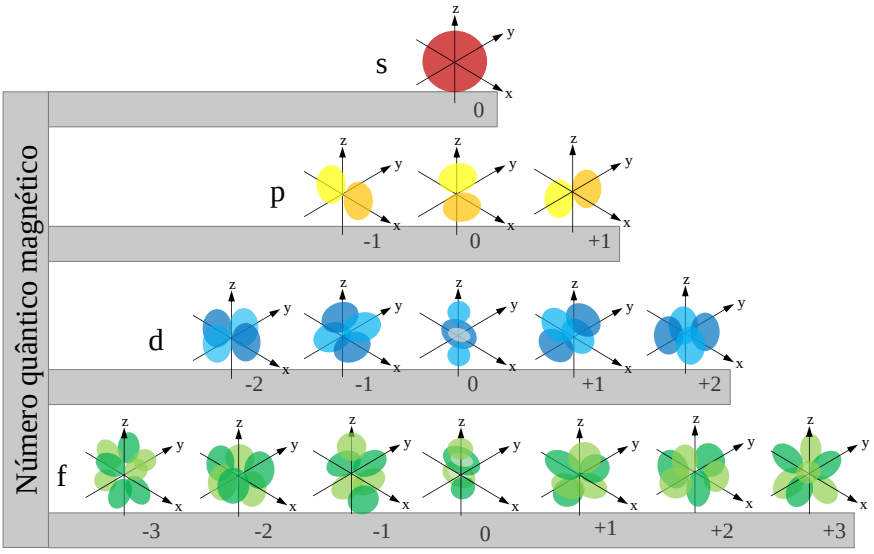

Figura 2. Orientação espacial das orbitais em cada subnível da distribuição eletrônica, evidenciando o numero quântico magnético.

Cada orbital possui, no máximo, dois elétrons e o número quântico *spin* (s ou m_s) refere-se ao sentido da rotação do elétron. Assim, o magnetismo em razão do *spin* de um elétron é anulado pelo magnetismo do *spin* oposto, ficando um sistema estável. No entanto, pela regra de preenchimento dos *spins*, os elétrons são posicionados todos em uma direção dentro de cada subnível e depois se preenche os elétrons na direção oposta. Assim, quando ha falta de elétrons dentro de alguns subnível o magnetismo não é anulado.

Desta forma, o átomo ou partícula apresentará momento magnético pela movimentação dos seus elétrons, a partir de: (1) da rotação orbital de um elétron sobre o núcleo de um átomo. Uma vez que todos os elétrons nas camadas completas ou em ligações covalentes estão emparelhados com um elétron de *spin* oposto em cada orbital, somente íons com camadas incompletas podem ter *spin* total diferente de zero. Na distribuição eletrônica, o valor de cada *spin* pode ser positivo, representado pela seta para cima ↑ (m_s = +½) ou negativo, representado pela seta para baixo ↓ (m_s = -½), na orbital completa, a soma dos *spins* individuais (+½ + -½) é igual a zero (Figura 3A); e (2) pelo giro de um elétron sobre seu próprio eixo (Figura 3B). Ambos os movimentos giratórios produzem um campo magnético, mas nos minerais naturais de óxido de ferro, a rotação do elétron sobre o seu próprio eixo é dominante (THOMPSON; OLDFIELD, 1986; COEY, 2009).

Elementos com camadas eletrônicas completas, como por exemplo, o Si^{4+} (distribuição eletrônica $1s^2 2s^2 2p^6$), apresentam configuração não magnética. Já o Fe^{3+} apresenta orbitais *3d* incompletos (distribuição

eletrônica $1s^2 2s^2 2p^6 3s^2 3p^6 3d^5$) (COEY, 2009; CURI et al., 2018) e, a falta de elétrons faz com que a soma dos *spins* seja diferente de zero o Fe^{3+} expresse o momento magnético.

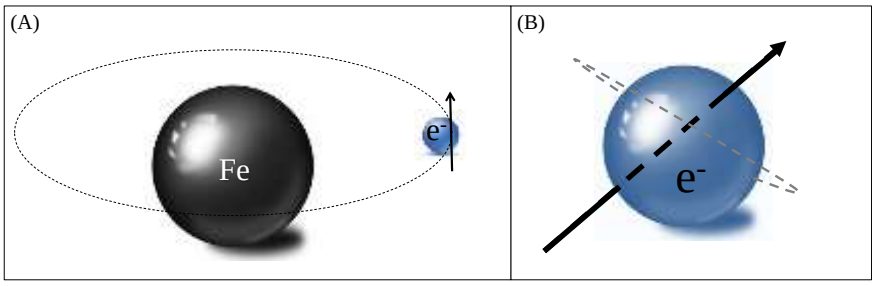

Figura 3. Desenho esquemático representando o movimento do elétron na orbital (A) e o movimento giratório em seu próprio eixo (*spin*) (B). Adaptado de Barrón (2017), comunicação pessoal.

No entanto, nem todos os minerais que contém Fe em sua estrutura apresentam momento magnético significativo. De acordo com Thompson; Oldfield (1986) e Coey (2009) as propriedades magnéticas dos minerais são classificadas como diamagnetismo, paramagnetismo, ferromagnetismo, ferrimagnetismo e antiferromagnetismo.

O diamagnetismo ocorre quando as várias orbitais e *spins* sofrem cancelamento de um componente sobre o outro e como consequência o mineral não expressa momento magnético ou expressa momento magnético negativo (Figura 4). Por ser extremamente fraco, este efeito é encoberto pelas demais propriedades magnéticas. Minerais como quartzo, feldspato, calcita e a água são diamagnéticos.

O paramagnetismo ocorre em minerais com intenso movimento térmico dos átomos presentes em sua estrutura e que, constantemente,

anulam o alinhamento dos momentos magnéticos, resultando em magnetização positiva pequena. No entanto, a magnetização é facilmente perdida após a remoção do campo magnético. Minerais como olivina, piroxênio, granada e biotita são paramagnéticos.

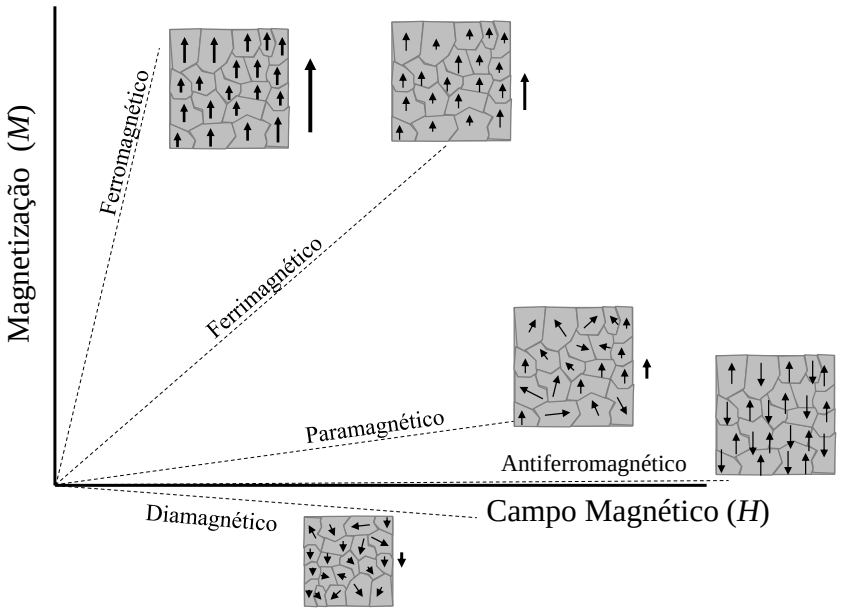

Figura 4. Principais ordenamentos magnéticos em elementos e minerais e sua representação esquemática. Adaptado de Barrón (2017), comunicação pessoal.

O ferromagnetismo ocorre no Fe e em outros elementos como Co e Ni. Quando esses elementos ou materiais que os contenham (ex: imã) são expostos a um campo magnético, alinham todos os momentos magnéticos. A magnetização resulta do somatório dos momentos magnéticos associados com cada elétron em cada átomo do elemento, que tem suas propriedades modificadas drasticamente em uma temperatura crítica denominada temperatura de Curie (THOMPSON; OLDFIELD,

1986; COEY, 2009; JORDANOVA, 2016). Este valor é específico e varia para cada elemento ou mineral. Abaixo da temperatura de Curie um elemento ferromagnético apresenta magnetização remanente muito forte e acima dessa temperatura apresenta características paramagnética.

A magnetização remanente dos materiais ferromagnéticos resulta do fenômeno de magnetização espontânea, que é a magnetização existente mesmo na ausência de um campo magnético (THOMPSON; OLDFIELD, 1986; COEY, 2009; JORDANOVA, 2016). O momento magnético nos materiais ferromagnéticos é muito superior aos dos materiais diamagnéticos e paramagnéticos, fazendo com que esta característica prevaleça em misturas de materiais com diferentes características magnéticas (THOMPSON; OLDFIELD, 1986; DEARING, 1994).

O ferrimagnetismo ocorre quando os *spins* estão alinhados antiparalelamente, porém a soma dos momentos em uma direção ultrapassa a de direção oposta, levando a uma magnetização liquida positiva, de maneira que a característica final é semelhante ao ferromagnetismo. A magnetita e a maghemita são exemplos de minerais ferrimagnéticos.

O antiferromagnetismo ocorre quando os *spins* de momentos magnéticos idênticos (mesmo tamanho de seta) estão alinhados em direções opostas, resultando em magnetização líquida do material positiva ou zero. Há uma variação deste arranjo denominada antiferromagnetismo inclinado, em que os vetores apresentam um pequeno ângulo de inclinação em relação ao eixo antiferromagnético e assim resultam num baixo momento magnético. Hematita e goethita são minerais antiferromagnéticos.

Quando um campo magnético é aplicado, o estado magnético dos minerais pode ser alterado e importantes informações podem ser obtidas. Um mineral que é submetido à aplicação de um campo magnético, aumenta sua magnetização até certo patamar. Quando o campo magnético é removido, a magnetização diminui, mas não retorna à zero, necessitando, para isso, a aplicação de um campo magnético em direção contrária. Nesse processo é gerada a curva de histerese magnética (Figura 5) (THOMPSON; OLDFIELD, 1986; COEY, 2009).

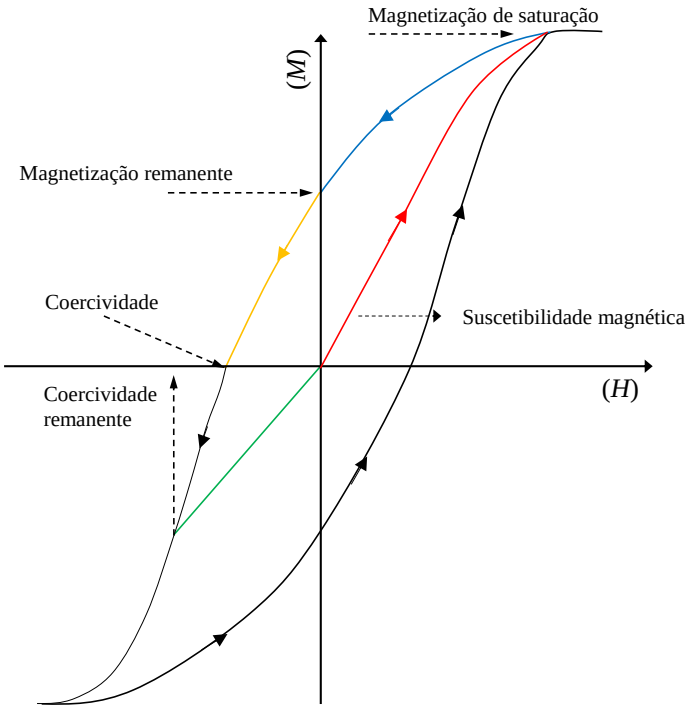

Figura 5. Representação esquemática da curva de histerese magnética, evidenciando os pontos de magnetização de saturação, magnetização remanente, coercividade, coercividade remanente e suscetibilidade magnética. M = magnetização; H = campo magnético.

A partir da curva de histerese (Figura 5), importantes parâmetros que permitem caracterizar os minerais magnéticos podem ser analisados: (1) a magnetização de saturação, definida como a magnetização máxima possível (M) de um material após a aplicação de um campo magnético externo (H). A saturação magnética é alcançada quando todos os momentos magnéticos estão alinhados com o campo magnético aplicado no sentido direto; (2) a magnetização remanente (linha azul), que é a magnetização residual no material quando se retira o campo magnético; (3) a coercividade, que é o campo magnético reverso, necessário (linha amarela) para que a magnetização retorne à zero (mas sem passar pela origem) e; (4) a coercividade remanente, que é definida como o campo magnético necessário (no sentido direto e de maior intensidade; linha verde) para que a magnetização retorne a zero passando pela origem. Além disso, a curva que passa pela origem (linha vermelha), no início do ciclo de histerese, representa a susceptibilidade magnética do material (Figura 5) (THOMPSON; OLDFIELD, 1986; DEARING, 1994; DUNLOP, 2002).

Os parâmetros obtidos graficamente pela curva de histerese também fornecem informações sobre a anisotropia cristalina dos minerais presentes na amostra, uma vez que o tamanho, a forma e a estrutura dos minerais podem influenciar nas propriedades magnéticas (DEARING, et al. 1996; PETERS; DEKKERS, 2003; LONG et al., 2015; NEDELKOSKI et al., 2017). A anisotropia magnética pode ser diferenciada em anisotropia magnetocristalina, anisotropia de forma e anisotropia de tensão (THOMPSON; OLDFIELD, 1986; COEY, 2009).

A anisotropia magnetocristalina surge a partir da rede cristalina dos minerais (geometria interna), uma vez que os vários eixos de um cristal têm propriedades magnéticas diferentes. Este tipo de anisotropia é importante para os minerais antiferromagnéticos, como hematita e goethita, que apresentam maior resistência à orientação dos *spins* quando o campo magnético é aplicado. Como consequência, esses minerais apresentam alta coercividade. A segunda forma de anisotropia está relacionada à forma dos minerais magnéticos. Minerais como a magnetita, que apresentam estrutura cristalina tipo espinélio (FABRIS et al., 1997; COSTA et al., 2009; COEY, 2009) são mais facilmente magnetizadas. A terceira forma de anisotropia pode ser considerada derivada da anisotropia magnetocristalina, uma vez que se refere a alteração do tamanho e distorções da rede cristalina quando o campo magnético é aplicado.

Na Tabela 1 são apresentados valores de medidas magnéticas de alguns minerais. Nota-se que minerais ferrimagnéticos como magnetita e maghemita apresentam maiores valores de suscetibilidade magnética, magnetização de saturação e magnetização remanente, e valores mais baixos de coercividade e coercividade remanente quando comparadas à hematita à goethita.

Além da curva de histerese, a suscetibilidade magnética pode ser obtida através de sensores próximos. Um dos equipamentos mais utilizados em estudos envolvendo material de solo é o sistema Bartington MS2 (INDA et al., 2013; BATISTA et al., 2013; RAMOS et al., 2017; CAMÊLO et al., 2017). Este sistema consiste na aplicação de um campo magnético de 80 A m^{-1} em uma amostra não magnetizada (DEARING,

1994). Dependendo da característica magnética da amostra (ferrimagnética, paramagnética, antiferrimagnéticas ou diamagnética) ela será mais ou menos magnetizada, conforme esquema apresentado na Figura 4. Este sistema tem como vantagens a facilidade de obtenção das leituras, viabilizando análises em um grande universo amostral, além de poder ser utilizada diretamente no campo.

Tabela 1. Propriedades magnéticas dos principais óxidos de Fe encontrado em solos tropicais.

Mineral	χ	Ms	Mr	Hc	Hcr
	10^{-6} m^3 kg^{-1}	-------- A m^2 kg^{-1} ---------		--------- 10^{-3} T ----------	
Mt	284 - 1233	50 - 90	0,3 - 33	0,1 - 35	8 - 70
Mh	283 - 845	62 - 66	4 - 10	7 - 9	17 - 31
Hm	0,13 - 3,83	0,1 - 0,5	0,003 - 0,35	4 - 520	30 - 821
Gt	0,46 - 5,92	0,02 - 0,6	0,015 - 0,12	25 - 890	500 - 4100

χ = suscetibilidade magnética; Ms = magnetização de saturação; Mr = magnetização remanente; Hc = coercividade; Hcr = coercividade remanente. Fonte: Peters; Dekkers (2003).

2.2. Domínios magnéticos

As medidas de histerese magnética estão também relacionadas com os domínios magnéticos. Juntamente com a anisotropia, os domínios magnéticos desempenham um papel importante no controle das propriedades magnéticas dos minerais (DUNLOP, 2002; THOMPSON; OLDFIELD, 1986).

Os domínios magnéticos são divisões energéticas que um material ou substância pode apresentar (THOMPSON; OLDFIELD, 1986). Cada

domínio pode ser magnetizado espontaneamente (quando não há aplicação de um campo magnético externo) em diferentes direções (Figura 6) e assim, a soma da magnetização dos domínios pode ser zero. O motivo pelo qual os domínios magnéticos se formam, é que essa organização faz com se produza um estado de menor energia total e o equilíbrio possa ser alcançado (THOMPSON; OLDFIELD, 1986; DEARING, 1994).

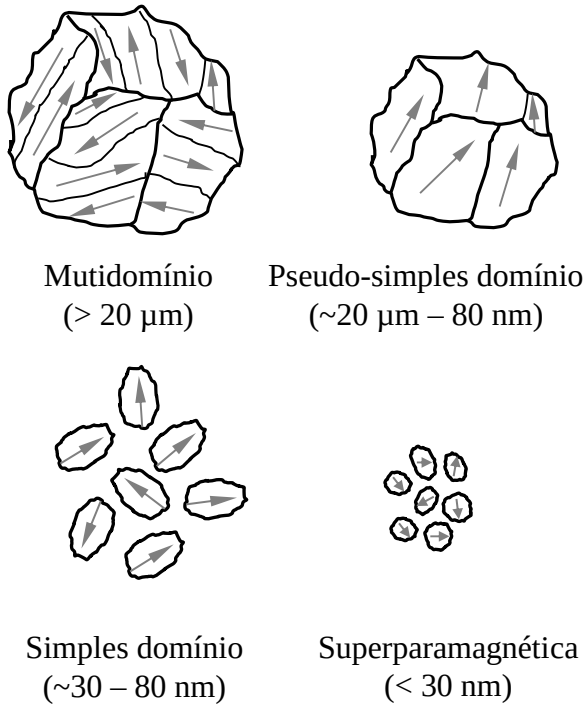

Figura 6. Desenho esquemático representando os domínios magnéticos de acordo com o tamanho das partículas.

Quanto aos domínios, as partículas podem apresentar multidomínio (MD), pseudo-simples domínios (PSD), simples domínio

(SD) e superparamagnetismo (SP) (Figura 6). Partículas grandes (> 20 µm) apresentam multidomínios por que, energeticamente, é mais favorável ter-se mais do que um domínio (DUNLOP; ÖZDEMIR, 1997; NEDELKOSKI et al., 2017). Partículas grandes o suficiente (~ 20 µm – 80 nm) para favorecer mais de um domínio, mas que mostram propriedades magnéticas dos grãos de domínio simples único; são denominados pseudo-simples domínio. Partículas menores (~30- 80 nm) apresentam simples domínio devido ao volume restrito das partículas. Já as partículas superparamagnéticas são muito pequenas (< 30 nm) e por isso apresentam também simples domínio, porém com forte magnetização. No entanto essas partículas são magneticamente instáveis devido à energia térmica. Essa característica é semelhante ao paramagnetismo, mas com uma susceptibilidade muito maior. Por isso, é denominado superparamagnético (DUNLOP; ÖZDEMIR, 1997; NEDELKOSKi et al., 2017; DEARING, 1999).

2.3. Maghemita pedogenética: principais características e sua quantificação

A maghemita é dominantemente considerada um óxido de Fe secundário. Seu nome deriva dos minerais magnetita e hematita, pois a estrutura cristalina (cúbica compacta) é semelhante à magnetita mas é um mineral polimorfo da hematita, com formula γFe_2O_3 (SCHWERTMANN; TAYLOR, 1989; COSTA et al., 2009). Sua presença é comum principalmente em solos tropicais e subtropicais, podendo ocorrer em todo o perfil do solo, ou em concreções e nódulos localizados. Em solos

brasileiros pode ser herdada do material de origem ou até mesmo formada pela oxidação da magnetita litogênica, entre outras possibilidades (CURI; FRANZMEIER, 1984; KÄMPF; CURI, 2000). Recentemente, alguns trabalhos demostraram ser possível a formação de maghemita via recristalização da ferrihidrita (BARRÓN; TORRENT; DE GRAVE, 2003; TORRENT; BARRÓN; LIU, 2006; LIU et al., 2008; MICHEL et al. 2010). Dentre os solos desenvolvidos de rochas máficas, a maghemita pode representar até 40% dos óxidos de Fe (COSTA et al., 1999), enquanto em solos desenvolvidos de dolomito ferruginoso pode representar até 47% (CARVALHO FILHO et al., 2015).

Embora se conheça a ocorrência da maghemita em solos brasileiros, existe uma grande lacuna no que diz respeito à sua formação pedogênica, mesmo sendo este mineral bastante comum em solos dos trópicos e subtrópicos (KÄMPF; CURI, 2000; COSTA et al., 2009; CARVALHO-FILHO et al., 2015; CAMÊLO et al., 2017; RAMOS et al., 2017).

A maghemita apresenta-se como um espinélio invertido com estrutura cristalina cúbica ou tetragonal (Figura 7). De acordo com Fabris et al (1997), sua formação a partir da magnetita (principal via) envolve a oxidação do Fe^{2+} da estrutura da magnetita à Fe^{3+} promovendo uma deficiência de cátions e a saída do Fe^{3+} da estrutura do espinélio, criando vacâncias. A substituição do Fe^{2+} para Fe^{3+} varia de zero na magnetita para 1/3 na maghemita, conforme fórmula abaixo:

$$[Fe^{3+}]\ \{Fe^{2+}_{1-3x}\ Fe^{3+}_{1+2x}\square_x\}O_4$$

Onde, □ indica a vacância e [ ] e { } representam a coordenação octaedral e tetraedral, respectivamente. A dimensão da cela unitária no sistema cúbico (de maior ocorrência) é de a_o = 0,8340 nm e no sistema

tetragonal é de a_o = 0,8346 e c_o = 2,501 nm. No entanto esses valores podem variar com o tipo e grau de substituição isomórfica do Fe^{3+} por outros cátions, dentro da cela unitária (COSTA et al., 2009; FABRIS et al., 1997; CARVALHO-FILHO et al., 2015; NONAKA et a., 2017).

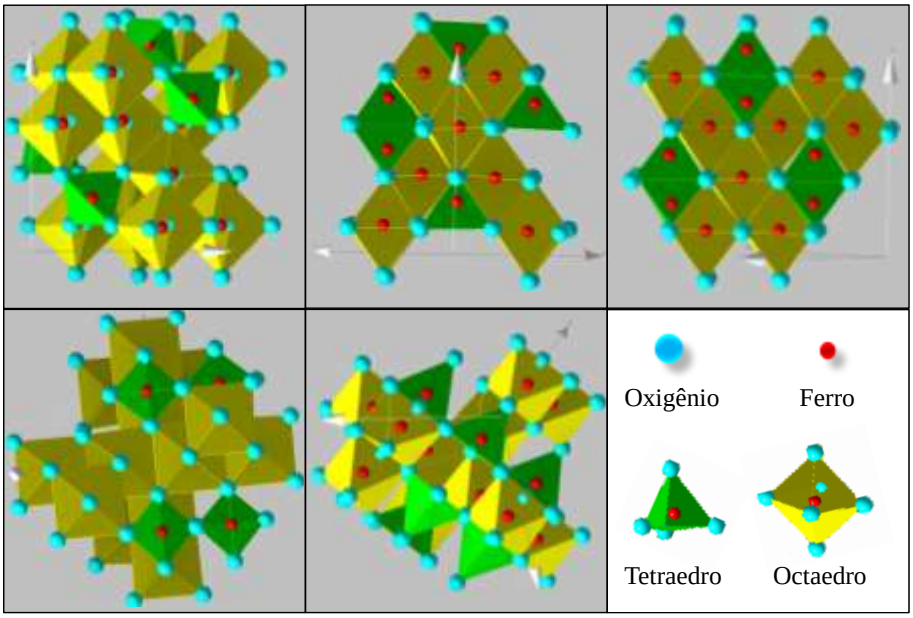

Figura 7. Modelo estrutural em diferentes rotações da coordenação tetraedral e octaedral do Fe na maghemita.

Na maghemita, assim como em outros minerais, pode ocorrer substituição isomórfica na rede cristalina, alterando suas características cristaloquímicas. Os principais metais que podem substituir o Fe^{3+} são Ti^{4+}, Al^{3+}, Mg^{2+}, Zn^{2+} e Mn^{2+}. Batista et al. (2008) avaliando as características de maghemitas sintéticas observou que o aumento da substituição de Fe^{3+} por Zn^{2+} aumentou a dimensão α_0 da cela unitária cúbica e reduziu o diâmetro médio do cristalito e a suscetibilidade

magnética. Já a substituição de Fe^{3+} por Al^{3+}, também em maghemitas sintéticas, diminuiu o diâmetro médio do cristalito, a dimensão a_o da cela unitária cúbica e a magnetização (BATISTA et al., 2013). Carvalho-Filho et al. (2015) observaram valores de substituição isomórfica em maghemita pedogenéticas variando de 0,0 a 0,23 mol mol^{-1} de Al, excedendo o maior valor comumente reportado pela literatura (0,20 mol mol^{-1} de Al), e sugerem que outros cátions podem estar substituindo o Fe na estrutura da maghemita.

Uma das principais características da maghemita é a propriedade magnética. Para que um material apresente propriedades magnéticas, é necessária uma resposta magnética quando se aplica um campo magnético externo. Esta resposta se deve às propriedades individuais dos átomos ou moléculas e às suas interações. Nos minerais, o caráter magnético é associado ao teor de Fe presente na estrutura, pois este elemento contém orbitais *3d* incompletas onde ocorre transição dos elétrons entre os orbitais, gerando assim o momento magnético (COEY, 2009; COSTA; BIGHAM, 2009).

A quantificação de goethita e hematita, óxidos cuja presença nos solos é mais abrangente do que a da maghemita, é tradicionalmente feita a partir da área da reflexão do mineral por DRX e pelos teores de Fe extraídos por DCB (CURI et al., 1987; COSTA et al., 1999., CARVALHO-FILHO et al., 2015). Para maghemita, no entanto, a área da reflexão é por vezes de difícil determinação, uma vez que este mineral, geralmente, ocorre em menores quantidades na fração argila, e a sua principal reflexão coincide com a reflexão da hematita. Assim, outros métodos para sua quantificação têm sido utilizados.

Historicamente, a quantificação de maghemita tem sido feita a partir da dissolução seletiva, proposta por Schwertmann; Fechter (1984), na qual é empregado um tempo de contato de 7,5 horas da amostra com o H_2SO_4 (1,8 mol L^{-1}). Contudo, neste tempo de contato, além de extrair toda a maghemita, podem ser extraídas porções consideráveis de goethita e hematita. Costa et al. (1999) constataram que a dissolução seletiva da maghemita foi completada após duas horas de contato com uma solução 1,8 mol L^{-1} de H_2SO_4. Os autores observaram também forte correlação entre a suscetibilidade magnética da fração argila e o teor de maghemita estimado pela difração de raios-X. Trabalhos nesta mesma linha, como os de Inda et al. (2013); Camargo et al. (2014) e Camêlo et al. (2017) confirmam que o tempo de dissolução da maghemita varia de acordo com a amostra, reforçando a necessidade da ampliação dos estudos sobre quantificação e caracterização da maghemita envolvendo um número maior de amostras representativas de solos formados sobre as mais distintas condições pedoclimáticas, com destaque para aquelas influenciadas pela diversidade de materiais de origem e seus efeitos covariantes.

Relacionado ao difratogramas de raios-X, o refinamento Rietveld por vezes também é utilizado na quantificação de maghemita (NONAKA et al., 2017). Este método consiste no ajuste computacional do difratograma experimental ao difratograma de uma amostra padrão, na qual se conhecem todos os parâmetros cristalográficos. A vantagem do refinamento Rietveld é que ele permite visualizar a posição e as intensidades dos minerais, mesmo que as reflexões estejam sobrepostas. Além disso, a partir do refinamento Rietveld podem ser obtidos os

parâmetros da célula e tamanho do cristal, entre outros parâmetros cristalográficos.

Outra forma indireta de quantificar a maghemita é através da suscetibilidade magnética. Santana (1984) estudando uma topossequência quantificou maghemita por difratometria diferencial de raios-X e, a partir destes dados e dos valores de suscetibilidade magnética da fração argila, constatou que a suscetibilidade magnética atribuída à maghemita era da ordem de 636×10^{-6} m^3 kg^{-1}. Posteriormente, Resende et al. (1988) calculou o teor de maghemita de solos, de diferentes localidades e teores de Fe, utilizando como referência este valor de suscetibilidade magnética da maghemita. Esta relação entre teor de maghemita no solo e o valor de suscetibilidade magnética foi também confirmado por Costa et al. (1999).

2.4. Aplicação das medidas magnéticas em estudos pedoambientais

No Brasil, os trabalhos pioneiros a utilizarem esta característica mineral e relaciona-las com classes de solos são os de Resende et al. (1986) e Curi; Franzmeier (1984; 1987) . À época havia a sugestão de utilizar a suscetibilidade magnética em níveis taxonômicos elevados como indicador de diferenças mineralógicas, sobretudo nos Latossolos Vermelhos, devido à sua origem poligenética (RESENDE et al., 1988).

A Tabela 2 apresenta valores de suscetibilidade magnética em diferentes solos. Os solos desenvolvidos sobre rochas com altos teores de Fe, como o basalto ou itabirito, por exemplo, apresentam valores de suscetibilidade magnética mais elevados do que os solos desenvolvidos de gnaisse, filito, micaxisto e rochas sedimentares. Os valores compilados

nesta tabela demonstram a capacidade da suscetibilidade magnética na distinção de solos originados de diferentes materiais de origem.

Tabela 2. Valores de suscetibilidade magnética do horizonte B de solos desenvolvidos de diferentes materiais de origem.

Referência	Rocha/Estado	Solo	$\chi^{(1)}$
(a)	Itabirito	Latossolos com > 18% de Fe_2O_3 e cores vermelhas (≤ 2,5 YR)	735 a 2.832
	Basalto		90 a 6.157
	Tufito		64 a 540
	Itabirito	Latossolos com > 18% de Fe_2O_3 e cores amarelas (> 2,5 YR)	21 a 588
	Tufito	Latossolos com 8-18% de Fe_2O_3 e cores vermelhas (< 2,5 YR)	81 a 149
	Sedimentar		56 a 115
	Gnaisse e migmatito	Latossolos com 8-18% de Fe_2O_3 e cores amarelas (> 2,5 YR)	1
	Charnokito		5
	Migmatito		22
	Sedimentar		12
	Sedimentar	Latossolos com > 8% de Fe_2O_3 e cores vermelhas (≤ 2,5 YR)	6 a 12
	Sedimentar	Latossolos com > 8% de Fe_2O_3 e cores vermelhas (> 2,5 YR)	1 a 7
(b)	Basalto/GO	Latossolo Vermelho	400
	Itabirito/MG	Latossolo Vermelho	2.830
(c)	Ígnea básica/PR	não especificado	100 a 779
	Metamórfica e sedimentar/PR	não especificado	≤ 50
(d)	Quartzito/MG	Cambissolo Háplico	10
	Mica-Xisto/MG	Argissolo Bruno-Acinzentado	26
	Gabro/MG	Latossolo Vermelho	140
	Itabirito/MG	Argissolo Vermelho-Amarelo	342
	Serpentinito/MG	Plintossolo Pétrico	192
	Metacalcário/MG	Latossolo Vermelho-Amarelo	32
	Gnaisse/MG	Argissolo Vermelho-Amarelo	3
	Filito/MG	Argissolo Vermelho	11
(e)	Sedimentos colúvio-aluviais/MG	Gleissolos Háplicos e Melânicos	< 2

Gnaise leucocrático/MG	Neossolos, Cambissolos, Nitossolos, Latossolos e Argissolos	2 a 25
Gnaise mesocrático/MG	Nitossolos, Latossolos e Argissolos	25 a 90
Gabro/MG	Cambissolos, Nitossolos, Latossolos e Argissolos	90 a 522

(1) χ = suscetibilidade magnética ($\times 10^{-7}$ m^3 kg^{-1}); (a) Resende et al. (1988) - faixa de valores dentro de cada material de origem de solos sob Cerrado ou Floresta, provenientes de diversas localidades; (b) Curi e Franzmeier (1987); (c) Silva; Souza Jr; Costa (2010) - rochas metamórficas e sedimentares: amostras oriundas do primeiro e do segundo planalto e da formação Caiuá, no terceiro planalto; Rochas ígneas: amostras do segundo planalto; (d) Araújo et al. (2014) - valores médios dos sub-horizontes B de cada solo; (e) Curi et al. (2018).

Posteriormente, Costa et al. (1999) trabalharam com suscetibilidade aliada a dissolução seletiva com H_2SO_4 no sentido de ajustar a metodologia de quantificação de maghemita em solos. Recentemente, a suscetibilidade magnética foi inserida na Pedometria, sendo utilizada como covariável ambiental para predizer outros atributos do solo (BAHIA et al., 2017; MARQUES Jr. et al., 2014; SIQUEIRA et al., 2016).

A Pedometria é um ramo recente da Pedologia no qual métodos estatísticos e matemáticos são utilizados para o estudo da distribuição e gênese dos solos (McBRATNEY et al., 2000). Um dos fatores relacionados à formação do solo mais usados nas predições das classes e propriedades do solo é a topografia, através dos modelos digitais de elevação e seus derivados - os modelos digitais de terreno (MDTs) (De MENEZES et al., 2016). Considerando a natureza contínua da variação dos MDTs, eles têm sido usados em modelos preditivos de solo, sendo uteis em ambientes onde a topografia está fortemente relacionada aos processos de formação do solo. (McKENZIE et al., 2000).

Neste sentido, diversos trabalhos envolvendo a Pedometria envolvem tanto os MDTs quanto a suscetibilidade magnética. Camargo et al. (2016) constataram que o fosfato adsorvido em solos desenvolvidos de arenitos pode ser predito a partir de uma função de pedotransferência usando óxidos de Fe e suscetibilidade magnética como preditores. Barrios et al. (2017) verificaram que a suscetibilidade magnética foi capaz de identificar mudanças nas características físicas, químicas e mineralógicas de Latossolos sob sistemas de colheita da cana-de-açúcar, com e sem queima. Ramos et al. (2017) utilizaram suscetibilidade magnética aliada à técnicas geoestatísticas para separar ambientes no Planalto Médio do Rio Grande do Sul. Propriedades magnéticas, como o tamanho da partícula magnética e seus domínios magnéticos, foram utilizadas em estudos envolvendo pedogênese (LONG et al., 2015; SRIVASTAVA; SANGODE; TORRENT, 2015) ou caracterização de paleoambientes (TORRENT; LIU; BARRÓN, 2010; WANG et al., 2016), além de estudos envolvendo erosão do solo (ROWNTREE et al., 2017) e mesmo poluição atmosférica (GRIMLEY et al., 2017), demostrando o grande potencial das medidas magnéticas como suporte a trabalhos em diversas áreas.

3. CONSIDERAÇÕES FINAIS

Em geral, as informações disponíveis sobre maghemita pedogenética são limitadas em relação à outros óxidos de Fe, especialmente hematita e goethita. Assim, o uso da suscetibilidade

magnética pode facilitar a quantificação de maghemita, especialmente em trabalhos que envolvam grande número de amostras. Além disso, a suscetibilidade e outras propriedades magnéticas podem auxiliar no entendimento da pedogênese em solos desenvolvidos de diferentes materiais de origem e apoiar trabalhos relacionados à classificação e mapeamento digital de solos.

REFERÊNCIAS

ARAÚJO, M. A. et al. Paragênese mineral de solos desenvolvidos de diferentes litologias na Região Sul de Minas Gerais. **Revista Brasileira de Ciência do Solo**, Viçosa, v.38, p.11-25, 2014.

BARRÓN, V.; TORRENT, J. Use of the Kubelka-Munk theory to study the influence of iron oxides on soil colour. **European Journal of Soil Science**, Hoboken, v. 37, p.499–510, 1986.

BARRÓN, V. Curso de magnetismo. Comunicação pessoal. 2017.

BARRÓN, V.; TORRENT, J.; DE GRAVE, E. Hydromaghemite, an intermediate in the hydrothermal transformation of 2-line ferrihydrite into hematite. **American Mineralogist**, Chantilly, v.88, p.1679–1688, 2003.

BAHIA, A.S.R.S. et al. Prediction and Mapping of soil attributes using diffuse reflectance spectroscopy and magnetic susceptibility. **Soil Science Society of America Journal,** Madison, v.81, n.6, p.1450-1462, 2017.

BARRIOS, M. R. et al. Magnetic susceptibility as indicator of soil quality in sugarcane fields. **Revista Caatinga**, Mossoró, v.30, n.2, p.287-295, 2017.

BATISTA, M.A. et al. Cristallochemical characterization of synthetic Zn-substituted maghemites (y-$Fe^{2-}{}_{x}Zn_{x}O_{3}$). **Revista Brasileira de Ciência do Solo**, Viçosa, v.32, n.2, p.561-568, 2008.

BATISTA, M.A. et al. Structural and magnetic characterization of maghemites prepared from al-substituted magnetites. **Revista Brasileira de Ciência do Solo**, Viçosa, v.37, p.1569–1575, 2013.

CAMARGO, L.A. et al. Clay mineralogy and magnetic susceptibility of Oxisols in geomorphic surfaces. **Scientia Agricola**, Piracicaba, v.71, p.244–256, 2014.

CAMARGO, L.A. et al. Pedotransfer functions to assess adsorbed phosphate using iron oxide content and magnetic susceptibility in an Oxisol. **Soil Use and Management**, Hoboken, v.32, n.2, p.172–182, 2016.

CAMÊLO, D.L. et al. Pedogenic Iron Oxides in Iron-Rich Oxisols developed from mafic rocks. **Revista Brasileira de Ciência do Solo**, Viçosa, v.41:e0160379, 2017.

CARVALHO FILHO, A. et al. Iron of diferent lithological origin in ferriferous quadrilateral (Minas Gerais, Brazil). **Applied Clay Science**, Amsterdã, v.118, p.1–7, 2015.

CERVI, E.S.; COSTA, A.C.S.; SOUZA Jr, I.G. Magnetic susceptibility and the spatial variability of heavy metals in soils developed on basalt, **Journal of Applied Geophysics**, Amsterdã, v.111, p.377-383, 2014.

COEY, J.M. **Magnetism and magnetic matter**. Cambridge University Press, Cambridge, 2009. 632pp.

COSTA, A. C. S. et al. Quantification and characterization of maghemite in soils derived from volcanic rocks in southern Brazil. **Clays and Clay Minerals**, Chantilly, v.47, p.466-473, 1999.

COSTA, A. C. S.; BIGHAM, J. M. Óxidos de Ferro. In: MELO, V.F.; ALLEONI, L.R.F., ed. **Química e Mineralogia do Solo: Parte I – Conceitos Básicos**. Viçosa: SBCS, 2009, p. 505-572.

CURI, N. et al. **Mapeamento de solos e magnetismo no campus da ufla como traçadores ambientais**. Lavras: Editora UFLA, 2018. 148pp.

CURI, N.; FRANZMEIER, D.F. Effect of parent rocks on chemical and mineralogical properties of some Oxisols in Brazil. **Soil Science Society of America Journal**, Madison, v.51, p.153-158, 1987.

CURI, N.; FRANZMEIER, D.F. Toposequence of Oxisols from the central plateau of Brazil. **Soil Science Society of America Journal**, Madison, v.48, p.341-346, 1984.

DEARING, J.A. **Environmental magnetic susceptibility**. Bartington Instruments, Witney, Oxon, England, 1994. 104pp.

DEARING, J.A. et al. Frequency-dependent susceptibility measurements of environmental materials. **Geophysical Journal International**, Oxford, v.124, p.228–240, 1996.

De MENEZES, M.D. et al. Spatial prediction of soil properties in two contrasting physiographic regions in Brazil. **Scientia Agricola**, Piracicaba, v.73, p.274–285, 2016.

DJERRAB, A. et al. Contribution of magnetic parameters to the identification of stratigraphic levels and pedogenesis (Angel Cave, Spain). **Estudios Geológicos**, Madrid, v.69, n.1, p.71-84, 2013.

DUNLOP, D.J. Theory and application of the day plot (Mrs/Ms versus Hcr/Hc). 2. Application to data for rocks, sediments, and soils. **Journal of Geophysical Research**, São Francisco, v.107, B32057, 2002.

DUNLOP, D. J.; ÖZDEMIR, Ö. **Rock Magnetism: Fundamentals and Frontiers**. Cambridge Univiversity Press, New York, 1997. 575 pp.

FABRIS, J.D. et al. Iron-rich spinels from Brazilian soils. **Hyperfine Interactions**, New York, v.110, p.23–32, 1997.

GRIMLEY, D.A. et al. Soil magnetic susceptibility: a quantitative proxy of soil drainage for use in ecological restoration. **Restoration Ecology**, Hoboken, v.16, n.4, p.657–667, 2008.

GRIMLEY, D. A. et al. Using magnetic fly ash to identify post-settlement alluvium and its record of atmospheric pollution, central USA. **Anthropocene**, v.17, p.84–98, 2017.

INDA, A.V. et al. Iron oxides dynamics in a subtropical Brazilian Paleudult under long-term no-tillage management. **Scientia Agricola**, Piracicaba, v.70, p.48–54, 2013.

JORDANOVA, N. Soil magnetism: applications in pedology, environmental science and agriculture. Academic Press, Elsevier, 2017. 466pp.

KÄMPF, N.; CURI, N. **Óxidos de ferro: indicadores de ambientes pedogênicos e geoquímicos**. In: Tópicos em Ciência do Solo, v.1, p.107-138, 2000.

LIU, Q.S. Magnetism of intermediate hydromaghemite in the transformation of 2-line ferrihydrite into hematite and its paleoenvironmental implications. **Journal of Geophysical Research**, São Francisco, v.113, B01103, 2008.

LONG, X. et al. Grain growth and transformation of pedogenic magnetic particles in red Ferralsols. **Geophysical Research Letters**, Washington, v.42, p.5762–5770, 2015.

LOURENÇO, A.M.; ROCHA, F., GOMES, C.R. Relationships between magnetic parameters, chemical composition and clay minerals of topsoils near Coimbra, central Portugal. **Natural Hazards Earth Systems Science**, v.12, p.2545-2555, 2012.

LU, S.G.; ZHU, L., YU, J.Y. Mineral magnetic properties of Chinese paddy soils and its pedogenic implications. **Catena**, Amsterdã, v.93, p.9-17, 2012.

MARQUES Jr, J. et al. Magnetic susceptibility and diffuse reflectance spectroscopy to characterize the spatial variability of soil properties in a Brazilian Haplustalf. **Geoderma,** Amsterdã, v.219–220, p.63-71, 2014.

McBRATNEY, A.B. et al. An overview of pedometric techniques for use in soil survey. **Geoderma**, Amsterdã, v.97, p.293-327, 2000.

McKENZIE, N.J. et al. The role of terrain analysis in soil mapping. In: Wilson, J., Gallant, J. (Eds). **Terrain Analysis: Principles and Applications**, John Wiley & Sons Ltd.: New York, NY, USA, 2000; pp. 245–265.

MICHEL, F.M. et al. Ordered ferrimagnetic form of ferrihydrite reveals links among structure, composition, and magnetism. **Proceedings of the National Academy of Sciences**, Washington, v.107, n.7, p.2787–2792, 2010.

NEDELKOSKI, Z. et al. Origin of reduced magnetization and domain formation in small magnetite nanoparticles. **Scientific Reporter**, London, v.7, 45997, 2017.

NONAKA, A.G. et al. Kinetics of thermal transformation of synthetic Al-maghemites into Al hematites. **Revista Brasileira de Ciência do Solo**, Viçosa, v.7, n.41, e0160384, 2017.

PETERS, C.; DEKKERS, M.J. Selected room temperature magnetic parameters as a function of mineralogy, concentration and grain size. **Physics and Chemistry of the Earth**, Amsterdã, v.28, p.659–667, 2003.

RAMOS, P.V. et al. Magnetic susceptibility of soil to differentiate soil environments in southern Brazil. **Revista Brasileira de Ciência do Solo**, Viçosa, v.41, e0160189, 2017.

RESENDE, M.; ALLAN, J.; COEY, J.M.D. The magnetic soils of Brazil. Earth Planet. **Earth and Planetary Science Letters**, Amsterdã, v.78, p.322–326, 1986.

RESENDE, M., et al. **Magnetic properties of Brazilian Oxisoils**. In: International soil classification workshop, 8., 1988, Rio de Janeiro, RJ. Proceedings… Embrapa, Rio de Janeiro. p.78–108. Available in. http://library.wur.nl/isric/fulltext/isricu_i9278_001.pdf

RIBEIRO, B.T. Portable X-ray fluorescence (pXRF) applications in tropical Soil Science. **Ciência e Agrotecnologia**, Lavras, v.41 n.3, p.245-254, 2017

ROWNTREE, K.M.; van der WAAL, B.W.; PULLEY, S. Magnetic susceptibility as a simple tracer for fluvial sediment source ascription during storm events. **Journal of Environmental Management**, Amsterdã, v.194, p.54–62, 2017.

SANTANA, D.P. **Soil formation in a Toposequence os Oxisols from Patos de Minas Region, Minas Gerais States, Brazil**. PhD. Thesis. Purdue University, Lafayette, Indiana, 1984.

SILVA, A.R.; SOUZA JUNIOR, I.G.; COSTA, A.C.S. Suscetibilidade magnética do horizonte B de solos do Estado do Paraná. **Revista Brasileira de Ciência do Solo**, Viçosa, v.34, p.329-338, 2010.

SCHWERTMANN, U.; TAYLOR, R.M. **Iron oxides**. In: Dixon, J.B., Weed, S.B., (Eds). Minerals in soil environments. Soil Science Society of America, Madison, 1989. p.379–438.

SIQUEIRA, D.S. et al. Magnetic susceptibility for characterizing areas with different potentials for sugarcane production. **Pesquisa Agropecuária Brasileira**, Brasília, v.51, n.9, p.1349–1358, 2016.

SRIVASTAVA, P.; SANGODE, S.J.; TORRENT, J. Mineral magnetic and diffuse reflectance spectroscopy characteristics of the Deccan volcanic bole beds: Implications to genesis and transformations of iron oxides. **Geoderma**, Amsterdã, v.239–240, p.317–330, 2015.

THOMPSON, R., OLDFIELD, F. Environmental magnetism. Allen and Unwin, London, Allen & Unwin, 1986. 237 pp.

TORRENT, J.; BARRÓN, V.; LIU, Q. Magnetic enhancement is linked to and precedes hematite formation in aerobic soil. **Geophysical Research Letters**, v.33, L02401, 2006.

TORRENT, J.; BARRÓN, V. **Diffuse Reflectance Spectroscopy**. In: Ulery, A.L., Drees, L.R. (Eds.). Methods of Soil Analysis Part 5. Mineralogical Methods. Soil Science Society of America, SSSA Book Series n. 5, p. 367-387, 2008.

TORRENT, J.; LIU, Q.S.; BARRÓN, V. Magnetic minerals in Calcic Luvisols (Chromic) developed in a warm Mediterranean region of Spain: origin and paleoenvironmental significance. **Geoderma**, Amsterdã, v.154, p.465–472, 2010.

VODYANITSKII, Y.N. et al. Geochemistry of Magnetite and Maghemite in Soils in European Russia. **Geokhimiya**, Moscou, v.3, p.314–327, 2009.

WANG, X. et al. Rock magnetic investigation of loess deposits in the Eastern Qingling Mountains (central China) and its implications for the environment of early humans. **Geophysical Journal International**, v.207, p.889–900, 2016.

SEGUNDA PARTE – ARTIGOS

Artigo elaborado de acordo com as normas do periódico Applied Clay Science (versão submetida).

ARTIGO 1 - Maghemite quantification and magnetic signature of Brazilian soils with contrasting parent materials

Giovana Clarice Poggere[a*], Alberto Vasconcellos Inda[b], Vidal Barrón[c], Nestor Kämpf[b], Angela Dayana Barrera de Brito[d], Julierme Zimmer Barbosa[e], Nilton Curi[a]

[a]Department of Soils, Federal University of Lavras, 37200-000, Lavras, Minas Gerais, Brazil.

[b]Department of Soils, Federal University of Rio Grande do Sul, Av. Bento Gonçalves 7712, 91540-000, Porto Alegre, Rio Grande do Sul, Brazil.

[c]Department of Agronomy, University of Córdoba, Edificio C4, Campus de Rabanales, 14071 Córdoba, Spain.

[d]Department of Physics, Federal University of Lavras, 37200-000, Lavras, Minas Gerais, Brazil.

[e]Department of Soils, Federal University of Paraná, Rua dos Funcionários, 1540, Cabral, 80035-070, Curitiba, Brazil.

*Corresponding author: gi.poggere@gmail.com

Abstract

Maghemite (Mh) is a ferrimagnetic mineral that governs magnetism in the clay fraction, especially in well weathered soils from tropical and subtropical regions. In this work, we assessed various methods for Mh quantification in Brazilian soils with contrasting parent materials (itabirite, basalt, gabbro, tuffite, gneiss, and amphibolite). The methods based on H_2SO_4 dissolution were found to overestimate the Mh content with respect to the standard method based on X-ray diffraction (XRD). This was particularly so in samples from gneiss and amphibolite and in samples with ligth contents of poorly crystalline Fe oxides. Mh contents based on magnetic susceptibility measurements or on the XRD-Rietveld refinement were closer to those provided by the standard method. Mh was found to accumulate in well weathered soils and soils with a high Fe_2O_3 content; by exception, soils from tuffite, which had high Fe_2O_3 contents (~330 g kg^{-1}), exhibited low Mh levels (~5.5 g kg^{-1}). Irrespective of the parent material, Mh particles typically fall in a single domain; however, they can also acquire multidomain characteristics, probably as a result of isomorphic substitution and aggregation with hematite.

Keywords: soil magnetism; iron oxides; tropical soils; mafic rocks.

1. Introduction

Maghemite (Mh) is a secondary Fe oxide occurring mainly in tropical and subtropical soils (Schwertmann and Taylor, 1989; Bigham et al., 2002; Fink et al., 2016). Mh may be inherited from the parent material or formed by oxidation of lithogenic magnetite (Mt), among other

pathways (Curi and Franzmeier, 1984, Fabris et al., 1995; Cornell and Schwertmann, 2003). In Brazil, Mh accounts for up to 40% of Fe oxides in some soils from volcanic rocks (Costa et al., 1999) or up to 47% in soils from ferruginous dolomite rocks (Carvalho Filho et al., 2015).

Mh confers soils magnetic properties such as magnetic susceptibility (χ), coercivity (Hc) and remanent magnetization (Mr) (France and Oldfield, 2000; Long et al., 2015; Attoucheik et al., 2017). The magnetic properties of minerals are associated with the Fe content of their structure because this element contains incomplete 3*d* orbitals involved in electron transitions between orbitals that produce a magnetic moment (Thompson and Oldfield, 1986). Besides Mh, the clay fraction of soils contains other major Fe oxides such as hematite (Hm) and goethite (Gt), which have a zero magnetic moment and are thus antiferromagnetic (France and Oldfield, 2000; Long et al., 2015).

The oxides Gt and Hm, which are present more frequently in soils than is Mh, have traditionally been quantified by chemical analysis of dithionite–citrate–bicarbonate (DCB) extracts (Curi et al., 1987; Costa et al., 1999; Carvalho Filho et al., 2015) or with physical techniques such as diffuse reflectance (Barrón and Torrent, 1986; Torrent and Barrón, 2008; Marques Jr et al., 2014) or by X-ray diffraction (XRD). However, XRD peak areas for Mh are occasionally difficult to determine because of the usually small amounts present in the clay fraction and of its strongest diffraction peak (a 311 reflection at 2.51–2.53 Å) coinciding with the Hm peak (a 110 reflection at 2.51 Å). One alternative method for Mh quantification is selective dissolution of Mh with H_2SO_4, which was initially proposed by Schwertmann and Fetcher (1984) and later modified

by Costa et al. (1999); others are based on magnetic susceptibility (Costa, 1999) or on application of Rietveld refinement to XRD data (Nonaka et al., 2017).

Mh content and magnetic susceptibility have been used in environmental studies on pedogenesis (Long et al., 2015) and in the characterization of paleoenvironments (Torrent et al., 2010; Wang et al., 2016), but also in soil mapping (Silva et al., 2016), soil fertility (Marques Jr. et al., 2014; Siqueira et al., 2016), soil erosion (Rowntree et al., 2017) and even atmospheric pollution research (Grimley et al., 2017). However, different Mh quantification methods have led also to different or even controversial results that have precluded comparison. In this work, different methods for quantifying Mh in soils and elucidated the properties of Mh from contrasting parent materials in Brazilian soils were assessed.

2. Material and methods

2.1. Samples and overall characterization

Samples from the A (0–20 cm) or B (80–100 cm) horizons of 18 soils were collected from different sites in Brazil (Table 1). The soils (Tables 1 and 2) spanned a wide range of Fe_2O_3 contents from low (gneiss and amphibolite), to medium or high (gabbro, tuffite, and basalt), and included iron-derived soils (itabirite) containing up to 71% Fe_2O_3, all measured by sulfuric digestion (Carvalho Filho et al., 2015).

Table 1. Localization of the Brazilian soils with their respective horizons, parent materials and climate.

Sample	Soil Taxonomy[(a)]	Hor.	Parent material	Localization	C[(b)]	T[(c)]	R[(d)]
						°C	mm
1-OX	Rhodic Hapludox	B	Itabirite	N.Lima/MG	Cwb	18	1558
2-OX	Rhodic Hapludox	B	Basalt	Cascavel/PR	Cfa	19	1875
3-OX	Rhodic Hapludox	A	Basalt	Sananduva/RS	Cfb	17	1900
4-OX	Rhodic Hapludox	A	Basalt	L.Vermelha/RS	Cfb	16	1939
5-MO	Typic Hapludoll	A	Basalt	Sta. C. do Sul /RS	Cfa	18	1924
6-OX	Rhodic Hapludox	B	Basalt	V.Bonita/SC	Cfb	16	1760
7-OX	Rhodic Hapludox	B	Basalt	A.Doce/SC	Cfb	15	1724
8-OX	Rhodic Hapludox	B	Gabbro	Lavas/MG			
9-OX	Rhodic Hapludox	B	Gabbro	Lavras/MG	Cwb	19	1621
10-EN	Typic Hapludents	A	Gabbro	Lavras/MG			
11-EN	Typic Hapludents	A	Gabbro	Lavras/MG			
12-OX	Rhodic Hapludox	B	Tuffite	P.Minas/MG			
13-MO	Typic Hapludoll	B	Tuffite	P.Minas/MG	Cwa	20	1448
14-IN	Typic Dystrudepts	B	Tuffite	P. Minas/MG			
15-OX	Rhodic Hapludox	B	Gneiss	Nazareno/MG	Cwb	18	1689
16-UL	Rhodic Hapludult	B	Gneiss	Lavras/MG	Cwb	19	1621
17-OX	Rhodic Hapludox	B	Amphi-bolite	Miraí/MG	Cwa	20	1322
18-MO	Typic Hapludoll	B	Amphi-bolite	Italva/RJ	Aw	22	1163

[(a)] Soil Survey Staff (2014); [(b)] Climate; [(c)] Mean annual temperature; [(d)] Cumulative annual rainfall.

Soil samples were passed through 2 mm sieves (air-dried fine earth, ADFE) and subjected to the following determinations: grain-size fractionation with the modified pipette method (Baver et al., 1972; Gee and Bauder, 1986); total organic carbon (TOC) by oxidation with potassium dichromate in sulfuric acid (Donagema et al., 2011); and oxide content by sulfuric digestion (Donagema et al., 2011). The ratios between Fe, Al and Si oxides were used to calculate the weathering indices *Ki* and *Kr* (Table 2).

Table 2. Chemical and physical properties of the soil samples.

Sample[(a)]	SiO_2	Al_2O_3	Fe_2O_3	TiO_2	P_2O_5	Ki[(b)]	Kr[(c)]	Al_2O_3/ Fe_2O_3	TOC[(d)]	Clay	Silt	Sand
	---------- % ----------								%	---- g kg^{-1} ---		
1-OX	1.9	15.1	64.8	3.1	0.09	0.22	0.06	0.37	1.41	540	150	310
2-OX	10.1	28.7	25.4	5.2	0.95	0.60	0.39	1.78	0.55	740	170	90
3-OX	22.1	18.8	21.9	5.6	0.18	2.00	1.14	1.35	2.04	590	360	500
4-OX	21.7	16.5	27.1	7.0	0.19	2.24	1.09	0.95	2.20	600	310	90
5-MO	21.5	13.9	18.3	4.2	0.14	2.63	1.43	1.20	1.88	300	370	330
6-OX	23.7	22.9	21.1	4.5	0.15	1.78	1.12	1.71	0.14	810	150	40
7-OX	26.3	22.0	22.8	2.9	0.15	2.06	1.24	1.51	0.67	670	250	80
8-OX	12.3	28.2	23.2	2.0	0.06	0.75	0.49	1.91	0.55	680	170	150
9-OX	13.6	15.5	13.0	1.5	0.12	1.51	1.07	2.50	1.49	460	180	360
10-EN	13.1	19.5	15.5	2.3	0.09	1.15	0.76	1.98	3.10	400	260	340
11-EN	21.7	22.7	14.3	2.0	0.07	1.64	1.17	2.49	1.20	480	200	320
12-OX	18.6	13.1	36.0	11.1	0.73	2.45	0.89	0.57	1.07	450	400	150
13-MO	15.2	10.7	32.8	11.1	1.37	2.44	0.82	0.51	0.67	460	280	260
14-IN	23.2	11.1	31.4	13.1	1.68	3.59	1.28	0.56	0.19	480	300	220
15-OX	11.8	32.6	16.4	2.8	0.07	0.62	0.47	3.11	1.07	660	220	120
16-UL	22.0	23.3	11.3	1.3	0.08	1.63	1.30	4.05	0.08	540	140	320
17-OX	24.8	17.5	18.9	3.1	0.12	2.43	1.56	1.79	0.02	430	320	250

18-MO	24.5	18.6	11.5	2.6	0.09	2.26	1.62	2.55	0.08	480	230	290

[(a)] sample 1: itabirite; samples 2 to 7: basalt; samples 8 to 11: gabbro; sample 12 to 14: tuffite; samples 15 and 16: gneiss; samples 17 and 18: amphibolite; [(b)] Ki = 1.7 × SiO_2/Al_2O_3; [(c)] Kr = 1.7 × SiO_2 / [Al_2O_3 + (0.64 × Fe_2O_3)]; [(d)] TOC = total organic carbon.

2.2. Fe and Al dithionite and oxalate

After grain-size fractionation according to Jackson (1979), the clay fraction was subjected in triplicate to four successive extractions with dithionite–citrate–bicarbonate at 80 °C for Fe in pedogenic Fe oxides (Fed) (Mehra and Jackson, 1960). Iron in poorly crystalline Fe oxides (basically ferrihydrite) was determined with 0.2 mol L^{-1} ammonium oxalate at pH 3.0 in the dark (Feo) (McKeague and Day, 1966). The resulting suspensions were centrifuged at 3500 rpm for 10 min, and Fe and Al quantified by inductively coupled plasma optical emission spectrometry (ICP-OES).

2.3. Iron oxides

The concentrated Fe oxides fraction was obtained by boiling the samples of clay, extracted from the soils in 5 mol NaOH L^{-1} (Kämpf and Shwertmann, 1982) to dissolve kaolinite and gibbsite, using 0.2 mol L^{-1} sodium metasilicate pentahydrate in the extractant to avoid dissolution and recrystallization of poorly crystalline, highly Al-substituted goethite (Kämpf and Schwertmann, 1982). After boiling in a sand bath for 1.5 h, the suspensions were centrifuged at 3500 rpm for 10 min and the supernatants discarded. Potentially formed artificial sodalite [$Na_4Al_3Si_3O_{12}$ (OH)] was removed by washing the residue with 90 mL of 0.5 mol HCl L^{-1} twice (Norrish and Taylor, 1961). Also, excess salts in

the final extract were removed by washing with 80 mL of 0.5 mol $(NH_4)_2CO_3$ L^{-1} twice and then with 80 mL of deionized water. The residue was oven dried at 60 °C and gently milled for further analysis.

2.4. Maghemite quantification

X-ray diffraction and Rietveld refinement

The Fe oxide concentrates were analyzed by XRD (powder method) on a Bruker D8 Discover A25 diffractometer using an Ni filter and CuKα radiation (ƛ = 1.541838 Å). The XRD, furnished with a vertical goniometer, was operated at 60 mA and 50 kV, using a goniometer angular velocity of 0.4 º2θ min^{-1} and an amplitude of 10 to 67 º2θ.

Initially, XRD was used to determine the proportions of Gt, Hm and Mh in the Fe oxide concentrate from the area of 110 reflection for Gt (Eq. 1), 012 for Hm (Eq. 2) (Schwertmann and Lathan, 1986) and 220 for Mh (Eq. 3) (Costa et al., 1999) (see Table S1 in Supplementary Material). The peak areas for Hm and Mh were multiplied by a factor of 3.5 because they amounted to about 35% of that for the highest peak. The total area was the combined area of Gt110, Hm012 × 3.5 and Mh220 × 3.5.

$$Gt\% = \left(\frac{area\ d_{110}}{total\ area}\right) \times 100 \quad (1)$$

$$Hm\% = \left(\frac{area\ d_{012} \times 3.5}{total\ area}\right) \times 100 \quad (2)$$

$$Mh\% = \left(\frac{area\ d_{220} \times 3.5}{total\ area}\right) \times 100 \quad (3)$$

The proportions of Gt, Hm and Mh were also determined by applying the Rietveld refinement (Mh-Rietveld) to the experimental XRD patterns (Young et al., 1995), using the software PowderCell v. 2.4 (see Table S1). The files with the crystal structure of the oxides were obtained from the American Mineralogist database (2017): amcsd 0002226 for Gt, amcsd 0000143 for Hm; amcsd 0020516 for Hm and amcsd 0019093 for An. The refinement included a polynomial function for the baseline; peak fitting with the pseudo-Voigt model; and using the Bragg angle parameters U, V and W to calculate the width at half height as WHH = (U tan 2θ + V tan θ + W)$^{1/2}$

The goodness of the refinement was assessed in terms of R_{exp} and the goodness of fit (GOF) (Young, 1995). Refinements for soil data are deemed good if $R_{exp} < 20$ and GOF < 5. Refinement was acceptable for all samples (R_{exp} ranged from 5 to 16 and GOF from 1 to 5; Table S2, Fig. S1).

With both methods, the Mh content of the clay fraction was calculated by considering the ratios A = Hm%/Mh% and B = Gt%/Mh% as calculated from the XRD patterns, as well as the difference Fed – Feo (Eq. 4).

$$Mh = \frac{Fe_d - Fe_o}{\frac{A}{1.43} + \frac{B}{1.59} + 0.699} \quad (4)$$

The extent of Al substitution in the Mh structure was estimated as Al (mol mol^{-1}) = [0.8343 – a_0]/2.22 × 10^{-4} (Schwertmann and Fechter, 1984), where a_0, the unit cell parameter for Mh, normal to 220 reflection plane, was determined with the Rietveld refinement. Crystal size (CS)

was calculated from the Scherrer equation (Klug and Alexander, 1974) (Eq. 5), where *K* is a constant (0.9); ƛ is the wavelength of the CuKα radiation; 57.3 a conversion factor for angles to radians and θ the Bragg angle of the measured diffraction line (hkl).

$$CS_{\perp(hkl)} = \frac{K\ x\ ƛ \times 57.3}{WHH_{(hkl)} \times \cos\theta} \quad (5)$$

Magnetic susceptibility

The third method used to estimate the Mh content of the clay fraction (Mh-χlf) was based on a calibration curve of magnetic susceptibility at a low frequency (χlf) for a mixture of synthetic Hm, Gt and Mh. The χlf value thus calculated for Mh was 486×10^{-6} m^3 kg^{-1} and the equation obtained was %Mh = 0.46 + 0.2 χlf (Table S3).

Details on the synthetic Hm and Gt can be found in Barrón et al. (1998) (sample A3) and Torrent et al. (1990) (sample 71), respectively. Mh was synthesized according to Taylor et al. (1987) by mixing Fe (II) [$FeCl_2 \cdot 4H_2O$] and Fe (III) [$Fe(NO_3)_3 \cdot 9H_2O$] in a mole ratio of 10:1 in deionized water and heating the solution at 90 °C for 1 h, after which 0.5 mol NaOH L^{-1} was added to pH 12.5 in order to precipitate Fe as Mt. The precipitate was washed with deionized water to an electrical conductivity below 20 μS cm^{-1} g^{-1} and then heated at 250 °C for 5 h to oxidize Mt to Mh. The crystal size of Mh and parameter a_0 for its unit cell as calculated from XRD data and the Rietveld refinement were 28 and 0.834 nm, respectively.

By way of alternative to the calibration curve method, Mh was also quantified from the direct relationship with χlf for the clay samples (Mh-χlf*), using χlf ($\times 10^{-6}$ m^3 kg^{-1}) as the Mh concentration (in g kg^{-1}).

Magnetic susceptibility (χ) was measured at 0.47 kHz (χlf) and 4.7 kHz (χhf), using a Bartington MS2B susceptibility meter. The absolute frequency-dependent susceptibility (χfd) was calculated as $\chi fd = \chi lf - \chi hf$, whereas the percent frequency-dependent susceptibility (% χfd) was calculated as $\% \chi fd = (\chi fd/\chi lf) \times 100$ (Dearing, 1994). These parameters provide information about pedogenic magnetic particles and the proportion of superparamagnetic particles (SP).

Selective dissolution with H_2SO_4

The fourth method used to quantify Mh was based on the selective dissolution of Mh according to Schwertmann and Fetcher (1984) as modified by Costa et al. (1999). The clay fraction from the soil samples was mixed with 1.8 mol H_2SO_4 L^{-1} and heated at 75 °C for 120 min in triplicate. The resulting suspensions were centrifuged at 3500 rpm for 5 min and the supernatants collected to determine the Fe content by ICP-OES.

The dissolution time was optimized with provision for the varied nature of the parent material. For this purpose, the clay samples were subjected to the same conditions as in the previous tests for variable times (5, 10, 20, 30, 45, 60, 90, 120, 240, 360 and 450 min) before measuring χlf in the residue. The time needed for complete dissolution of Mh was calculated from the dissolution curve for each soil at the point where χlf decreased to less than 10% of the initial value (Table S4).

The Mh content was determined from the amount of Fe extracted after 120 min (Mh-H_2SO_4) and from the applicable dissolution time (Mh-H_2SO_4*), which was multiplied by a factor of 1.43 to calculate the amount of Fe_2O_3.

2.5. Magnetic hysteresis loops

Clay hysteresis loops were obtained by using a LakeShore 7404 vibrating sample magnetometer. The clay fraction of each soil was placed in gelatin capsules and subjected to a magnetic field of ± 1.2 Tesla (T) at a scanning rate of 5 Oe/s. The hysteresis cycles of all samples were measured at 298 K.

The hysteresis loops allowed four major variable for magnetic minerals to be determined, namely: Saturation magnetization (Ms), defined as the maximum possible magnetization of a material upon application of an external field. Magnetic saturation is reached when all magnetic moments are aligned with the applied magnetic field; Remanent saturation magnetization (Mrs), which is residual magnetization remaining in the material when the applied magnetic field is zero; Coercivity (Hc), defined as the applied field for which magnetization is zero; Remaining coercivity (Hcr), which is the field needed for magnetization to fall to zero after the applied field is removed. These variable were used to calculate the ratio (Mr/Ms)/(Hcr/Hc) and the results to construct a Day graph (Day et al., 1977) as modified by Dunlop et al. (2002).

3. Results

3.1. Fe contents

As can be seen from Table 3, Fed contents differed markedly among samples as a consequence of the widely variable degree of weathering and parent material of the soils. The lowest Fed, Gt, and Hm contents were found in the less developed soils from each parent material (e.g., samples 5-MO, 10-EN, 14-IN and 16-UL). The Feo/Fed ratio, which was lower than 0.04 for most samples, indicates a prevalence of crystalline Fe oxide forms, which is typical of well weathered soils such as Oxisols. Feo/Fed ratios above 0.04 were found for the less developed soils (Entisols, Inceptisols and Mollisols), especially in tuffite-containing samples. Also, the Fed/Fes ratio was lower in the less developed soils (Table 3), indicating a smaller contribution of pedogenic Fe forms to total Fe after sulfuric digestion (Table 2) in there soils.

3.2. Methods for maghemite quantification

Mh contents were compared among methods by using XRD as standard by virtue of its wide use to quantify minerals and, particularly, Mh in soils (Curi and Franzmeier, 1987; Costa et al., 1999; Carvalho Filho et al., 2015; Nonaka et al., 2017). The Mh content estimated with the Rietveld refinement (Mh-Rietveld) was similar and highly correlated with XRD values (Mh-XRD) (Table 4; Fig. 1), and so were the Gt and Hm contents estimated with the refinement (R^2 0.94 and 0.98, respectively; angular coefficient 1.04 and 1.01, respectively; $p < 0.0001$) (see Fig. S2). The Mh content obtained by using the calibration curve method with synthetic Mh (Mh-χlf) was overestimated by a factor of up

to 17; on the other hand, those directly obtained from χlf values (Mh-χlf*) were closer to the Mh-XRD contents (Table 4; Fig. 1).

Table 3. Fe in pedogenic iron oxides (Fed) and its relationship with Fe in poorly crystalline iron oxides (Feo/Fed) and Fe of sulfuric digestion (Fed/Fes), goethite (Gt) and hematite (Hm) contents.

Sample	Parent material	Fed	Feo/Fed	Fed/Fes	Gt[(a)]	Hm[(a)]
		g kg^{-1}			--------g kg^{-1}------	
1-OX	Itabirite	324	0.02	0.71	138	203
2-OX	Basalt	149	0.02	0.84	21	153
3-OX		111	0.04	0.72	22	115
4-OX		119	0.03	0.63	90	76
5-MO		70	0.08	0.55	66	33
6-OX		116	0.02	0.79	141	34
7-OX		100	0.03	0.62	138	14
8-OX	Gabbro	148	0.02	0.91	68	131
9-OX		90	0.04	0.98	58	71
10-EN		69	0.05	0.64	60	38
11-EN		67	0.05	0.67	42	49
12-OX	Tuffite	184	0.02	0.73	87	171
13-MO		123	0.08	0.53	126	47
14-IN		88	0.14	0.40	91	31
15-OX	Gneiss	105	0.01	0.91	112	48
16-UL		68	0.02	0.86	65	36
17-OX	Amphibolite	132	0.03	0.99	88	104
18-MO		64	0.05	0.80	47	46

[(a)] determined by XRD and Fed; nd: not determined.

Table 4. Maghemite (Mh) determined by different methods, parameter of Mh unit cell (*a*), Al-for-Fe isomorphic substitution (IS) in the Mh and crystal size of Mh (CS).

Sample	Parent material	Mh XRD	Mh Rietveld	Mh χlf	Mh χlf*	Mh H_2SO_4	Mh H_2SO_4*	*a*	IS	CS
		---------- g kg^{-1} ----------						nm	mol mol^{-1}	nm
1-OX	Itabirite	130	100	307	147	230	230	0.833	0.08	28
2-OX	Basalt	38	23	118	55	125	125	0.832	0.12	37
3-OX		20	20	65	30	111	84	0.831	0.13	27
4-OX		9.1	5.6	31	13	101	72	0.831	0.16	19
5-MO		2.2	4.2	17	6.0	71	65	0.831	0.16	16
6-OX		2.0	1.5	10	2.8	73	36	0.826	0.28	34
7-OX		2.2	3.2	7.1	2.5	81	10	0.831	0.17	26
8-OX	Gabbro	17	15	67	31	99	79	0.831	0.13	44
9-OX		2.2	1.5	20	7.3	61	32	0.831	0.15	36
10-EN		3.5	2.6	16	5.4	121	74	0.829	0.25	23
11-EN		5.7	6.2	15	5.6	38	23	0.829	0.25	27
12-OX	Tuffite	10	16	37	16	150	98	0.828	0.29	13
13-MO		5.2	2.6	25	10	120	74	0.829	0.25	25
14-IN		1.5	0.7	9.8	2.5	101	37	0.827	0.36	45
15-OX	Gneiss	0.0	0.0	8.1	1.7	46	4.1	nd	nd	nd
16-UL		0.7	0.5	8.0	1.6	27	2.7	nd	nd	nd
17-OX	Amphibolite	2.2	1.0	5.3	1.2	117	14	nd	nd	nd
18-MO		0.3	0.5	5.2	1.1	71	14	nd	nd	nd

nd: not determination.

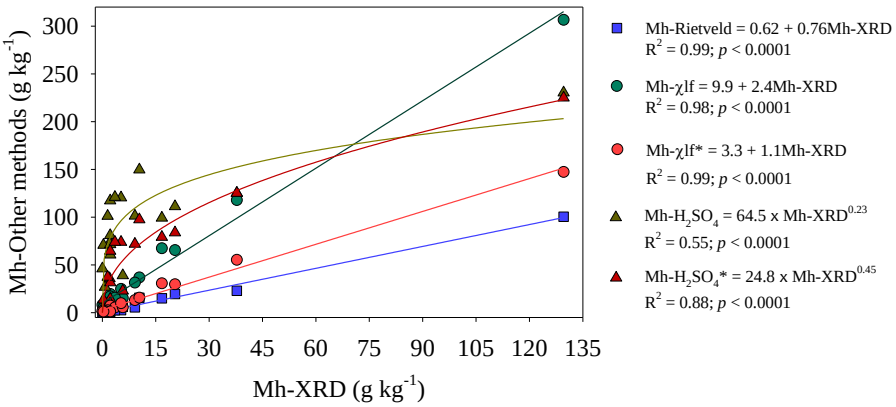

Fig. 1. Regressions among the Mh contents as determined by XRD spectroscopy (Mh-XRD) and with the Rietveld refinement (Mh-Rietveld), χlf from a calibration curve with synthetic Mh (Mh-χlf), directly from χlf (Mh-χlf*), by sulfuric dissolution for 120 min (Mh-H_2SO_4) and by sulfuric dissolution for a variable time and monitoring of χlf (Mh-H_2SO_4*).

The largest differences in the Mh methods were those of H_2SO_4 dissolution for 120 min (Mh-H_2SO_4), mainly in the samples with Mh-XRD contents below 5 g kg^{-1} and derived from gneiss and amphibolite (38–237 times higher than with the Mh-XRD method; Table 4). Some clay samples exhibited smaller peaks for Hm and, especially, Gt (e.g., 1-OX), whereas others showed little difference (e.g., 2-OX; Fig. 2). This result suggests that dissolving these oxides in H_2SO_4 may lead to overestimated Mh contents. Although sulfuric dissolution with χlf monitoring (Mh-H_2SO_4*) also overestimated Mh contents, the largest differences (23–68 times relative to Mh-XRD) were observed in samples with increased contents of Fe in poorly crystalline oxides (5-MO, 13-MO and 14-IN; Table 4).

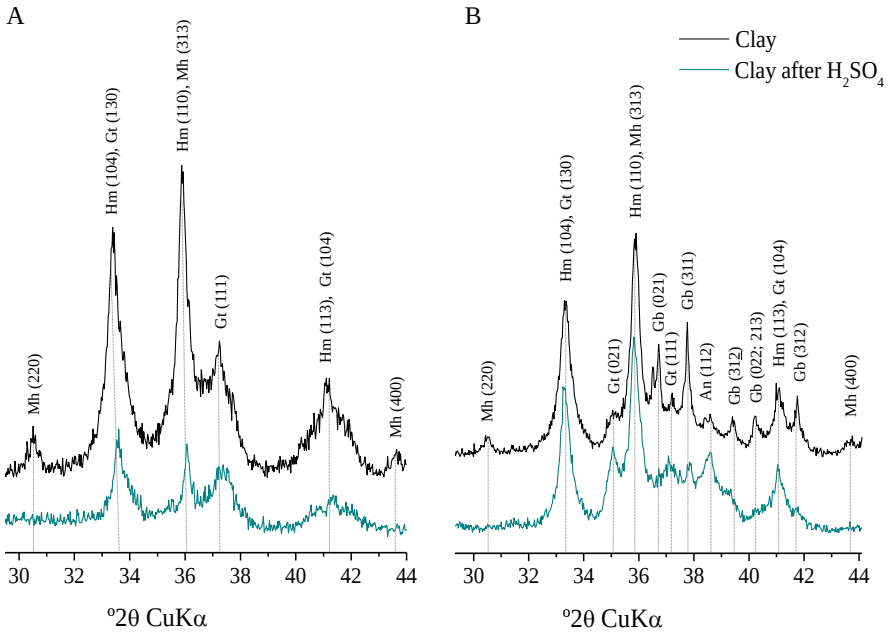

Fig. 2. X-ray diffraction patterns for clay samples 1-LV (A) and 2-LV (B) before and after dissolution with H_2SO_4 for 120 min.

3.2. Magnetic signature

As can be seen from Fig. 3, hysteresis loops for clay samples with contrasting parent materials exposed differences in magnetic profile in individual samples and also in samples sharing the same parent material. Although, apparently, the parent material stratified samples with contrasting magnetic profiles, soil types dictated the magnetic profile for samples with the same parent material under similar environmental conditions, which reflected in the hysteresis loops for the gabbro and tuffite soil samples.

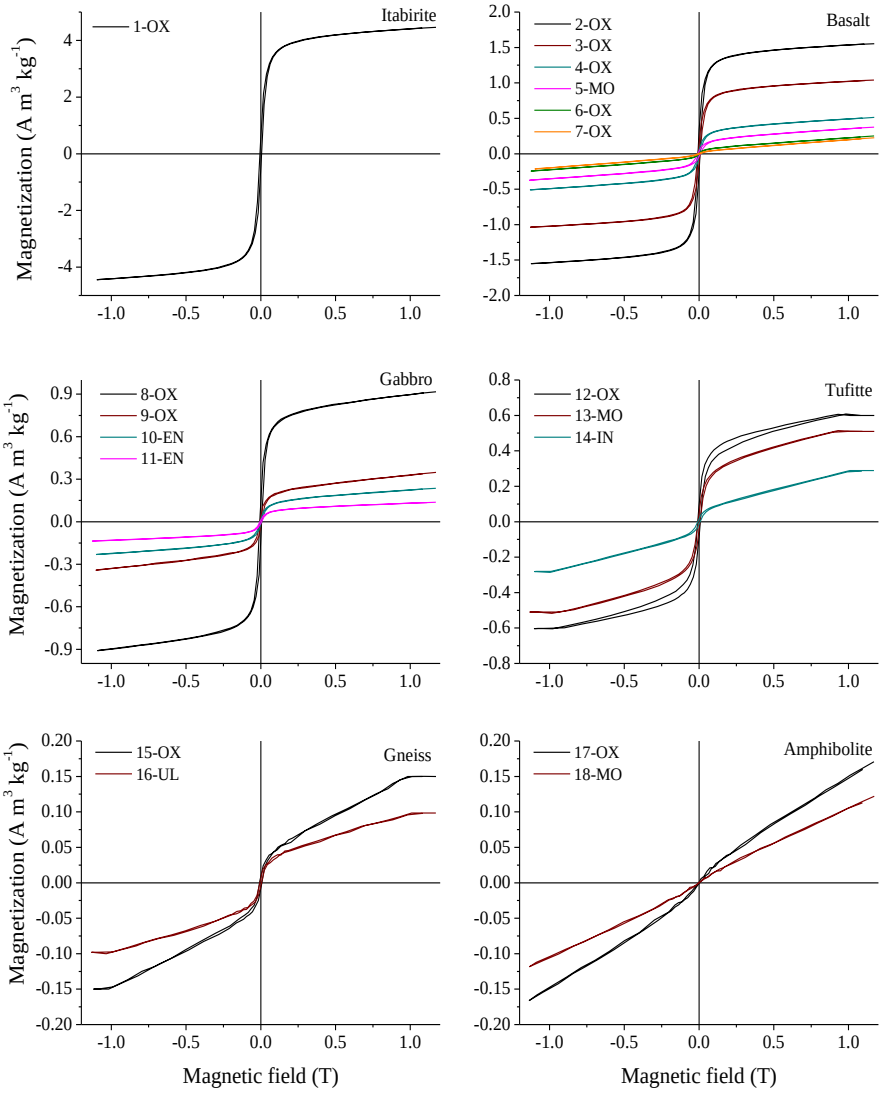

Fig. 3. Hysteresis loops for soil clay according to parent material.

The clay samples of itabirite, gabbro and basalt reached saturation magnetization (Ms) upon application of a 1.2 T magnetic field, with 452 $\times 10^{-2}$ A m^2 kg^{-1} for itabirite soil, (22 –156) $\times 10^{-2}$ A m^2 kg^{-1} for basalt

soils and (15–92) × 10^{-2} A m^2 kg^{-1} for gabbro soils. The Ms estimated for the clay samples of tuffite and gneiss as calculated by eliminating paramagnetic contribution were (29–60) × 10^{-2} and (10–15) × 10^{-2} A m^2 kg^{-1}, respectively (Table 5). The correlations between Ms and Mh contents (r = 0.99, p < 0.05), Ms and *Ki* (r = –0.51, p < 0.05), and Ms and *Kr* (r = –0.70, p < 0.05) (Table S5) indicate that increased Mh contents led to also increased Ms values, and also that soils with increased clay mineral contents (increased *Ki* and *Kr* values) required higher magnetic fields to reach saturation.

Irrespective of parent material, the (Mr/Ms)/(Hcr/Hc) ratio was consistent with the presence of Mh particles consisting of single-domain (SD) and multidomain (MD) grains (Fig. 4). On the other hand, the %χfd values above 10% (Table 5) indicate a prevalence of SD particles and/or superparamagnetic particles (SP) (Dearing et al., 1996). Also, as can be seen in Table 4, the size of Mn crystallites ranged from 13 to 54 nm, which suggests that the samples consisted mainly of SD particles.

Table 5. Magnetic susceptibility at low frequency (χlf) and relative to Mh (χMh), dependent frequency (χfd), percent of frequency dependent (%χfd) and magnetic parameters obtained by the hysteresis loops (Ms, Mr, Hc, Hcr).

Sample	Parent material	χlf[(a)]	χfd[(a)]	%χfd	χMh[(b)]	Ms[(c)]	Mr[(c)]	Hc[(d)]	Hcr[(d)]
1-OX	Itabirite	147.3	32	11	682	452	58.5	6.1	23.5
2-OX	Basalt	55.3	17.2	16	692	156	30.3	7.1	21.6
3-OX		29.7	8.2	14	712	105	14.6	7.0	26.6
4-OX		13.1	3.5	14	743	53	5.4	5.9	21.3
5-MO		6.0	1.3	11	940	38	3.7	8.7	23.1
6-OX		2.8	0.8	14	730	26	0.9	3.9	17.4
7-OX		2.5	0.3	13	310	22	0.6	6.7	19.5
8-OX	Gabbro	30.7	9.6	17	1047	92	12.9	6.7	25.0
9-OX		7.3	2.2	16	1368	35	3.2	5.5	27.2
10-EN		5.4	1.1	11	566	24	1.5	4.8	24.0
11-EN		5.6	1.3	13	331	15	1.0	5.8	21.4
12-OX	Tuffite	15.7	3.9	12	882	60	9.3	8.7	21.5
13-MO		9.9	2.3	12	747	51	4.4	7.0	25.3
14-IN		2.5	0.7	13	464	29	1.5	8.5	25.0
15-OX	Gneiss	1.7	0.5	14	nd	15	0.8	7.8	21.7
16-UL		1.6	0.5	15	nd	10	0.6	6.7	17.1
17-OX	Amphibolite	1.2	0	0	nd	nd	nd	nd	nd
18-MO		1.1	0	3	nd	nd	nd	nd	nd

[a] $\times 10^{-6}$ m^3 kg^{-1};[b] The χ of Mh was determined by χMh = (χlf × 100) / Mh%, being the Mh percent (estimated by XRD) and the χlf ($\times 10^{-6}$ m^3 kg^{-1}) determined in Fe oxides concentrate; [c] saturation magnetization (Ms), remanent magnetization (Mr), $\times 10^{-2}$ A m^2 kg^{-1}; [d] magnetic coercivity (Hc), remanent magnetic coercivity (Hcr) $\times 10^{-3}$ T; nd: not determined.

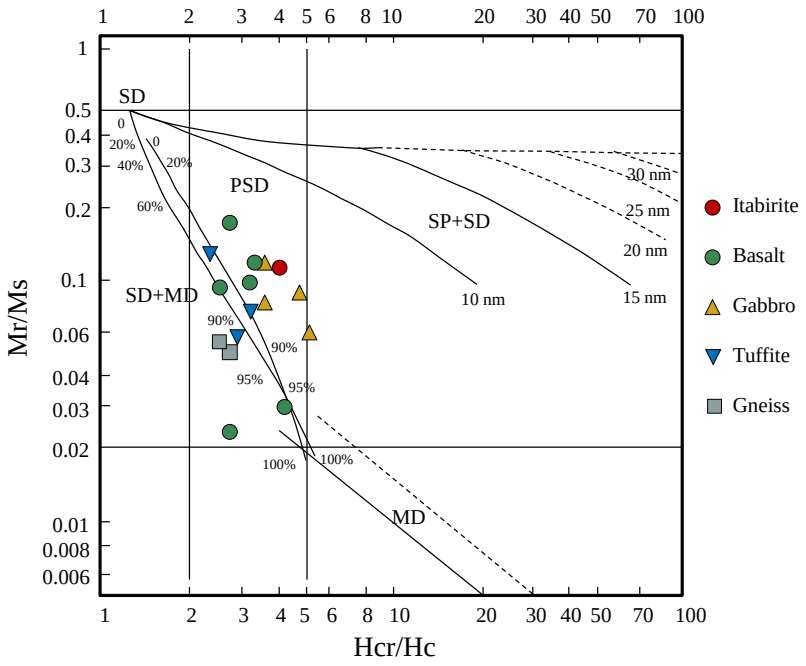

Fig. 4. Day plot for soil clay from contrasting parent materials showing the distribution of magnetic particles: SD single-domain, PSD pseudo single-domain; MD multidomain and SP superparamagnetic.

3.3. Relationship between Mh and soil properties

The increase in Mh and Hm contents was followed by a decrease in Gt contents (Figs 5A and 5B). The Mh-XRD results exhibited positive correlations ($p < 0.05$) with Ms ($r = 0.99$), Mr ($r = 0.97$) and Fe_2O_3 determined by sulfuric digestion ($r = 0.83$) (Table S5), which indicates that the soils with the highest Fe contents were also those containing the greatest amounts of Mh. On other hand, the Mh-XRD content exhibited negative correlations ($p < 0.05$) with SiO_2 as measured by sulfuric digestion ($r = –0.70$), *Ki* ($r = –0.54$) and *Kr* ($r = –0.67$) (Table S5), which

indicates that Mh tended to accumulate in the more strongly weathered soils. The degree of Al-for-Fe isomorphic substitution in Mh was negatively correlated with χlf (r = –0.59, p < 0.05) (Table S5).

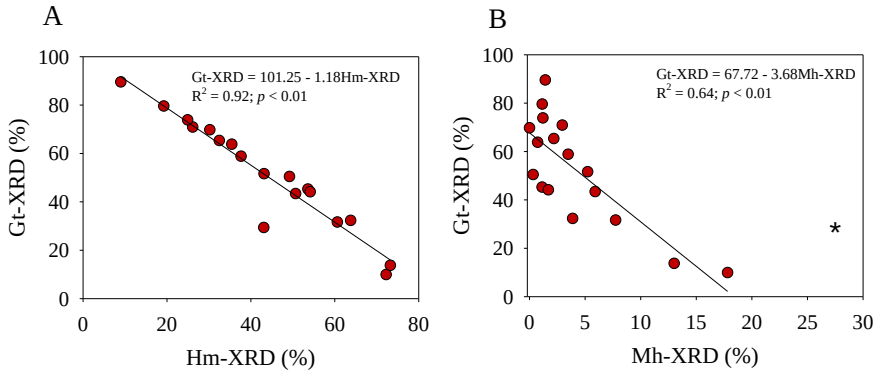

Fig. 5. Regression curves between the proportions of Gt and Hm (A), and Gt and Mh (B). The asterisk denotes the clay in the itabirite soil, which was excluded from the analysis.

4. Discussion

4.1. Mh quantification methods

As can be seen from Table 4, the different Mh quantification methods gave widely variable results (e.g., 100–307 g kg^{-1} for sample 1-OX). These results testify to the need to standardize existing methods for reliability with a view to characterizing magnetic soils and their implications.

The XRD method, which is widely used to identify and quantify soil minerals, is subject to some limitations for Mh, namely: (i) the strongest Mh peak (d311) falls in the same position as the Hm peak with a

75% relative intensity (d110), which results in masking the main Mh peak because Hm is usually present in greater amounts in Fe oxide concentrates; (ii) the intensity of the second strongest Mh peak (a 220 reflection), typically overlap-free, is only 35% that of the 311 reflection, which makes detection difficult in samples with low Mh contents (Carvalho Filho et al., 2015); and (iii) crystal defects due to isomorphic substitution or a small crystal size also diminish the intensity of XRD peaks (Carvalho Filho et al., 2015). The close relationship between Mh-Rietveld and Mh-XRD data (R^2 = 0.99, p < 0.0001), suggests that the Rietveld refinement may be an effective choice for estimating Mh in soils. This refinement has the advantage that it allows the position and intensities of mineral peaks to be determined even in the presence of overlap; also, it allows one to calculate cell parameters and crystal size, among other crystallographic variables.

The increased Mh-H_2SO_4 contents compared with other methods indicate that sulfuric dissolution is of limited use with clay from different parent materials. Also, ensuring acceptable precision with this method requires using Fe oxide concentrates, which increases the difficulty of, or even precludes, analyzing samples with low oxide contents. It should be noted that the principle behind H_2SO_4 dissolution is the stability of Fe oxides against an acid solution. Based on the formation sequence Mt → Mh → Hm, maghemite is assumed to be metastable relative to Hm (Fabris et al., 1997; Torrent et al., 2006), so it will be dissolved preferentially, but not exclusively (Schwertmann and Fetcher, 1984) (Fig. 2), and cause Mh to be overestimated.

The sulfuric dissolution method, even if modified by Schwertmann and Fetcher (1984) and supplemented with χlf monitoring, also overestimated Mh contents, mainly in soils with increased Feo/Fed ratio (e.g., tuffite soils). By analyzing Fe oxide concentrates with basaltic andesite, quartz latite and rhyodacite as parent materials, Costa et al. (1999) found a 1.8 mol H_2SO_4 L^{-1} solution to result in complete selective dissolution of Mh within 120 min. Also, Inda et al. (2013) used a treatment time of 45 min on a Rhodic Paleudult sample and found an Mh content of 11.5 g kg^{-1}, which was four times higher than the value estimated from χlf (1.8×10^{-6} m^3 kg^{-1} as calculated for an Mh sample with χlf = 600×10^{-6} m^3 kg^{-1}). Camargo et al. (2014) used H_2SO_4 concentrations from 0.8 to 1.8 mol L^{-1} and contact times from 45 to 120 min to dissolve Oxisols from altered sandstones and found the optimum acid concentration and time to be 1.3 mol L^{-1} and 120 min, respectively. These results show that the H_2SO_4 concentration and time to be used depend on the nature of the sample and, especially, on its Fe and Mh contents, which precludes recommending a universal time–concentration pair for all soils.

Quantification in terms of χlf for synthetic Mh (486×10^{-6} m^3 kg^{-1}), Mh-χlf, also led to overestimated Mh contents (Fig. 1). The greatest difficulty with this method is selecting the χlf value for Mh best representing the body of clay samples. Reported χlf values for Mh ranged from 283 to 845×10^{-6} m^3 kg^{-1} (Peters and Dekkers, 2003) as compared to 636–910×10^{-6} m^3 kg^{-1} for Brazilian soils (Resende et al., 1988; Costa et al., 1999) and 310–1368×10^{-6} m^3 kg^{-1} for our soils. Peters and Dekkers (2003) reported a χlf value 0.97 10^{-6} m^3 kg^{-1} for Hm and of 1.17

$\times 10^{-6}$ m^3 kg^{-1} for Gt, which confirms that Mh is virtually the only Fe oxide with a substantial χlf value in the clay fraction.

However, the Mh contents estimated from χlf for clays (Mh-χlf*) were closer to Mh-XRD contents (Mh-χlf* = 3.33 + 1.1 Mh-XRD; R^2 = 0.98; Fig. 1). This result is consistent with those of Costa et al. (1999), whose regression equation for soils from basaltic andesite, quartz latite and rhyodacite (viz., χlf = 6.6 + 0.90 Mh-XRD; R^2 = 0.89; with χlf $\times 10^{-6}$ m^3 kg^{-1}) was similar to that to obtained here for soils from itabirite, basalt, gabbro, tuffite, gneiss and amphibolite. Therefore, Mh contents can be accurately estimated from χlf even in soils differing in parent material and degree of weathering. These further results support the advantages previously noted by Resende et al. (1988) and Costa et al. (1999) of using χlf for Mh quantification. In addition, this method is easy to implement, requires no handling of chemical reagents and uses reproducible χlf measurements.

4.2. Pedogenetic implications and magnetic signature

The increased Fe contents and decreased Si contents estimated with sulfuric digestion were accompanied by increased Mh contents, and also increased χlf and χfd values. However, the soil samples from tuffite did not follow this trend; rather, they exhibited high Fe but low Mh contents and χlf values. Tuffite is an igneous rock deriving from volcanic ash and containing large amounts of poorly crystalline minerals (Fabris et al., 1995). Also, soil samples from tuffite were found to contain increased amounts of TiO_2, with sulfuric digestion, as well as substantial amounts of anatase (9 to 17%) with the Rietveld method. These lithogenic minerals undergo high Mg and Ti isomorphic substitution, so pedogenic

Mh also exhibits poor crystallinity and a high degree of isomorphic substitution (Fabris et al., 1995; Fabris et al., 1998) possibly by Mg and Ti, which decrease χlf.

Mh tends to accumulate with incressing soil weathering. This finding confirms the negative correlation of the weathering indexes *Ki* and *Kr* with Mh and Ms (Table S5). In indicator fact, low *Ki* values are typical of weathered soils, as low *Kr* values high proportions of oxides relative to kaolinite. Also, the samples with increased Mh contents exhibited increased values (Table 5) and χfd has been used as a proxy for pedogenetic Mh (Torrent et al., 2010; Liu et al., 2010).

In general, magnetite (Mt) or titanomaghemite (Ti-Mt) from rocks are transformed into Mh or, directly, into Hm (Resende et al., 1986; Torrent et al., 2006; Fabris et al., 1998). The accumulation of Mh as an intermediate in Hm formation in soil is due, among other factors, to the particle size of Mh, which can govern transformation rates, and also the degree of Hm formation to the detriment to Gt since these oxides follow opposing formation pathways and there is no record of Gt formation from Mh (Long et al., 2015). This relationship was also apparent in the clay samples from basalt Oxisols if one considers the differences in temperature. Thus, the sample 2-LV, which is site with annual mean temperature of 19 ºC, presented more Hm and Mh (72 and 18%, respectively), whereas sample 7-NB, from a site with a mean temperature of 15 °C, presented more Gt (90%) (Table 1). As shown by Cornell and Schwertmann (2000), however, the formation of Fe oxides is also influenced by other factors such as pH, water activity and organic matter content.

The negative correlation between χlf and isomorphic substitution was a result of ferrimagnetic element (Fe^{3+}) exchange with a paramagnetic element (e.g., Al^{3+}) and it was previously observed by Batista et al. (2013) in synthetic Mh. Some values of Al-for-Fe isomorphic substitution (Table 4) exceeded the commonly reported values for Mh (Schwertmann and Fechter, 1984; Schwertmann and Latham, 1986; Costa et al., 1999), ~0.20 mol Al mol^{-1}, especially in the soil samples from tuffite (12-OX, 13-MO, 14-IN). Similar results were obtained by Carvalho Filho et al. (1995) in clays with high Fe contents from Quadrilátero Ferrífero soils (Minas Gerais, Brazil), suggesting that other cations (e.g., Ti, Mg) may substitute Fe in the Mh structure (Fabris et al., 1998) and increase the Al/(Al+Fe) ratio as a result.

An increasing of Mh content leds to an Ms increasing and to as easier saturation as a result. Samples with higher Mh content such as 1-OX render hysteresis curves typical of ferrimagnetic maghemite, with Ms values up to 452×10^{-2} A m^2 kg^{-1}. On the other hand, samples containing antiferrimagnetic minerals such as Hm or Gt in high proportions exhibited decreasing of Ms and Mr values. This result was expected since both Hm and Gt may have a weak ferromagnetic order associated with defects, gaps or impurities present in the material. Although these ferromagnetic particles do not possess a high magnetic anisotropy, they exhibit high coercivity at small particle sizes (very fine particles) (Chen et al., 2016). In fact, the higher is the proportion of antiferrimagnetic minerals, the higher the applied magnetic field need be to cause saturation. Pure Hm samples require 4–7 T (France and Oldfield, 2000) and Gt 7–57 T for complete saturation (Rochette et al., 2005).

Based on the Day plot (Day et al., 1977) as fit by Dunlop et al. (2002) (Fig. 4), Mh consisted of a mixture of SD/MD and SD particles. The SD particles were about 30–80 nm in size, whereas the MD particles were 20 μm and the superparamagnetic particles ca. 0.05 μm. In our samples, the particle size of Mh as determined by XRD (13–45 nm, Table 4) and the %χfd values (≥ 3; Table 5) was related to SD and SP particles. However, structural perturbations such as isomorphic substitutions in the Mh structure or even an increase in fine antiferromagnetic particles can promote the emergence of a greater number of magnetic domains and lead to the formation of MD particles. This was confirmed by analyzing synthetic Mt in high-resolution transmission microscopy, which revealed that more than one magnetic domain in small particles (12–14 nm) was a response to defects in mineral structure (Nedelkoski et al., 2017). In addition, aggregation of Mh and Hm (Peters and Dekkers, 2003), the particle size and properties of which under these conditions are typical of MD, may interfere with magnetization.

Final considerations

In general, available information about pedogenetic Mh is limited in relation to other Fe oxides. As shown by this study, χlf is able to make Mh quantification easier, especially with large numbers of samples. Also, the magnetic properties of Mh change with the degree of soil weathering and the nature of the parent material, which can be useful support to soil classification and digital soil mapping.

5. Conclusions

The results obtained in this work allow us to draw two main conclusions, as follow:

i) If XRD-quantified Mh contents are taken to be the standard, H_2SO_4 dissolution is unsuitable for quantifying this compound because it also dissolves other Fe oxides and overestimates Mh. In contrast, the Rietveld refinement and χlf values are suitable choices for Mh quantification, the latter having the advantage that it affords determination in the clay fraction. One should bear in mind that Mh is the only clay mineral with expressive magnetism in tropical and subtropical soils, so, by comparing existing analytical methods, this study has confirmed that χlf is a fensible choice for quantifying Mh in soils.

ii) Mh formation was more marked in soils from itabirite and mafic rocks as a result of their Fe_2O_3 contents and of accumulation in the more weathered soils developed from these parent materials. However, soils from tuffite, a mafic rock, are an exception since they have a high Fe_2O_3 content (~330 g kg^{-1}) but a low Mh content (~5.5 g kg^{-1}), probably as result of their poorly crystalline Fe oxides and marked isomorphic substitution. The hysteresis loop parameters Ms and Mr were the most closely related to Mh contents in clay fraction. Also, irrespective of parent material, particle size and %χfd values suggest that Mh consists largely of single-domain and superparamagnetic particles. However, because of

isomorphic substitutions in the crystal structure of Mh and to the presence of minerals such as Hm and Gt, samples can gather multidomain particles.

Acknowledgments

The authors are grateful to the CAPES Foundation (Brazilian Ministry of Education) for additional funding and award of a doctoral fellowship to G. C. Poggere (PDSE 88881-132582/2016-01); to the National Council for Scientific and Technological Development (CNPq); to the Minas Gerais State Agency for Research and Development (FAPEMIG). This work was also partly co-funded by Spain's Ministry of Education and Science and the European Regional Development Fund.

References

Attoucheik, L., Jordanova, N., Bayou, B., Lagroix, F., Jordanova, D., Maouche, S., Henry, B., Boutaleb, A., 2017. Soil metal pollution from former Zn–Pb mining assessed by geochemical and magnetic investigations: case study of the Bou Caid area (Tissemsilt, Algeria). Environ. Earth Sci, 76:298.

American Mineralogist. http://rruff.geo.arizona.edu/AMS/amcsd.php

Barrón, V., Herruzo, M., Torrent, J., 1988. Phosphate adsorption by aluminous hematites of diferente shapes. Soil Sci. Soc. Am. J., 52, 647–651.

Barrón, V., Torrent, J., 1986. Use of the Kubelka-Munk theory to study the influence of iron oxides on soil colour. J. Soil Sci., 37, 499–510.

Batista, M.A., Costa, A.C.S., Bigham, J.M., Paesano Junior, A., Berndt, G., Inoue, T.T., Nonaka, A.G., 2013. Structural and magnetic characterization of maghemites prepared from al-substituted magnetites. Rev. Bras. Ci. Solo, 37, 1569–1575.

Baver, L.D., Gardner, W.H., Gardner, W.R., 1972. Soil Physics 5 ed. John Wiley & Sons, Nova Iorque (498 pp)

Bigham, J.M.; Fitzpatrick, R.W.; Schulze, D. Iron oxides. In: Dixon, J.B.; Schulze, D.G. Soil mineralogy with environmental applications. Madison: SSSA, 2002. p. 323-366.

Camargo, L.A., Júnior, J.M., Pereira, G.T., Bahia, A.S.R.S., 2014. Clay mineralogy and magnetic susceptibility of Oxisols in geomorphic surfaces. Sci. Agric., 71, 244–256.

Carvalho Filho, A., Inda, A.V., Fink, J.R., Curi, N., 2015. Iron of diferent lithological origin in ferriferous quadrilateral (Minas Gerais, Brazil). Appl. Clay Sci., 118, 1–7.

Chen, L., Zhou, C.H., Fiore, S., Tong, D.S., Zhang, H., Li, C.S., Ji, S.F., Yu, W.H., 2016. Functional magnetic nanoparticle/clay mineral nanocomposites: preparation, magnetism and versatile applications. Appl. Clay Sci., 127–128, 143–163.

Costa, A.C.S., Bigham, J.M., Rhoton, F.D., Traina, S.J., 1999. Quantification and characterization of maghemite in soils derived from volcanic rocks in southern Brazil. Clay Clay Miner., 47, 466–473.

Curi, N., Franzmeier, D. F., 1987. Effect of parent rocks on chemical and mineralogical properties of some Oxisols in Brazil. Soil Sci. Soc. Am. J., 51, 153–158.

Day, R., Fuller, M., Schmidt, V.A., 1977. Hysteresis properties of titanomagnetites: grain size and composition dependence. Phys. Earth Planet. Inter., 13, 260–267.

Dearing, J.A., 1994. Environmental magnetic susceptibility. Bartington Instruments, Witney, Oxon, England (104 pp)

Dearing, J.A., Dann, R.J.L., Hay, K., Lees, J.A., Loveland, P.J., Maher, B.A., OGrady, K., 1996. Frequency-dependent susceptibility measurements of environmental materials. Geophys. J. Int., 124, 228–240.

Dunlop, D.J., 2002. Theory and application of the day plot (Mrs/Ms versus Hcr/Hc). 2. Application to data for rocks, sediments, and soils. J. Geophys. Res., 107, B32057.

Dunlop, D. J., Özdemir, Ö., 1997. Rock Magnetism: Fundamentals and Frontiers. Cambridge Univ. Press, New York (575 pp)

Donagema GK, Campos DVB, Calderano SB, Teixeira WG, Viana JHM., 2011. Manual de métodos de análise de solos. 2nd ed. Embrapa Solos, Rio de Janeiro (230pp)

Fabris, J.D., Coey, J.M.D., Mussel, W.N., 1998. Magnetic soils from mafic lithodomains in Brazil. Hyperfine Interact., 114, 249–258.

Fabris, J.D., Jesus Filho, M.F., Coey, J.M.D., Mussel, W.N., Goulart, A.T., 1997. Iron-rich spinels from Brazilian soils. Hyperfine Interact., 110, 23–32.

Fabris, J.D., Coey, J.M.D., QI, Q., Mussel, W.N., 1995. Characterization of Mg-rich maghemite from tuffite. Am. Mineral., 80, 664–669.

France, D.E., Oldfield, F., 2000. Identifying goethite and hematite from rock magnetic measurements of soils and sediments. J. Geophys. Res. Solid Earth, 105, (B2),2781–2795.

Fink, J.R., Inda, A.V., Tiecher, T., Barrón, V., 2016. Iron oxides and organic matter on soil phosphorus availability. Ciênc. Agrotec., 40, 369–379.

Gee, G.W., Bauder, J.W., 1986. Particle-size analysis. In: Klute, A. (Ed.), Methods of Soil Analysis, Part 1: Physical and Mineralogical Methods. Soil Science Society of America, Madison, pp. 383–412.

Grimley, D.A., Anders, A.M., Bettis, E.A., Bates, B.L., Wang, J.J., Butler, S.K., Huot, S., 2017. Using magnetic fly ash to identify post-settlement alluvium and its record of atmospheric pollution, central USA. Anthropocene, 17, 84–98.

Inda, A.V., Torrent, J., Barrón, V., Bayer, C., Fink. J.R., 2013. Iron oxides dynamics in a subtropical Brazilian Paleudult under long-term no-tillage management. Sci Agric., 70, 48–54.

Jackson, M.L., 1979. Soil chemical analysis - advanced course: A manual of methods useful for instruction and research in soil chemistry, physical chemistry of soils, soil fertility, and soil genesis. 2nd ed. Dept. Soil Sci. Univ. of Wisconsin, Madison (895 pp)

Kämpf, N., Schwertmann, U., 1982. The 5 M NaOH concentration treatment for iron oxides in solis. Clay. Clay Miner., 30, 401–408.

Klug, H.P., Alexander, L.E., 1974. X-ray diffraction procedures for polycrystalline and amorphous materials 2nd ed. John Wiley and Sons, New York (992 pp)

Liu, Q., Hu, P., Torrent, J., Barrón, V., Zhao, X., Jiang, Z., Sua, Y., 2010. Environmental magnetic study of a Xeralf chronosequence in northwestern Spain: Indications for pedogenesis. Palaeo3 293, 144–156.

Long, X., Ji, J., Balsam, W., Barrón, V., Torrent, J., 2015. Grain growth and transformation of pedogenic magnetic particles in red Ferralsols. Geophys. Res. Lett., 42, 5762–5770.

Marques Jr, J., Siqueira, D.S., Camargo, L.A., Teixeira, D.D.B., Barrón, V., Torrent, J., 2014. Magnetic susceptibility and diffuse reflectance spectroscopy to characterize the spatial variability of soil properties in a Brazilian Haplustalf. Geoderma, 219–220, 63-71.

Mckeague JA, Day JH., 1966. Dithionite and oxalate-extractable Fe and Al as aids in differentiating various classes of soils. Can J Soil Sci., 46, 13–22.

Mehra, J.P., Jackson, M.L., 1960. Iron oxides removal from soils and clays by a dithionite-citrate-bicarbonate system buffered with bicarbonate sodium. Clay. Clay Miner., 7, 317–27.

Nedelkoski, Z., Kepaptsoglou, D., Lari, L., Wen, T., Booth, R. A., Oberdick, S.D., Galindo, P.L., Ramasse, Q.M., Evans, R.F.L., Majetich, S., Lazarov, V.K., 2017. Origin of reduced magnetization and domain formation in small magnetite nanoparticles. Sci. Rep., 7, 45997.

Nonaka, A.G., Batista, M.A., Costa, A.C.S., Inoue, T.T., Bonadio, T.G.M., Souza Junior, I.G., 2017. Kinetics of thermal transformation of synthetic Al-maghemites into Al hematites. Rev. Bras. Ciênc. Solo, 41, e0160384.

Norrish, K., Taylor, M., 1961. The isomorphous replacement of iron by aluminium in soil goethites. J. Soil Sci., 12, 294–306.

Resende, M., Santana, D.P., Franzmeier, D.P., Coey, J.M.D. Magnetic properties of Brazilian Oxisoils. In: International soil classification workshop, 8., 1988, Rio de Janeiro, RJ. Proceedings… Embrapa, Rio de Janeiro. p.78–108. Available in. http://library.wur.nl/isric/fulltext/isricu_i9278_001.pdf

Resende, M., Allan, J., Coey, J.M.D., 1986. The magnetic soils of Brazil. Earth Planet. Sc. Lett., 78, 322–326.

Rochette, P., Mathé, P.E., Esteban, L., Rakoto, H., Bouchez, J.L., Liu, Q., Torrent, J., 2005. Nonsaturation of the defect moment of goethite and fine-grained hematite up to 57 Teslas. Geophys. Res. Lett., 32, L22309.

Rowntree, K.M., van der Waal, B.W., Pulley, S., 2017. Magnetic susceptibility as a simple tracer for fluvial sediment source ascription during storm events. J. Environ. Manage., 194, 54–62.

Schwertmann, U., Fechter, H., 1984. The influence of aluminum on iron oxides: XI. Aluminum-substituted maghemita in soils and its formation. Soil Sci. Soc. Am. J., 48, 1462–1463.

Schwertmann, U., Latham, M., 1986. Properties of iron oxides in some New Caledonian Oxisols. Geoderma, 39, 105–123.

Schwertmann, U., Taylor, R.M., 1989. Iron oxides. In: Dixon, J.B., Weed, S.B., (Eds). Minerals in soil environments. Soil Science Society of America, Madison. p.379–438.

Siqueira, D.S., Marques JR, J., Teixeira, D.D.B., Matias, S.S.R., Camargo, L.A., Pereira, G.T., 2016. Magnetic susceptibility for characterizing areas with different potentials for sugarcane production. Pesq. Agropec. Bras., 51, 1349–1358.

Silva, S.H.G., Poggere, G.C., Menezes, M.D.D., Carvalho, G.S., Guilherme, L.R.G., Curi, N., 2016. Proximal Sensing and Digital Terrain Models Applied to Digital Soil Mapping and Modeling of Brazilian Latosols (Oxisols). Remote Sens., 8, 614-636.

Soil Survey Staff, 2014. Keys to Soil Taxonomy, Twelfth ed. USDA - Natural Resources Conservation Service, Washington.

Taylor, R., M., Maher, B.A., Self, P.G., 1987. Magnetite in soils: I. The synthesis of single-domain ad superparamagnetic agnetite. Clay Miner., 22, 411–422.

Thompson, R., Oldfield, F., 1986. Environmental magnetism. Allen and Unwin, London, p. 227.

Torrent, J., Barrón, V., 2008. Diffuse Reflectance Spectroscopy. In: Ulery, A.L., Drees, L.R. (Eds.). Methods of Soil Analysis Part 5. Mineralogical Methods. Soil Science Society of America, SSSA Book Series n. 5, p. 367-387, 2008.

Torrent, J., Barrón, V., Schwertmann, U., 1990. Phosphate adsorption and desorption by goethites differing in crystal morphology. Soil Sci. Soc. Am. J., 54, 1007-1012.

Torrent, J., Barrón, V., Liu, Q., 2006. Magnetic enhancement is linked to and precedes hematite formation in aerobic soil. Geophys. Res. Lett., 33, L02401.

Torrent, J., Liu, Q.S., Barrón, V., 2010. Magnetic minerals in Calcic Luvisols (Chromic) developed in a warm Mediterranean region of Spain: origin and paleoenvironmental significance. Geoderma, 154, 465–472.

Wang, X., Lu, H., Zhang, W., Hu, P., Zhang, H., Han, Z., Wang, Z., Li, B., 2016. Rock magnetic investigation of loess deposits in the Eastern Qingling Mountains (central China) and its implications for the environment of early humans. Geophys. J. Int., 207, 889–900.

Young, R.A., Sakthivel, A., Moss, T.S., Paiva-Santos, C.O., 1995. DBWS-9411 - an upgrade of the DBWS*.*programs for Rietveld refinement with PC and mainframe computers. J Appl Cryst., 28, 336-337.

Young, R.A., 1995. The Rietveld Method; I. U. C., Oxford University Press Inc., New York.

Supporting information for:

Maghemite quantification and magnetic signature of Brazilian soils with contrasting parent materials

Giovana Clarice Poggere, Alberto Vasconcellos Inda, Vidal Barrón, Nestor Kämpf, Angela Dayana Barrera de Brito, Julierme Zimmer Barbosa, Nilton Curi

Table S1. Percent of goethite (Gt), hematite (Hm) and maghemite (Mh) estimated by XRD and by Rietveld refinement.

Sample	Parent material	XRD			Rietveld		
		Gt	Hm	Mh	Gt	Hm	Mh
		---------- % ----------					
1-OX	Itabirite	29.4	43.1	27.5	33.7	45.1	21.2
2-OX	Basalt	9.9	72.2	17.8	11.5	77.7	10.8
3-OX		13.8	73.2	13	14.3	73.2	12.5
4-OX		51.6	43.1	5.2	49.5	47.3	3.2
5-MO		65.3	32.5	2.2	53.6	35.0	3.9
6-OX		79.6	19.2	1.1	70.1	29.1	0.9
7-OX		89.6	9.0	1.4	87.4	8.7	2.0
8-OX	Gabbro	31.6	60.6	7.7	35.0	58.1	6.9
9-OX		44.2	54.1	1.7	45.4	51.9	1.1
10-EN		58.9	37.7	3.5	44.5	52.9	2.6
11-EN		43.4	50.7	5.9	27.3	65.7	6.4
12-OX	Tuffite	32.3	63.8	3.9	26.0	52.4	4.9
13-MO		70.9	26.1	2.9	60.2	23.6	1.3
14-IN		73.9	24.9	1.2	78.8	11.3	0.5
15-OX	Gneiss	69.8	30.2	0.0	73.5	26.5	0.0
16-UL		63.8	35.5	0.7	64.3	35.7	0.5
17-OX	Amphibolite	45.3	53.6	1.1	41.4	58.5	0.8
18-MO		50.5	49.2	0.3	46.4	53.6	0.5

Table S2. Parameters of the adjust of the experimental diffractograms and calculated by the Rietveld refinement.

Sample	Parent material	R_p	R_{pw}	R_{exp}	Gof
1-OX	Itabirite	6.66	8.81	7.57	1.35
2-OX	Basalt	7.37	9.82	7.33	1.79
3-OX		7.05	9.32	5.86	2.53
4-OX		6.36	8.25	5.71	2.09
5-MO		6.71	8.97	5.38	2.78
6-OX		6.7	8.67	5.66	2.35
7-OX		8.84	11.7	7.06	2.75
8-OX	Gabbro	6.94	9.17	5.88	2.43
9-OX		8.15	10.72	5.35	4.01
10-EN		7.71	10.07	6.45	2.44
11-EN		8.47	11.04	6.25	3.12
12-OX	Tuffite	8.39	10.86	5.86	3.43
13-MO		11.02	14.36	9.66	2.21
14-IN		10.5	14.76	6.71	4.84
15-OX	Gneiss	12.19	15.78	16.09	0.96
16-UL		8.83	11.23	13.62	0.68
17-OX	Amphibolite	8.81	11.5	15.99	0.52
18-MO		6.97	9.18	12.58	0.53

Table S3. Percent of synthetic goethite (Gt), hematite (Hm) and maghemite (Mh) and value of magnetic susceptibility (χlf).

Point	Synthetic			χ_{lf}	Regression between χlf and Mh (R^2; *p*)
	Gt	Hm	Mh		
	--------- % ----------			$\times 10^{-6}$ m^3 kg^{-1}	%Mh = 0.4609 + 0.205χlf
1	53	45	2	6	(0.999; 0.01)
3	47	48	5	23	
4	46	45	9	43	
5	45	43	12	57	
6	34	41	25	119	
7	0	0	100	486	

Table S4. Dissolution time for each sample considering the decrease of the magnetic susceptibility (χlf) and Fe content extracted at the respective times.

Sample	Parent material	Time of dissolution	χlf initial	χlf final	Decrease	Fe
		minutes	$\times 10^{-6}$ m^3 kg^{-1}		%	g kg^{-1}
1-OX	Itabirite	120	147.3	6.6	4	161.0
2-OX	Basalt	120	55.3	1.7	3	87.6
3-OX		60	29.7	1.1	4	58.6
4-OX		60	13.1	0.4	3	50.3
5-MO		90	6.0	0.3	5	45.2
6-OX		45	2.8	0.2	7	25.1
7-OX		10	2.5	0.1	4	6.7
8-OX	Gabbro	45	30.7	0.9	3	55.4
9-OX		45	7.3	0.4	5	22.1
10-EN		45	5.4	0.3	6	51.7
11-EN		45	5.6	0.3	5	16.0
12-OX	Tuffite	60	15.7	0.5	3	68.2
13-MO		45	9.9	0.9	9	51.7
14-IN		10	2.5	0.1	4	26.1
15-OX	Gneiss	10	1.7	0.1	6	2.9
16-UL		10	1.6	0.1	6	1.9
17-OX	Amphibolite	10	1.2	0.1	8	10.1
18-MO		10	1.1	0.1	9	9.5

Table S5. Correlations among chemical, mineralogical and magnetic attributes and oxide content. Cells in red are significant r values ($p < 0.05$) and cells in gray show the significance (p).

	Hm(*)	Mh(*)	χlf	Ms	Mr	Hc	Hcr	*a*	Al(†)	SiO_2(!!)	Al_2O_3(!!)	Fe_2O_3(!!)	Ki	Kr
Gt	-0.113	0.200	0.144	0.170	0.049	-0.127	-0.314	-0.243	0.205	-0.060	-0.165	0.485	0.038	-0.184
	0.657	0.426	0.567	0.529	0.858	0.639	0.235	0.402	0.483	0.812	0.512	0.041	0.882	0.464
Hm		0.726	0.767	0.772	0.831	0.148	0.246	0.472	-0.485	-0.598	-0.008	0.656	-0.439	-0.601
		0.001	0.000	0.000	0.000	0.585	0.359	0.088	0.079	0.009	0.976	0.003	0.068	0.008
Mh			0.994	0.995	0.973	-0.075	0.137	0.562	-0.548	-0.700	-0.071	0.835	-0.544	-0.666
			0.000	0.000	0.000	0.784	0.612	0.036	0.042	0.001	0.779	0.000	0.020	0.003
χlf				0.997	0.990	-0.050	0.179	0.599	-0.593	-0.733	-0.039	0.825	-0.571	-0.705
				0.000	0.000	0.854	0.507	0.024	0.026	0.001	0.879	0.000	0.013	0.001
Ms					0.982	-0.038	0.196	0.582	-0.575	-0.707	-0.112	0.849	-0.506	-0.698
					0.000	0.890	0.467	0.029	0.032	0.002	0.680	0.000	0.045	0.003
Mr						0.007	0.183	0.615	-0.607	-0.726	-0.028	0.801	-0.547	-0.732
						0.978	0.497	0.019	0.021	0.001	0.918	0.000	0.029	0.001
Hc							0.204	0.099	0.096	0.070	-0.202	0.153	0.387	0.080
							0.448	0.736	0.744	0.798	0.453	0.570	0.139	0.767
Hcr								0.304	-0.197	-0.369	-0.381	0.162	0.058	-0.193
								0.291	0.499	0.160	0.145	0.548	0.831	0.475
a									-0.939	-0.525	0.215	0.252	-0.567	-0.454
									0.000	0.054	0.461	0.385	0.034	0.103
Al										0.495	-0.368	-0.183	0.671	0.460
										0.072	0.195	0.531	0.009	0.098
SiO_2											-0.180	-0.535	0.770	0.919
											0.475	0.022	0.000	0.000
Al_2O_3												-0.374	-0.673	-0.336
												0.126	0.002	0.173
Fe_2O_3													-0.165	-0.588
													0.513	0.010
Ki														0.781
														0.000

(*) Hm, Gt and Mh by XRD; (†) Al (mol mol^{-1}) from isomorphic substitution; (!!) sulfuric attack.

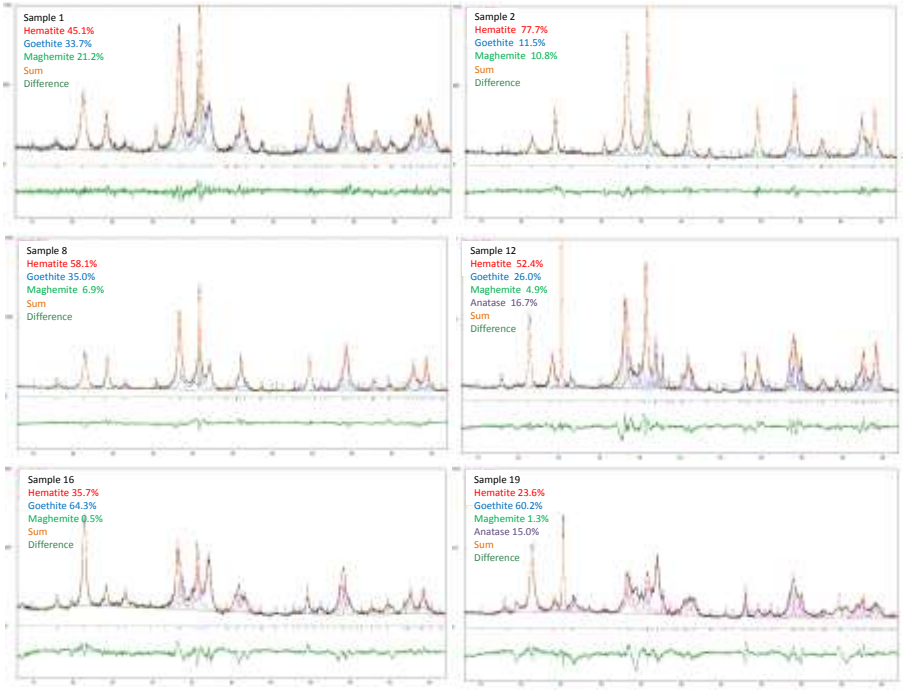

Fig. S1. Example of adjust of the diffractograms by Rietveld refinement determined in Fe oxides concentrate.

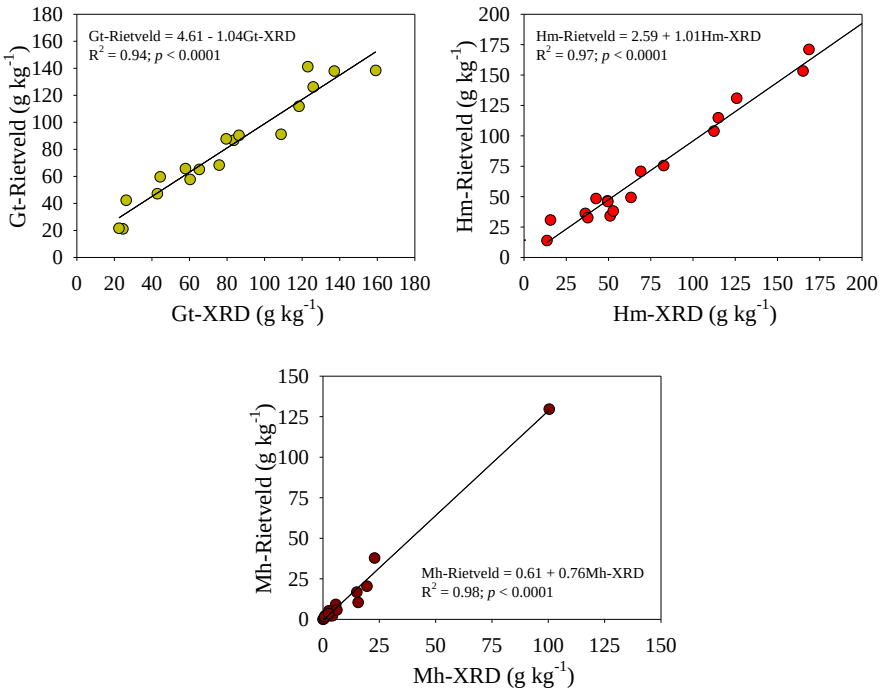

Fig. S2. Content of goethite (Gt), hematite (Hm) and maghemite (Mh) estimated by XRD and by Rietveld refinement.

Artigo elaborado de acordo com as normas do periódico Remote Sensing (versão aceita e publicada).

ARTIGO 2 - Proximal Sensing and Digital Terrain Models Applied to Digital Soil Mapping and Modeling of Brazilian Latosols (Oxisols)

Sérgio Henrique Godinho Silva [1], Giovana Clarice Poggere [2], Michele Duarte de Menezes [2], Geila Santos Carvalho [2], Luiz Roberto Guimarães Guilherme [2] and Nilton Curi [2,*]

[1] Institute of Agricultural Sciences, Federal University of Jequitinhonha and Mucuri Valleys, Campus Unaí, Av. Vereador João Narciso, 1380, Cachoeira, Unaí 38610-000, Brazil; sergiohgsilva@gmail.com

[2] Department of Soil Science, Federal University of Lavras, P.O. Box 3037, Lavras 37200-000, Brazil; gi.poggere@gmail.com (G.C.P.); michele.menezes@dcs.ufla.br (M.D.d.M.); geilacarvalho@dcs.ufla.br (G.S.C.); guilherm@dcs.ufla.br (L.R.G.G.)

* Correspondence: niltcuri@dcs.ufla.br; Tel.: +55-35-3829-1267

Academic Editors: José A.M. Demattê, LenioSoares Galvao and Prasad S. Thenkabail
Received: 25 May 2016; Accepted: 21 July 2016; Published: 25 July 2016

Abstract: Digital terrain models (DTM) have been used in soil mapping worldwide. When using such models, improved predictions are often attained with the input of extra variables provided by the use of proximal sensors, such as magnetometers and portable X-ray fluorescence scanners (pXRF). This work aimed to evaluate the efficiency of such tools for mapping soil classes and properties in tropical conditions. Soils were classified and sampled at 39 locations in a regular-grid design with a 200-m distance between samples. A pXRF and a magnetometer were used in all samples, and DTM values were obtained for every sampling site. Through visual analysis, boxplots were used to identify the best variables for distinguishing soil classes, which were further mapped using fuzzy logic. The map was then validated in the field. An ordinary least square regression model was used to predict sand and clay contents using DTM, pXRF and the magnetometer as predicting variables. Variables obtained with pXRF showed a greater ability for predicting soil classes (overall accuracy of 78% and 0.67 kappa index), as well as for estimating sand and clay contents than those acquired with DTM and the magnetometer. This study showed that pXRF offers additional variables that are key for mapping soils and predicting soil properties at a detailed scale. This would not be possible using only DTM or magnetic susceptibility.

Keywords: magnetic susceptibility; portable X-ray fluorescence scanner; data mining; fuzzy logics; ordinary least square multiple linear regression

1. Introduction

The small scale of most soil maps in Brazil is not suitable for land use planning and for defining soil and water conservation practices, which need to be done in more detail, i.e., at the level of watersheds [1], as established by the current legislation in Brazil [2]. The lack of financial support along with the large area of the country and the scarcity of roads are some of the main issues restricting the creation of more detailed soil maps, since they require intensive field work for sampling and classifying soils. In this sense, digital soil mapping and modeling are viewed as an alternative to increase not only soil information [3], but also the accuracy required for detailed soil maps, by the adoption of new tools and techniques to analyze, integrate and visualize soil and environmental datasets [4]. In recent years, extra effort has been put into the creation and use of new covariates that represent soil-forming factors [5,6], which are crucial for achieving adequate accuracy in soil mapping and a better understanding of soil modeling. Thus, the investigation of the main drivers of pedogenesis, as well as their geographic patterns is a key point for a successful mapping and modeling.

The study area of this work comprises the complete soil-landscape variations of Latosols (Oxisols), whose distribution pattern is commonly observed in the surrounding region. Previous studies have pointed out parent material and age as the main drivers of soil differentiation in the region [7,8]. Such studies attempted to define soil-landscape relationships from erosional surfaces and their relationship with parent material, soil classes and properties. One of the main findings of these studies performed by [7,8] was the low predictive power of topography. It is important to emphasize that during those preliminary findings, geographic information systems and digital elevation models were not available. Besides the predominance of Latosols (Oxisols), these studies highlighted important parent material contrasts, including soils derived from gabbro, leucocratic gneiss (predominance of lighter minerals), and mesocratic gneiss (higher contents of darker minerals), exerting strong influence on soil properties. These studies also indicated the importance of having detailed geologic maps in the region, as well as in most areas of Brazil, which might improve soil maps and prediction models. Such findings reveal the need for new techniques that may well improve the tacit models developed by pedologists. By providing new insights on soil-landscape relationships and detailed information on parent material differentiation, such techniques could offer more specific terrain

models through remote sensing data and increase the amount of information about soils, thus improving soil mapping and modeling in the area.

One of the most common soil-forming factors used in the predictions of soil classes and properties is topography [4,9–11], by analyses of a digital elevation model and its derivatives (digital terrain models (DTMs)), e.g., slope, terrain curvatures, topographical wetness index, aspect, etc. Such maps have been extensively used in recent years, since soils occur in response to water movement throughout the landscape, which is controlled by local relief [11]. Additionally, considering the continuous nature of DTM variation (raster-based distribution), they have been used in soil predictive models for providing spatially-exhaustive auxiliary variables [12,13], although it is commonly known that soils result from a complex interaction of soil-forming factors [14]. In this sense, the use of DTM is considered very useful in environments where topography is strongly related to the processes driving soil formation [11,15].

Despite the fact that DTMs have been used worldwide as adequate predictors of soil properties, recent studies are searching for new tools associated with soil attributes, especially those concerning chemical features. For example, some soil chemical elements or properties could function as tracers or indicators of different parent materials, which, in turn, could be related to soil classes and properties. At last, this information could potentially improve soil mapping and modeling. In this sense, equipment that performs fast analyses in the field and provides a large spectrum of data, such as proximal sensors, has been recently adopted to help soil mapping. Proximal sensing includes proximal or remote in situ and ex situ (field and laboratory) non-invasive or intrusive and mobile or stationary devices [16]. Some examples are magnetometers, which quantify the magnetic susceptibility of different materials, and portable X-ray fluorescence (pXRF) scanners, used to identify and quantify chemical elements and compounds present in soil samples [17].

Magnetic susceptibility is obtained from the ratio of induced magnetization in relation to the intensity of the magnetizing field and is being considered a simple, sensitive, inexpensive and non-destructive analysis [18]. It has been used as a proxy method for heavy metals [18,19] and pollution screening [20,21], sediment tagging and tracing [22] in erosion studies [22,23], for discriminating individual soils and horizons [24], for soil survey purposes [25,26] and to quantity magnetic minerals in soils and to relate soil-forming process [25,27–29]. For soil minerals, such studies involve measuring the response of the material of concern to a series of externally-applied magnetic fields, which, in soils, results mainly from the presence of magnetite and maghemite [24,30]. Thus, the major interest of soil magnetic studies is iron oxides, as different iron forms and dynamics reflect different soil-forming factors and processes [25].

Portable X-ray fluorescence scanners (pXRF) are another class of sensors used in recent studies involving soils to assess total elemental contents and to make predictions regarding soil properties [17,31–33]. In theory, a pXRF is able to detect many elements of the periodic table, since each one has a typical fluorescence energy. Such sensors have the advantage of being a portable proximal sensing tool that provides immediate estimates of contents of various chemical elements in soils, with none or minimum sample pre-processing [32,33]. Results showed that pXRF devices provide adequate analytical accuracy when compared to conventional laboratory-based methods [17,32,34,35]. On the other hand, few efforts have been made to apply proximal sensors on predictions of soil physical properties [33]. Furthermore, parent material and the intensity of both weathering and pedogenesis may exert strong influences on soil physical properties, such as soil particle size distribution [36], because its pattern represents a unique combination of primary and secondary minerals, reflecting the elemental composition of soils [33]. However, these technologies still require tests to help soil mapping, especially in regions with a lack of detailed soils and geology information, such as in tropical environments. Digital mapping and modeling techniques have made progress due to increased data availability and their combination with theoretical and conceptual soil models [37], as well as the integration of pedological knowledge into digital soil mapping [38]. Thus, proximal sensing along with geographic information systems, predictive models and pedological knowledge can be used to characterize the spatial distribution of soils across the landscape [11].

Thus, considering the contrast of parent material in the study area and the potential of proximal sensors in detecting soil chemical composition that is related to parent material [32,39], this study attempts to: (i) evaluate the efficiency of proximal sensors (magnetometer and pXRF) in addition to DTM to create a detailed soil map of an area with highly variable geology; and (ii) generate models for predicting soil particle size distribution based on data obtained from those sensors, DTM and parent material in Latosols (Oxisols), in Brazil. Such tools were evaluated in two ways: areal-based (detailed soil class maps) and point-based (OLS multiple linear regression) to assess their efficiency regarding different types of predictions.

2. Materials and Methods

2.1. Study Area and Laboratory Analyses

The study was carried out in an area located on the Campus of Federal University of Lavras, which is dominated by Latosols (Oxisols), a class representing the majority of the soils of Southern Minas Gerais state, Brazil

(Figure 1). This area (~150.18 ha) does not have either a detailed soil map or a detailed geologic map and is located between latitudes 7651,207 and 765,3478 m and longitudes 501,962 and 503,957 m, Zone 23 K. The climate of the region is Cwa (C: subtropical climate; w: rainy summers; a: warm summers), characterized by rainy and warm summers and cold and dry winters, according to the Köppen classification system, with mean annual temperature and rainfall of 19 °C and 1530 mm, respectively [40].

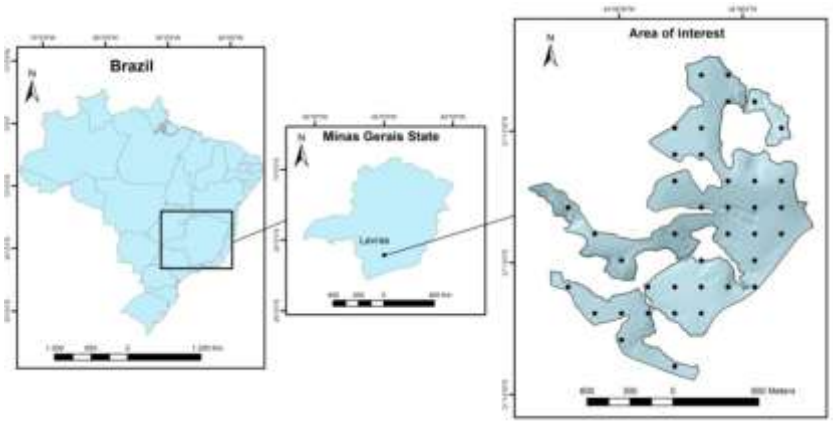

Figure 1. Location of the study area and sampling design for the classification of soils and the collection of samples for laboratory analyses.

The area encompasses a great geologic variety, with the dominance of leucocratic and mesocratic gneisses, the latter containing greater contents of Fe and darker minerals than the former, as well as a gabbro intrusion and sediments of varying nature.

A total of 39 sampling sites were selected throughout the study area, in a regular-grid design with a distance of 200 m between samples (Figure 1), covering different land uses, which included cultivated (pasture (signal grass) and coffee), and non-cultivated areas (native vegetation, semiperennial tropical forest). At each location, soils were classified according to the Brazilian Soil Classification System [41] into typic Dystrophic Yellow Latosol (LA), typic Dystrophic Red-Yellow Latosol (LVA), both developed from leucocratic gneiss, typic Dystrophic Red Latosol developed from mesocratic gneiss (LVm) and typic Dystropherric Red Latosol developed from gabbro (LVg). Such soils were classified as Latosols due to the presence of the B latosolic diagnostic horizon (similar to the oxic horizon in the U.S. Soil Taxonomy), followed by the dominant color of the B horizon (Munsell color 2.5YR or redder (red), 7.5YR or yellower (yellow), in between 2.5YR and 7.5YR (red-yellow)). The term Dystrophic is used when base saturation is smaller than 50%, whereas Dystropherric describes a dystrophic soil with Fe_2O_3 contents (obtained through a sulfuric acid digestion) ranging from 18% to

36%. The expression "typic" is used for reporting no intergrade regarding other soil classes.

Soil samples were collected from A and B horizons and submitted to analyses of particle size distribution by the pipette method [42,43]. Briefly, the sand fraction was separated using a 0.05-mm sieve; the silt and clay fractions were separated from each other after the sedimentation of the silt fraction, by pipetting a volume of the solution containing only the clay fraction, followed by oven-drying the solution and weighting the remaining clay fraction; the silt fraction is obtained by subtracting the weights of sand and clay fractions from the total weight of the soil. Chemical analyses included: soil pH (water, at 1:2.5 ratio); exchangeable Ca^{2+}, Mg^{2+} and Al^{3+} extracted with 1 $mol \cdot L^{-1}$ KCl [44]; available K and P extracted with Mehlich-l solution [45], $H^{+} + Al^{3+}$ using the SMP extractor [46]; organic carbon by wet oxidation with potassium dichromate in sulfuric acid medium; and remaining P [47]. Table 1 presents the physical and chemical characterization of soils developed from each parent material.

Table 1. Mean values of the physical and chemical properties of the soils sampled.

Soil Properties	LA [1] (2)		LVA [1] (10)		LVm [1] (16)		LVg [1] (11)	
	Horizons							
	A	B	A	B	A	B	A	B
pH	5.6	5.7	5.5	5.1	5.9	5.4	6.0	5.1
K (mg dm^{-3})	122.0	15.0	153.0	19.6	176.9	30.6	166.4	30.2
P (mg dm^{-3})	7.6	0.4	5.2	0.6	8.7	1.2	20.8	1.0
Ca^{2+} (mg dm^{-3})	3.2	1.6	3.0	1.1	5.1	2.2	4.3	0.9
Mg^{2+} (mg dm^{-3})	1.5	0.3	1.0	0.3	2.0	0.4	1.8	0.2
Al^{3+} ($cmol_c$ dm^{-3})	0.0	0.1	0.3	0.4	0.1	0.2	0.2	0.3
$H^{+} + Al^{3+}$ ($cmol_c$ dm^{-3})	2.1	1.7	4.5	3.5	3.3	3.8	3.7	4.5
SB [2] ($cmol_c$ dm^{-3})	5.0	1.8	4.4	1.4	7.6	2.7	6.5	1.2
t [3] ($cmol_c$ dm^{-3})	5.0	1.9	4.6	1.7	7.6	2.8	6.7	1.5
T [4] ($cmol_c$ dm^{-3})	7.1	3.5	8.9	4.9	10.9	6.5	10.2	5.7
V [5] (%)	70.3	52.0	56.4	34.7	67.3	43.3	64.1	23.4
m [6] (%)	0.0	3.1	6.2	24.4	1.4	11.4	4.8	19.1
SOM [7] (%)	3.7	1.1	5.6	1.5	6.5	2.1	6.6	2.8
P-Rem (mg dm^{-3})	26.6	9.8	23.1	7.3	20.2	7.2	15.6	3.1
Clay (g kg^{-1})	470.0	540.0	451.0	566.0	501.0	595.0	535.0	659.0
Silt (g kg^{-1})	140.0	85.0	18.2	119.0	230.0	158.0	312.0	186.0
Sand (g kg^{-1})	390.0	375.0	367.0	315.0	269.0	247.0	153.0	155.0

[1] LA: Yellow Latosol; LVA: Red-Yellow Latosol; LVm: Red Latosol developed from mesocratic gneiss; LVg: Red Latosol developed from

gabbro. Numbers between parentheses show the number of soil samples classified as those soil classes; [2] SB: sum of bases; [3] t: effective cation exchange capacity; [4] potential cation exchange capacity; [5] V: base saturation; [6] m: aluminum saturation; [7] SOM: soil organic matter.

Magnetic susceptibility per unit of mass (χ_{BF}) was determined using the Barrington MS2B magnetometer in air-dried samples passed through a 2-mm sieve. Data were obtained at low frequency (χ_{BF} = 0.47 kHz) and calculated through the expression $\chi_{BF} = (10 \times \kappa)\ m^{-1}$, where κ is dimensionless [48]; studying different soils and parent materials in the region of Lavras, it was noticed that soil classes comprising the same taxonomic order (Latosols and Argisols) developed from different parent materials showed contrasting magnetic susceptibility values, which demonstrates the potential of using magnetic susceptibility for characterizing soils with varying parent materials.

For the analyses of total elemental contents in soil samples, a portable X-ray fluorescence analyzer (pXRF) (Bruker model S1 Titan LE) was used to scan samples that were previously air-dried and passed through a 2-mm sieve. Samples were placed in plastic holders, and the scanning was performed during 60 s in two beams. The software used in pXRF is GeoChem General, and the device contains a 50-kV and 100-μA X-ray tube, which provides fairly selective detection of various elements, ranging from Mg to U, with limits of detection (LOD) in the parts per million range (ppm) for many of these elements. Calibration of the pXRF was checked with the analysis of a standard soil sample (CS). The average of the measured values for selected elements found in CS was within acceptable limits: Al_2O_3 (99%), SiO_2 (95%), K_2O (90%), Mn (85%), Fe (130%) and Cu (93%). Furthermore, quality control and quality assurance protocols were performed by analyses of NIST Standard Reference Materials with varying elemental concentrations (SRM 2710a and SRM 2711a). Each of these control samples (NIST and CS) were analyzed ten times. The recoveries (%) for NIST 2710a and NIST 2711a were, respectively: Al (36; 69), Si (46; 41), P (75; 22), K (67; 33), Ca (76; <LOD), Ti (77; 55), V (155; 135), Mn (87; 55), Fe (92; 77), Cu (110; 104), Zn (129; 135) and Zr (257; 54). Selected data obtained with pXRF for the 39 samples collected in the field (MgO, SiO_2, Cl, K_2O, Ti, Fe, Zn, Zr, Mn, Cr, Ni, Cu and Ce) were used as covariates to help soil and geologic mapping.

X-ray diffractometry (XRD) analyses were performed to identify Fe oxide minerals present in the soil clay fraction, which was previously treated with 5 $mol \cdot L^{-1}$ NaOH [49] for iron concentration and dissolution of kaolinite, gibbsite and other minerals in the samples. Afterwards, non-oriented plates (Koch plate) were prepared for XRD analyses in the range from 15 to 45°2θ, using halite as an internal pattern to correct for instrumental distortions.

2.2. Soil Classes Mapping

A digital elevation model (DEM) of 5-m resolution was created from contour lines of 1 m of vertical distance by the Topo to Raster function in ArcGIS 10.1(ESRI). From this DEM, 9 terrain variables commonly used for predictions and mapping of soil classes and properties [10,50–55] were selected using both ArcGIS 10.1 and SAGA GIS [56], including: slope, topographic wetness index (TWI), SAGA wetness index (SWI), cross-sectional and longitudinal curvatures, vertical distance to channel network and valley depth, in addition to elevation and Geomorphons [57]. Geomorphons consist of an algorithm that classifies the landscape into 10 possible landforms, and thus, it is expected to contribute to distinguishing geomorphology patterns that may be related to varying soil classes and properties.

Terrain information in addition to magnetic susceptibility and pXRF data for the 39 sites were grouped into four soil classes found in the study area during the field work, and box plots were generated in order to help identify the variables (terrain and laboratory data) that contributed the most to distinguishing soil classes. Similar boxplot analyses have been performed by [52,58–60] to identify the best variables regarding the prediction of soil properties. In this procedure (analysis of boxplots), the variables whose values per soil class presented different ranges, without overlapping the range of values of other soil classes, were considered appropriate to distinguish soil classes and, hence, adequate to be used for soil mapping.

Next, the mean value of these previously-mentioned variables was calculated per each soil class, being considered representative of the typical condition for each soil class of occurrence. The standard deviation of each variable for each soil class was also calculated per soil class based on data obtained from the 39 sampling sites. Both the mean and the standard deviation of the chosen variables per soil class were used as rules for predicting the spatial occurrence of soil classes through ArcSIE, the soil inference function, an ArcGIS extension that has been successfully used for soil mapping [59,61–64]. For example, according to the sampling sites, a soil class was found to occur at places where slope values range from 12% to 20% (mean ± standard deviation), with a mean value (typical condition) of 16% coupled with SWI ranging from 2 to 4 and a mean value of 3. Based on this kind of information (rules, typical conditions and range of values of variables for all of the soil classes occurring in the area), ArcSIE uses fuzzy logic and similarity vectors to predict soil classes and properties on the landscape [65] identifying the places that are more related to the typical conditions of each soil class. For that, ArcSIE generates membership maps in raster format in which every pixel shows the value of similarity to a typical condition, ranging from 0 (low similarity) to 1 (great similarity). Subsequently, a final map is generated representing the places that are more likely for each soil class to occur, according to the rules inserted into ArcSIE.

For the soil mapping procedure, DTM information was continuously available for the entire study area, but variables obtained from pXRF and magnetic susceptibility data at the 39 sampled sites needed to be extrapolated to the entire area using the inverse distance weighting (IDW) method, with the purpose of being used as continuous variables for soil mapping through ArcSIE. The values inferred at non-sampled areas by IDW are estimated using a linear combination of values at the sampled points, weighted by an inverse function of the distance from the point of interest to the sample points. The weights (λ_i) are expressed as:

$$\lambda_i = \frac{\frac{1}{d_i^p}}{\sum_{i=1}^{n} \frac{1}{d_i^p}} \quad (1)$$

where d_i is the distance between x_0 and x_0, p is a power parameter and n represents the number of sampled points used for the estimation. This interpolation was performed in ArcGIS 10.1 (ESRI), where a power parameter equal to 2 (default) was chosen. Mean error (ME) and root mean square error (RMSE) were calculated for assessing the accuracy of interpolation, as follows:

$$ME = \frac{1}{n}\sum_{i=1}^{n}(ei - mi) \quad (2)$$

$$RMSE = \sqrt{\frac{1}{n}\sum_{i=1}^{n}(ei - mi)^2} \quad (3)$$

where n is the number of observations, ei is the estimated value from pXRF and magnetic susceptibility data and mi is the correspondent measured value.

The accuracy assessment of the soil classes map generated in ArcSIE was performed through the comparison of the soil class presented on the map with the real soil class at 14 places (field validation) randomly chosen within the study area. From this analysis, overall accuracy (percentage of correctly-predicted soil classes), Kappa index, omission and commission errors and user's and producer's accuracy were calculated for each soil class. The formulas for calculating the Kappa index and producer's and user's accuracies are presented below:

$$Kappa = \frac{Po - Pe}{1 - Pe} \quad (4)$$

where *Po* is the proportion of correctly-classified samples and *Pe* is the probability of random agreement. The Kappa index ranges from −1 to 1, although the results are commonly found between 0 and 1,indicating increasing accuracy as the values get closer to 1 [66]:

$$User's\ accuracy = \frac{Xii}{\sum_{i=1}^{r} Xij} \quad (5)$$

$$Producer's\ accuracy = \frac{Xjj}{\sum_{j=1}^{r} Xij} \quad (6)$$

where X_{ii} and X_{jj} represents the number of correctly-classified samples and X_{ij} indicates the total number of samples of a soil class in a row (user's accuracy) or column (producer's accuracy) of a confusion matrix.

2.3. Soil Particle Size Distribution Predictive Models

The ordinary least square multiple linear regression (OLS) was used for fitting the prediction models of sand and clay contents (dependent variables) in ArcGIS 10.1 from proximal sensors, DTM and the previously obtained soil classes map (explanatory variables). First, the exploratory analysis module was applied to the data to provide a suitable set of explanatory variables, to determine if the OLS assumptions were met and to measure the prediction power of the candidate variables in order to generate effective and reliable prediction models. Only models that met the criteria were considered as suitable models. Statistically-significant explanatory variables, models with higher adjusted R^2, Akaike's information criterion, multicollinearity checked by means of the variance inflation factor, the normality of regression residuals and parsimony were all carefully considered and analyzed for the selected models.

In order to properly assess the accuracy of the models, independent sand and clay datasets were used. Such data were not used for developing the models. Mean error and root mean square of prediction error were calculated, according to Equations (2) and (3), as previously mentioned. Furthermore, in order to assess the predictive power of the variables, five types of prediction models were refined for clay and sand contents, according to the explanatory variable source: (i) only with DTM; (ii) proximal sensors plus parent material (based on soil classes map); (iii) proximal sensors plus parent material plus DTM; (iv) only proximal sensors; and (v) proximal sensors plus DTM.

3. Results

3.1. Digital Soil Mapping

Boxplots of the analyzed variables are shown on Figure 2. The fluorescence energy is characteristic of the elements present in a sample of interest, and so, theoretically, the spectrum of atomic weights greater than 19 may be determined by the pXRF detector. However, because of low energy responses, not all elements of the periodic table can be effectively measured, and there is also a limit of detection depending on the content of the element of interest in the sample [67]. pXRF could identify 13 elements and/or compounds for at least one soil class, increasing the number of potentially useful variables to distinguish different Latosols, making up a total of 23 variables, including both the ones related to terrain features and those obtained from laboratory analyses (pXRF and magnetic susceptibility). Only elements with low error or uncertainty were selected. This error is a deviation calculated by the equipment, according to its calibration. Four out of the 23 variables were considered more capable of distinguishing at least one of the four possible soil classes (Figure 2), according to the boxplots, three of them being related to proximal sensing analyses (magnetic susceptibility, Fe and SiO_2) and one related to terrain (SWI). Regarding all of the terrain-related variables, only SWI presented high potential for distinguishing a soil class (LA) due to the lowest values found for that soil class in comparison with the others. In contrast, all of the other terrain-related variables contain values within a similar interval among the four soil classes.

Magnetic susceptibility, Fe and SiO_2 contents presented distinguished ranges of values for the soil classes, in addition to SWI. Soils derived from gabbro had higher magnetic susceptibility and Fe contents, while LA presented the greatest concentration of SiO_2. Other chemical compounds were not considered adequate for distinguishing one soil class from the others because they could be estimated only in some soil classes (e.g., Ni, Cr, Cu, Ce and MgO) or because their values were within the same range for all soil classes (K_2O, Ti, Mn, Cl, Zn and Zr).

Redder soils (LVA, LVm and LVg) had greater contents of Fe and Ti and some elements that were not present in LA, such as Ni, Cr and Cu. This latter soil class contains MgO and Ce, which were not detected by pXRF for the other soils, and greater amounts of SiO_2 and Cl than the redder soils.

Table 2 shows the mean and the standard deviation of the variable values obtained by analyses of the soil samples grouped according to the soil class. It can be noticed that the greatest magnetic susceptibility, as well as Fe and Ti contents were found for LVg, followed by LVm, and also that they decreased as the soil became yellower. On the other hand, SiO_2, Cl and K_2O contents decreased as the soil became redder. Zn and Zr contents were greater for LVm and LVA, respectively.

Table 2. Mean and standard deviation (SD) of the variable values.

Variable	LA	LVA	LVm	LVg
MS [1] (10^{-7} m^3 kg^{-1})	4.8	15.7	43	194
SM SD	0.26	16.9	27	97
MgO (ppm)	23,545	-	-	-
MgO SD	20,543	-	-	-
SiO_2 (ppm)	19,568	17,265	16,946	16,289
SiO_2 SD	1870	1858	1961	2033.7
Cl (ppm)	1461	1160	1113	984.9
Cl SD	36	40	48.6	60.8
K_2O (ppm)	1432	1397	1324	945
K_2O SD	146	150	159.2	157.9
Ti (ppm)	5900	6799	8379	9221
Ti SD	155	165	186.2	196.7
Fe (ppm)	31,880	46,103	66,450	96,410
Fe SD	304	358	439.6	531
Zn (ppm)	18	23	35.3	32.2
Zn SD	8	9	9.8	10.7
Zr (ppm)	170	187	182	167.6
Zr SD	9	10	10.8	11.6
Mn (ppm)	91	152	372	-
Mn SD	53	62	79.3	-
Cr (ppm)	-	-	454	1103
Cr SD	-	-	55.9	68.3
Ni (ppm)	-	-	121	105.7
Ni SD	-	-	23.5	28.1
Cu (ppm)	-	-	29	36.8
Cu SD	-	-	9.6	11.3
Ce (ppm)	1538	-	-	-
Ce SD	468	-	-	-

[1] Magnetic susceptibility.

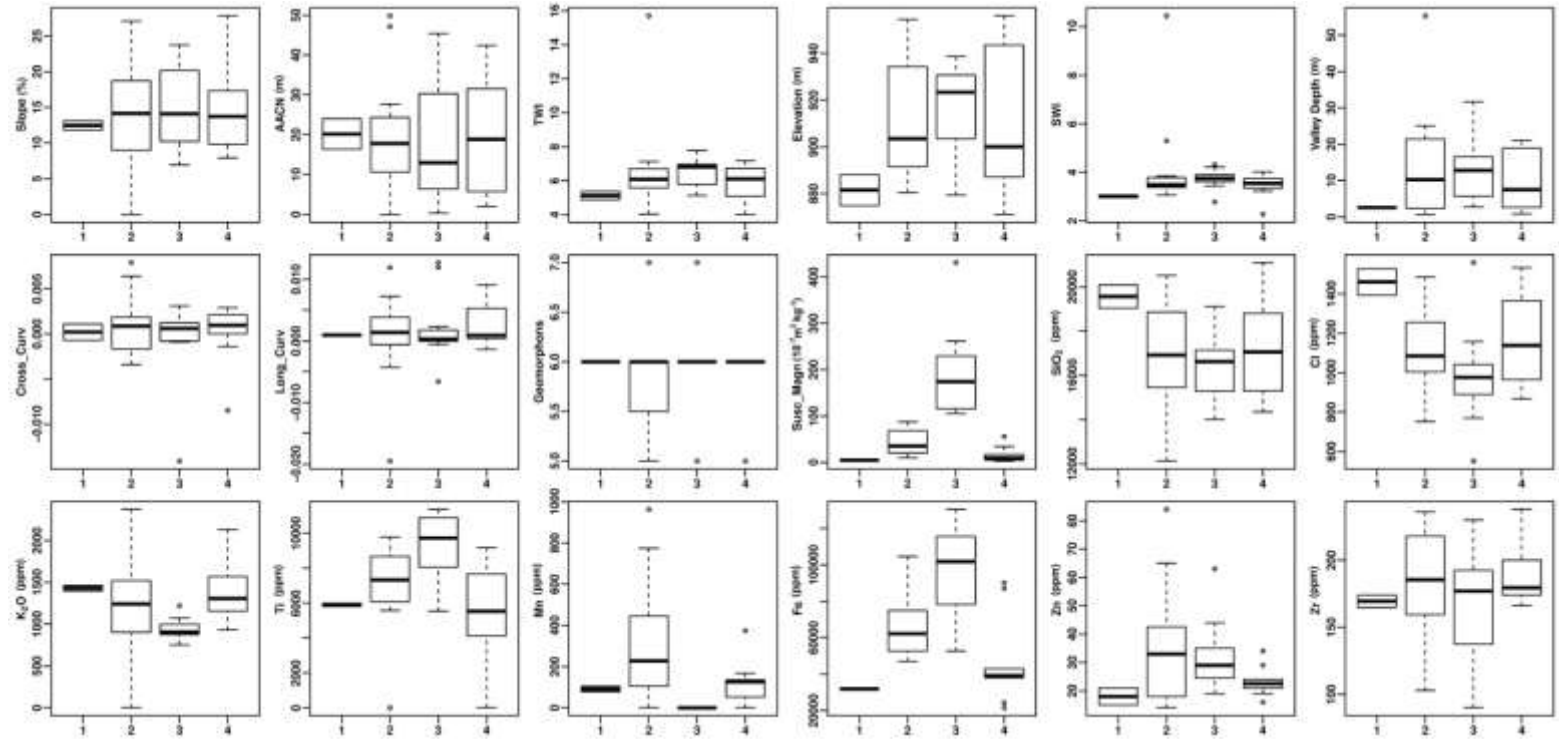

Figure 2. Boxplots of the variables used for distinguishing the four soil classes of the study area. 1, LA; 2, LVm; 3, LVg; 4, LVA.

Figure 3 shows the maps of the four variables considered more capable of distinguishing the soil classes. Magnetic susceptibility ranged from 2.9 to 431 χ_{BF} in the study area, and higher values covaried with larger contents of Fe, which, in turn, ranged from 21,531 to 130,434 ppm. SiO_2 contents ranged from 12,135 to 21,100 ppm, while SWI ranged from 1.3 to 10.4, being greater as the chance of accumulating water increases on the landscape [68]. The accuracy indexes of magnetic susceptibility, Fe and SiO_2 IDW maps were, respectively: ME = −3.603 and RMSE = 60.604; ME = −340.103 and RMSE = 22867.917; ME = −137.973 and RMSE = 1707.471.

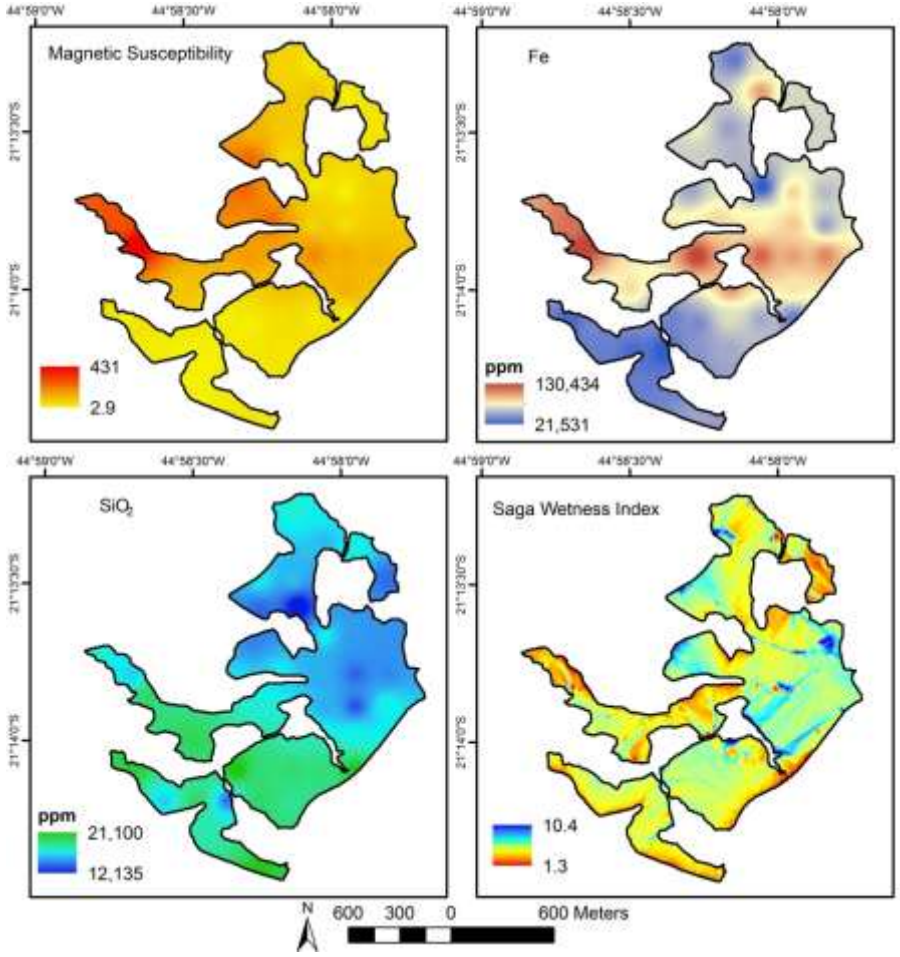

Figure 3. Maps of the variables used for distinguishing soil classes in the study area.

Table 3 represents the values used in ArcSIE to generate the soil class map. The similarity column in Table 3 represents the similarity to the typical condition: when it is 100%, it corresponds to the typical condition for a soil

class to occur (mean value obtained from the collected samples), whereas 50% represents the values resulting from the standard deviation subtracted from (lower limit) and added to (upper limit) the mean value, indicating the range of values for a soil class to occur, with at least 50% membership in relation to the typical condition. Data in Table 3 show that Fe was the unique variable used for mapping all four soil classes, while the other three variables were employed for at least one soil class, such as SWI, although in all cases, a soil class required more than one variable to be mapped.

Table 3. Values used in ArcSIE in order to map the soil classes' distribution in the study area. SWI, SAGA wetness index.

	Similarity [1]	**LA**	**LVA**	**LVm**	**LVg** [2]
	50%	31,610	23,100	48,450	70,410
Fe	100%	31,880	46,100	66,450	96,410
	50%	32,150	69,100	84,450	-
	50%	18,840	14,970	14,750	-
SiO_2	100%	19,570	17,270	16,950	-
	50%	20,300	19,570	19,150	-
	50%	4.54	-	16	97
SM	100%	4.80	-	43	194
	50%	5.06	-	70	-
	50%	2.9	-	-	-
SWI	100%	3.0	-	-	-
	50%	3.1	-	-	-

[1] Similarity to the typical condition. [2] The curve type for LVg is S-shaped, while for other soils, it is bell-shaped.

The geologic variety contributed to the formation of Latosols with contrasting physical, chemical and mineralogical properties [7,48,69], as shown in Table 1 and Figure 4. Leucocratic gneisses tend to form Yellow- or Red-Yellow Latosols, while mesocratic gneisses develop Red Latosols, as well as the gabbro-derived soils, yet the latter contain different properties in relation to the former, such as the presence of maghemite (Figure 4), higher Fe contents and magnetic susceptibility values (Table 2).

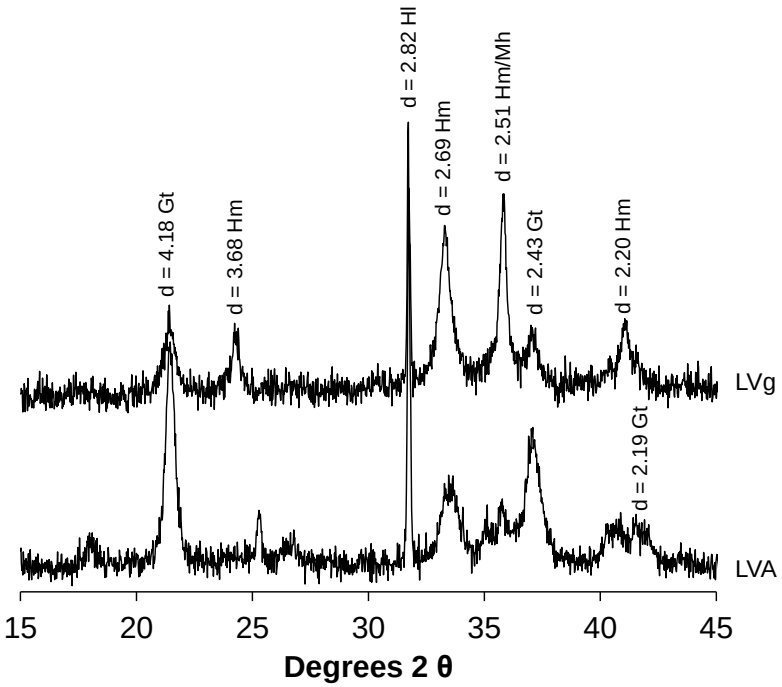

Figure 4. X-ray diffractograms of the concentrated Fe clay fraction of the B horizon of soils derived from gabbro (LVg) and gneiss (LVA). Gt, goethite; Hm, hematite; Mh, maghemite.

The predicted soil map is shown in Figure 5. It can be noticed that LVA is the soil class that occupies the largest portion of the area, corresponding to 40.79% (61.25 ha). It is followed by LVg, with 33.70% (50.60 ha), mainly occurring in the center of the study area, from east to west. In sequence, LVm is found in 25.50% (38.30 ha). Lastly, LA occurs in 0.01% (0.016 ha) of the area, at places where SWI is lower.

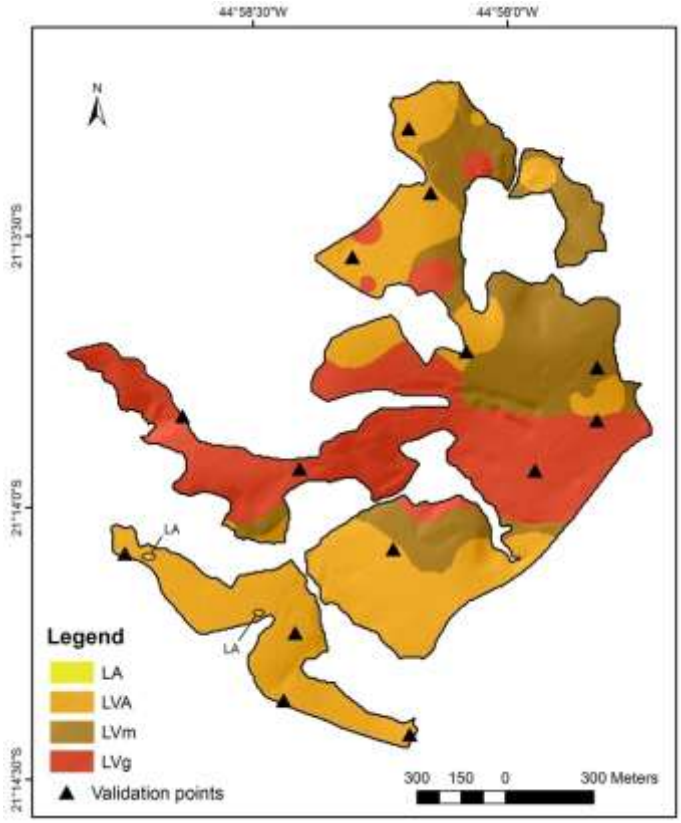

Figure 5. Predicted soil map of the study area and location of the validation points.

The indexes for the predicted soil map accuracy were assessed according to a confusion matrix (Table 4), from where it was found an overall accuracy of 78.57%, meaning that 11 out of the 14 validation points match the predicted soil class. The validation resulted in a Kappa index of 0.6719, corresponding to a substantial classification [66]. Furthermore, the omission error for LVA was the greatest (lowest producer's accuracy), while commission error was the greatest for LVm (lowest user's accuracy).

Table 4. Confusion matrix, omission and commission errors and producer's and user's accuracies for the predicted soil map.

	LVg	LVm	LVA	LA	Omission Error	Producer's Accuracy	Commission Error	User's Accuracy
LVg	4	0	1	0	0	100	20	80
LVm	0	2	2	0	0	100	50	50
LVA	0	0	5	0	37.5	32.5	0	100
LA	0	0	0	0	0	100	0	100

3.2. Soil Particle Size Distribution Predictive Models

Tables 5 and 6 show, respectively, the parameters of clay and sand predictive models from OLS multiple linear regression, as well as the R^2, adjusted R^2, the variance inflation factor (VIF) and the summary of variable significance. VIF less than 7.5 means no redundancy among explanatory variables. The summary of variable significance provides information about variable relationships and how consistent those relationships are. For each explanatory variable, the OLS tool calculates a coefficient to determine if such a variable can help to explain clay and sand contents. These coefficients (and their statistical significance) can be changed depending on the combination of variables in the model. The summary of variables' significance provides information about variable relationships and how consistent those relationships are. Larger values (%) mean stronger predictors, as they were considered statistically significant in most of the cases during the analysis, i.e., they are consistently significant, and the relationships are stable. All equations are models that met the OLS requirements. Considering the adjusted R^2, the models are considered suitable, since all of them were able to explain more than 58% of the total variance, with sand models performing better than clay models. However, adjusted R^2 is not the unique parameter that determines the modeling performance. All of the explanatory variables were statistically significant, and all of the residuals of regression showed normality.

Differently from the digital soil map, only SiO_2, Cl, K_2O, Ti, Fe, Zn and Zr from pXRF were used for developing models, because their contents were above the detection limit for all sampling points. The models that had only DTM as explanatory variables did not meet the OLS requirements, with adjusted R^2 around 0.15.

Proximal sensors showed higher predictive power and consistency (higher variable significance) than DTM, with no multicollinearity among them. TWI, SWI and valley depth showed multicollinearity, while proximal sensors and parent material did not present multicollinearity. Parent material was statistically significant (0.01 level) in most cases (variable significance), which reinforces the importance of soil class and parent material for the prediction of soil properties, such as soil particle size distribution. For the prediction of clay content, Fe and magnetic susceptibility were selected in the models that did not consider parent material (models using only proximal sensors and proximal sensors plus DTM). Considering the adjusted R^2, the model with proximal sensors showed greater predictive power. However, for the prediction of sand content, models that excluded parent material showed lower adjusted R^2.

Considering the selected explanatory variables and the scatterplot graphics (Figure 6), clay content values increase as follows: leucocratic gneiss → mesocratic gneiss → gabbro. This was followed by increasing Ti

and decreasing K_2O and Zn contents. Sand content increases according to the sequence gabbro → mesocratic gneiss → leucocratic granite gneiss, followed by increasing SiO_2, Zr and Cl contents.

Table 7 shows the accuracy of the models, from an independent dataset. In general, the R^2 are higher than 0.50, and the models presented a positive bias (positive ME), with small RMSE, which means high accuracy. The R^2 of clay content is the lowest considering scatterplots; on the other hand, the ME and the RMSE are the lowest. In general, when compared to the validation indexes from other studies that used proximal sensors, the models in our study performed well. In the studies of [33,70–72], the RMSE values range from 2.66 to 7.9, which is similar to the RMSE values of our study.

Table 5. Ordinary least square multiple linear regression models of the parameters for clay content developed from proximal sensors (PS) portable X-ray fluorescence and magnetic susceptibility, parent material (PM) and digital terrain models (DTM).

Explanatory Variable	Clay (PS + PM) and Clay (DTM + PS + PM)			Clay (PS)			Clay (DTM + PS)		
	Coefficient	VIF [1]	Variable Significance (%)	Coefficient	VIF	Variable Significance (%)	Coefficient	VIF	Variable Significance (%)
Intercept	72.177			92,361			79,406		
MS [2]	-		67.75	0.028 *	1.980	76.77	0.035 **	1.347	79.95
SiO_2	-		6.85	-	-	10.10	-	-	8.09
Cl	-		100.00	−0.012 **	1.311	100.00	-	-	100.00
K_2O	−0.013 **	1.334	100.00	−0.010 **	1.313	100.00	−0.009 **	1.363	100.00
Ti	−0.001 *	1.750	4.84	-	-	0.00	-	-	6.12
Fe	-		9.58	−0.00005 **	1.803	3.03	-	-	11.90
Zn	−0.196 **	1.213	77.43	−0.164 **	1.146	87.88	−0.165 **	1.101	70.29
Zr	0.038 *	1.310	11.54	-	-	8.08	-	-	11.35
Geomorphons	-		4.84	-	-	-	-	-	0.27
DEM [3]	-		9.58	-	-	-	-	-	8.97
SWI [4]	-		13.81	-	-	-	-	-	12.85
WI [5]	-		5.62	-	-	-	-	-	4.89
Slope	-		70.17	-	-	-	−0.372 *	1.173	64.65
AACHN [6]	-		4.84	-	-	-	-	-	2.31
Valley depth	-		9.58	-	-	-	-	-	5.30
Parent material	4.527 **	1.740	67.75	-	-	-	-	-	-
R^2	0.66			0.71			0.67		
Adjusted R^2	0.61			0.67			0.64		

[1] VIF, variance inflation factor; [2] MS, magnetic susceptibility; [3] digital elevation model; [4] SWI, SAGA wetness index; [5] WI, wetness index; [6] AACHN, altitude above the channel network; model variable significance: * = 0.05, ** = 0.01.

Table 6. Ordinary least square multiple linear regression models of parameters for sand content developed from proximal sensors (PS) portable X-ray fluorescence and magnetic susceptibility, parent material (PM) and digital terrain models (DTM).

Explanatory Variable	Sand (PS + PM)			Sand (DTM + PS + PM)			Sand (PS)			Sand (DTM + PS)		
	Coefficient	VIF [1]	Variable Significance (%)	Coefficient	VIF	Variable Significance (%)	Coefficient	VIF	Variable Significance (%)	Coefficient	VIF	Variable Significance (%)
Intercept	−1.726			0.487648			−30,497			9.134		
MS [2]	-		47.85	-		72.13	-	-	78.79	−0.036 **	1.708	92.11
SiO_2	0.001 *	1.278	78.53	0.001 *	1.337	61.88	0.001 **	1.218	85.86	0.001 **	1.103	63.83
Cl	0.013 **	1.322	100.00	0.012 **	1.334	99.95	0.017 **	1.202	100.00	-	-	99.93
K_2O	-		27.61	-		39.98	-	-	34.34	-	-	49.22
Ti	-		6.13	-		13.70	−0.001 *	1.157	10.10	-	-	17.61
Fe	-		59.51	-		78.52	-	-	90.91	−0.0001 **	1.825	94.09
Zn	-		1.23	-		5.00	-	-	2.02	-	-	6.59
Zr	0.050 *	1.121	16.56	0.046 *	1.130	24.32	0.101 **	1.173	22.22	-	-	28.96
Geomorphons	-		-	-		3.45	-	-	-	-	-	4.42
DEM [3]	-		-	-		47.45	-	-	-	-	-	50.44
SWI [4]	-		-	-		11.03	-	-	-	-	-	10.67
WI [5]	-		-	-		7.52	-	-	-	-	-	9.11
Slope	-		-	0.270 *	1.076	47.45	-	-	-	0.432 **	1.122	32.29
AACHN [6]	-		-	-		5.20	-	-	-	-	-	6.12
Valley depth	-		-	-		5.36	-	-	-	-	-	6.80
Parent material	−5.154 **	1.333	100.00	−5.560 **	1.380	99.64	-	-	-	-	-	-
R^2		0.73			0.77			0.63			0.69	
Adjusted R^2		0.70			0.73			0.58			0.66	

[1] VIF, variance inflation factor; [2] MS, magnetic susceptibility; [3] digital elevation model; [4] SWI, SAGA wetness index; [5] WI, wetness index; [6] AACHN, altitude above the channel network; model variable significance: * = 0.05, ** = 0.01.

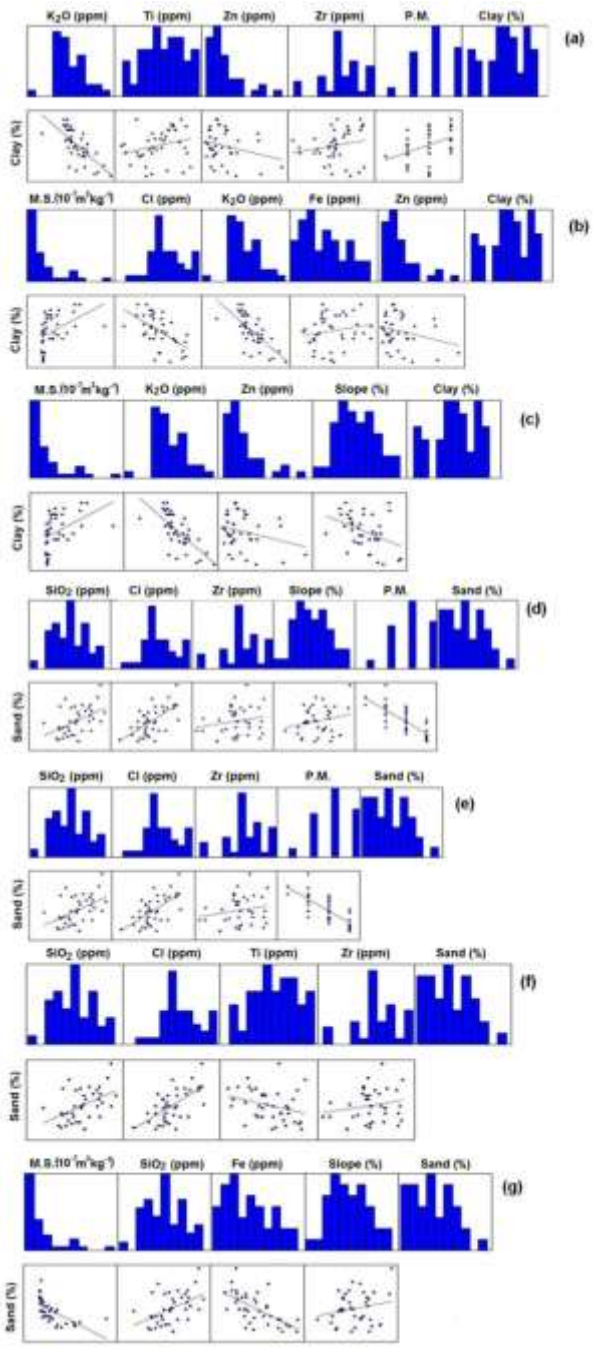

Figure 6. Scatterplots considering only the explanatory variables of predictive models for clay and sand contents. In (**a**–**c**), models for clay, and in (**d**–**g**), models for sand. (a,d) Using parent material (PM), proximal sensors (PS) and digital terrain models (DTM) as explanatory variables; (b,f) using only PS; (c,g) using only PS and DTM; and (e) using PS and PM.

The model for clay using PS and P.M. resulted in the same model as using PS, PM, and DTM. MS = magnetic susceptibility.

Table 7. Accuracy assessment of predictive clay and sand models.

Model	ME	RMSE	R^2
Clay (PS [1] + PM [2]) and (DTM [3] + PS + PM)	13.56	3.68	0.52
Clay (PS)	2.21	6.26	0.39
Clay (DTM + PS)	−4.32	12.37	0.37
Sand (PS + PM)	25.84	5.08	0.69
Sand (DTM + PS + PM)	24.11	4.91	0.67
Sand (PS)	48	136.47	0.72
Sand (DTM + PS)	−10.81	30.41	0.87

[1] PS, proximal sensor; [2] PM, parent material; [3] DTM, digital terrain model.

4. Discussion

4.1. Soil Classes Mapping

Through the analysis of boxplots (Figure 2), it can be noticed that the terrain attributes most commonly used for the predictions of both soil classes and properties were not capable of solely distinguishing most Latosols in the study area, except for SWI, which could distinguish LA from the other Latosols.

The magnetic susceptibility data and some elements/compounds assessed by the pXRF technique, mainly SiO_2 and Fe, could aid in predicting soil classes, probably because of their relationships to soil parent material [73]. The work in [48], studying eight soils and their correspondence to the parent material in the region of Lavras, found that a gabbro-derived soil contained higher contents of Fe_2O_3 and magnetic susceptibility value and a lower content of SiO_2 when compared to soils derived from gneiss, which agrees with the findings of our study, as estimated here by pXRF.

Among the gneisses, soils derived from mesocratic ones are expected to contain higher contents of Fe and lower contents of SiO_2, in comparison with soils derived from leucocratic gneisses, as supported by our pXRF analyses (Table 2). Similar results were found by [7,8], studying soils of the same region.

Regarding magnetic susceptibility, [74] found lower values of magnetic susceptibility in soils derived from rocks, such as gneiss, granite, quartzite, marble and dolomite, due to their lower content of Fe when compared to soils derived from mafic rocks. The presence of gneiss, granite, quartzite, marble and dolomite reduces the chances of ferromagnetic minerals to be formed [75], which is in agreement with the lower Fe content and magnetic susceptibility

values found for gneiss-derived soils (LA, LVA and LVm) in comparison to the gabbro-derived soil (LVg) found in our study. Those authors also found higher magnetic susceptibility values for soils derived from diabase and basalt, the latter being the extrusive rock correspondent to gabbro, ranging from 225 to 7790 × 10^{-8} $m^3 \cdot kg^{-1}$, which contributed to the distinction of those soils from other soils derived from different parent materials. The work in [76], studying magnetic susceptibility in samples of soils derived from sandstone and basalt with the goal of separating soils from different landscape segments in the Jaboticabal region (São Paulo state, Brazil), found that this variable could help with the separation of soils derived from these two rock types.

The higher magnetic susceptibility value for LVg than for Latosols derived from gneiss is probably due to the presence of maghemite, as supported by the X-ray diffractograms (Figure 4). Contrary to magnetite and maghemite, generally found in the sand and clay fractions, respectively [77], goethite and hematite, also present in the studied soils, tend to contain null or low values of magnetic susceptibility [78], similarly to the findings of this study (Figure 4 and Table 3).

According to the soil map of the study area, LVA was the dominant class. This result was also reported by other works related to soil mapping in this same region, such as [79,80].

In Brazil, due to the lack of detailed soil surveys, the establishment of differential soil properties at inferior taxonomic levels has been discussed, and a consensus has not been reached yet. This might be one of the causes of the mismatches between taxonomical and mapping units in detailed soil maps in Brazil. In this sense, the importance of numerical classification models has increased as an alternative for mapping [26,81,82]. Keeping in mind such limitations and options to overcome it, this study proposes the use of numerical soil properties from proximal sensors, which could function as a basis for establishing the boundaries of different types of Latosols at lower taxonomic levels, coupled with a data mining tool for extracting and applying information.

According to the validation indexes, this approach properly fits to the study area, thus contributing to the identification of taxonomic units and their distribution through the landscape (mapping units). The accuracy assessment presented values of overall accuracy within the range defined by the Technical Manual of Pedology [83], which establishes the basis for soil surveys in Brazil, considering reliable soil maps those that present more than 70% of overall accuracy. The remaining 30% are considered inclusions of other soil classes within a mapping unit, which are not included in the legends of soil maps. Thus, the soil maps generated in this work can be considered adequate. Furthermore, soil maps have the ability to provide information about the spatial distribution of surficial geology [84], and, thus, such maps can be used

for several soil property predictions, which was performed in this study for modeling soil particle size distribution, as an example.

4.2. Soil Particle Size Distribution Prediction Models

The main goal here was not only to develop soil particle size distribution prediction models, but also to understand which covariates (proximal sensors, DTM or soil classes map) could better explain this soil property, using the OLS multiple regression, a data mining tool [9]. From the OLS multiple linear regression results, it is clear that the soil class itself and the elemental composition obtained from pXRF that is related to parent material were the best explanatory variables, consistently increasing the prediction power of models.

Chemical elements obtained from pXRF were able to predict soil particle size distribution, which, in turn, depends on parent material, as well as on weathering and leaching [33]. Considering those explanatory variables of prediction models, as clay content increases, K_2O and Zn decreases, Ti increases and the soils tend to be Red Latosols derived from gabbro [73]. Although low K contents were found in those soils, which was expected due to the very low contents of K-bearing minerals in those parent materials and the intense and prolonged weathering-leaching processes to which those soils were subjected [73,85–87], there was a trend of reducing K content and increasing clay content (as an influence of parent materials) in soils developed from varying parent materials, following the sequence leucocratic gneiss → mesocratic gneiss → gabbro. The same trend of reducing K content and increasing clay contents was reported by [48], studying soils derived from the same parent materials of this current work. As sand content increases, SiO_2, Cl and Zr are greater, and the soils tend to be Yellow Latosols derived from leucocratic gneiss [8]. Cl was an important chemical component in the predictive models, and according to [88], Cl contents tend to be higher in igneous rocks. The same authors stated that Zr content in soils generally is inherited from parent rocks. SiO_2 content in the sand fraction was selected to be used on the models, probably because particles in the sand fraction in these extremely weathered-leached soils, such as those in tropical conditions, e.g., in Brazil, are by far dominantly composed of quartz, followed by other very resistant minerals in much smaller quantities, such as magnetite, concretions and nodules of Fe, as reported by [86].

Analyzing the low predictive power of DTM in the models, it is important to highlight that such maps serve only as a proxy of the current environmental conditions, which in many cases are different from the past conditions in which pedogenesis took place [6,89]. Considering that Latosols, soils formed in ancient landscapes, resulted from an environment of soil formation that does not currently exist [87], the contemporary landscape analyzed by DTM might not translate to the preterit soil-forming

conditions [13]. Since DTM did not significantly improve the predictive power of soil properties' prediction, it is preferable to create models that contain less independent variables, reducing time and cost for processing data. These findings suggest that, for tropical conditions, alternative variables that help the predictions of soil classes and properties, such as those provided by pXRF and magnetic susceptibility, may contribute to soils' differentiation and, hence, for the creation/improvement of detailed soil maps, following the world trend for that, as the GlobalSoilMap [90], AfSoilsGrid250m [91] and SoilGrids1Km [92] projects. Furthermore, in tropical developing countries, such as Brazil, most geologic maps, which could contribute to detailed soil mapping, are at small scales, limiting the detailed scale soil maps, coupled with the lack of financial support for soil surveys. Thus, the use of new tools, such as pXRF and magnetic susceptibility, may be of great help in creating/improving detailed soil maps in a fast and reliable way at lower cost, while contributing substantially to a better planning of soil use and management in a sustainable manner.

It is important to emphasize that this work did not have the intention to obtain real values of element contents in soils using pXRF, which would require total element analyses in the laboratory (e.g., with wavelength dispersive (WDXRF) or energy dispersive (EDXRF) X-ray fluorescence equipment) to be correlated with those obtained by pXRF (some of the authors of this paper are currently working on such a study for several tropical soils). This would probably make the soil mapping procedure more costly and time consuming, which is contrary to the idea of using pXRF as a field support for soil mapping [17,31–33] by providing results in a fast way. Furthermore, the estimated values of the elements for the soil classes were consistent with values reported by other studies related to soil characterization in this same region [7,8,48] and contributed to distinguishing soil classes by providing more variables for soil mapping and modeling.

5. Conclusions

The findings of this work suggest that soil classes under tropical conditions may be variable according to the places where they occur on the landscape. This is especially noticed for more detailed soil mapping, in which information about parent material variability becomes even more important. It also demonstrates that the use of other variables, such as magnetic susceptibility data and those provided by analyses with pXRF, in addition to DTM, are needed and may contribute to create detailed soil maps.

Proximal sensors were useful to generate detailed soil class maps and predictive models of soil particle size distribution with suitable accuracy. Therefore, for the region of study, considering the aforementioned limitations, the use of proximal sensors is recommended for digital mapping

and modeling. This approach could make soil mapping faster, less expensive and more accurate.

Acknowledgements: The authors thank the funding agencies Conselho Nacional de Desenvolvimento Científico e Tecnológico (CNPq), Coordenação de Aperfeiçoamento de Pessoal de Ensino Superior (CAPES) and Fundação de Amparo à Pesquisa do Estado de Minas Gerais (FAPEMIG) for the financial support for the development of this work and for scholarships provided to Nilton Curi and Luiz Roberto Guimarães Guilherme.

Author Contributions: Sérgio Henrique Godinho Silva, Giovana Clarice Poggere, Michele Duarte de Menezes and Nilton Curi conceived and performed the study and wrote the manuscript. Luiz Roberto Guimarães Guilherme provided the equipment and wrote the manuscript. Geila Santos Carvalho performed laboratory analyses and contributed to the manuscript writing.

Conflicts of Interest: The authors declare no conflicts of interest.

References

1. Dos Santos, W.J.R.; Curi, N.; Silva, S.H.G.; da Fonseca, S.; da Silva, E.; Marques, J.J. Detailed soil survey of an experimental watershed representative of the Brazilian Coastal Plains and its practical application. *Ciênc. Agrotecnol.* **2014**, *38*, 50–60.
2. SBCS Brazilian Soil Science Society Bulletin. Available online: http://www.sbcs.org.br/wp-content/uploads/2016/01/boletim_v41_n3.pdf (accessed on 2 March 2016).
3. Da Silva, E.; Curi, N.; Ferreira, M.M.; Volpato, M.M.L.; dos Santos, W.J.R.; Silva, S.H.G. Pedotransfer functions for water retention in the main soils from the Brazilian Coastal Plains. *Ciênc. Agrotecnol.* **2015**, *39*, 331–338.
4. Grunwald, S. Multi-criteria characterization of recent digital soil mapping and modeling approaches. *Geoderma* **2009**, *152*, 195–207.
5. Hengl, T.; MacMillan, R.A.; Nikolic, M. Mapping efficiency and information content. *Int. J. Appl. Earth Obs. Geoinf.* **2013**, *22*, 127–138.
6. Samuel-Rosa, A.; Heuvelink, G.B.M.; Vasques, G.M.; Anjos, L.H.C. Do more detailed environmental covariates deliver more accurate soil maps? *Geoderma* **2015**, *243–244*, 214–227.
7. Curi, N.; Lima, J.M.; Andrade, H.; Gualberto, V. Geomorfologia, física, química e mineralogia dos principais solos da região de lavras (MG). *Ciênc. Prát.* **1990**, *14*, 297–307.
8. Marques Júnior, J.; Curi, N.; Lima, J.M. Evolução diferenciada de latossolo vermelho-amarelo e latossolo vermelho-escuro em função da litologia gnáissica na região de lavras (MG). *Rev. Bras. Ciênc. Solo* **1992**, *16*, 235–240.
9. McBratney, A.B.; Mendonça-Santos, M.L.; Minasny, B. On digital soil mapping. *Geoderma* **2003**, *117, 3-52*.
10. Adhikari, K.; Kheir, R.B.; Greve, M.B.; Bøcher, P.K.; Malone, B.P.; Minasny, B.; McBratney, A.B.; Greve, M.H. High-resolution 3-D mapping of soil texture in Denmark. *Soil Sci. Soc. Am. J.* **2013**, *77*, 860–876.

11. Scull, P.; Franklin, J.; Chadwick, O.A.; McArthur, D. Predictive soil mapping: A review. *Prog. Phys. Geogr.* **2003**, *27*, 171–197.
12. Hengl, T.; Heuvelink, G.B.M.; Rossiter, D.G. About regression-kriging: From equations to case studies. *Comput. Geosci.* **2007**, *33*, 1301–1315.
13. De Menezes, M.D.; Silva, S.H.G.; de Mello, C.R.; Owens, P.R.; Curi, N. Spatial prediction of soil properties in two contrasting physiographic regions in Brazil. *Sci. Agric.* **2016**, *73*, 274–285.
14. Jenny, H. *Factors of Soil Formation a System of Quantitative Pedology*; McGraw-Hill Book Co., Inc.: New York, NY, USA, 1941.
15. McKenzie, N.J.; Gessler, P.E.; Ryan, P.J.; O'Connell, D. The role of terrain analysis in soil mapping. In *Terrain Analysis: Principles and Applications*; Wilson, J., Gallant, J., Eds.; John Wiley & Sons Ltd.: New York, NY, USA, 2000; pp. 245–265.
16. McBratney, A.B.; Minasny, B.; Whelan, B. Defining proximal soil sensing. In Proceedings of the The Second Global Workshop on Proximal Soil Sensing, Montreal, PQ, Canada, 15–18 May 2011.
17. Horta, A.; Malone, B.; Stockmann, U.; Minasny, B.; Bishop, T.F.A; McBratney, A B.; Pallasser, R.; Pozza, L. Potential of integrated field spectroscopy and spatial analysis for enhanced assessment of soil contamination: A prospective review. *Geoderma* **2015**, *241–242*, 180–209.
18. Liu, D.; Ma, J.; Sun, Y.; Li, Y. Spatial distribution of soil magnetic susceptibility and correlation with heavy metal pollution in Kaifeng, China. *Catena* **2016**, *139*, 53–60.
19. Wang, X.S. Assessment of heavy metal pollution in Xuzhou urban topsoils by magnetic susceptibility measurements. *J. Appl. Geophys.* **2013**, *92*, 76–83.
20. Karimi, R.; Ayoubi, S.; Jalalian, A.; Sheikh-Hosseini, A.R.; Afyuni, M. Relationships between magnetic susceptibility and heavy metals in urban topsoils in the arid region of Isfahan, central Iran. *J. Appl. Geophys.* **2011**, *74*, 1–7.
21. Schmidt, A.; Yarnold, R.; Hill, M.; Ashmore, M. Magnetic susceptibility as proxy for heavy metal pollution: A site study. *J. Geochem. Explor.* **2005**, *85*, 109–117.
22. Guzmán, G.; Barrón, V.; Gómez, J.A. Evaluation of magnetic iron oxides as sediment tracers in water erosion experiments. *Catena* **2010**, *82*, 126–133.
23. Jordanova, D.; Jordanova, N.; Petrov, P. Pattern of cumulative soil erosion and redistribution pinpointed through magnetic signature of chernozem soils. *Catena* **2014**, *120*, 46–56.
24. De Jong, E.; Pennock, D.J.; Nestor, P.A. Magnetic susceptibility of soils in different slope positions in Saskatchewan, Canada. *Catena* **2000**, *40*, 291–305.
25. Maher, B.A. Characterisation of soils by mineral magnetic measurements. *Phys. Earth Planet. Inter.* **1986**, *42*, 76–92.
26. Siqueira, D.S.; Marques, J.; Pereira, G.T.; Teixeira, D.B.; Vasconcelos, V.; Carvalho Júnior, O.A.; Martins, E.S. Detailed mapping unit design based on soil-landscape relation and spatial variability of magnetic susceptibility and soil color. *Catena* **2015**, *135*, 149–162.

27. Hanesch, M.; Scholger, R. The influence of soil type on the magnetic susceptibility measured throughout soil profiles. *Geophys. J. Int.* **2005**, *161*, 50–56.
28. Hanesch, M.; Rantitsch, G.; Hemetsberger, S.; Scholger, R. Lithological and pedological influences on the magnetic susceptibility of soil: Their consideration in magnetic pollution mapping. *Sci. Total Environ.* **2007**, *382*, 351–363.
29. Lu, S.G.; Xue, Q.F.; Zhu, L.; Yu, J.Y. Mineral magnetic properties of a weathering sequence of soils derived from basalt in Eastern China. *Catena* **2008**, *73*, 23–33.
30. Mullins, C.E. Magnetic susceptibility of the soil and its significance in soil science—A review. *J. Soil Sci.* **1977**, *28*, 223–246.
31. Hseu, Z.; Chen, Z.; Tsai, C.; Jien, S. Portable X-ray fluorescence (pXRF) for determining Cr and Ni contents of serpentine soils in the field Zeng-Yei. In *Digital Soil Morphometrics*; Hartemink, A.E., Minasny, B., Eds.; Progress in Soil Science; Springer International Publishing: Cham, Switzerland, 2016; pp. 37–50.
32. Stockmann, U.; Cattle, S.R.; Minasny, B.; McBratney, A.B. Utilizing portable X-ray fluorescence spectrometry for in-field investigation of pedogenesis. *Catena* **2016**, *139*, 220–231.
33. Zhu, Y.; Weindorf, D.C.; Zhang, W. Characterizing soils using a portable X-ray fluorescence spectrometer: 1. Soil texture. *Geoderma* **2011**, *167–168*, 167–177.
34. VanCott, R.J.; McDonald, B.J.; Seelos, A.G. Standard soil sample preparation error and comparison of portable XRF to laboratory AA analytical results. *Nucl. Instrum. Methods Phys. Res. Sect. A Accel. Spectrom. Detect. Assoc. Equip.* **1999**, *422*, 801–804.
35. Weindorf, D.C.; Sarkar, R.; Dia, M.; Wang, H.; Chang, Q.; Haggard, B.; McWhirt, A.; Wooten, A. Correlation of X-ray fluorescence spectrometry and inductively coupledplasma atomic emission spectroscopy for elemental determination in compostedproducts. *Compost Sci. Util.* **2008**, *16*, 79–82.
36. Sparks, D.L. *Environmental Soil Chemistry*, 2nd ed.; Elsevier: San Diego, CA, USA, 2003.
37. Hartemink, A.E.; Minasny, B. Towards digital soil morphometrics. *Geoderma* **2014**, *230–231*, 305–317.
38. Walter, C.; Lagacherie, P.; Follain, S. Integrating pedological knowledge into digital soil mapping. In *Digital Soil Mapping: An Introductory Perspective*; Lagacherie, P., McBratney, A.B., Voltz, M., Eds.; Elsevier: Amsterdam, The Netherlands, 2007; pp. 281–300.
39. Camargo, L.A.; Marques Júnior, J.; Pereira, G.T.; Bahia, A.S.R.D.S. Clay mineralogy and magnetic susceptibility of oxisols in geomorphic surfaces. *Sci. Agric.* **2014**, *71*, 244–256.
40. Gomide, P.H.O.; Silva, M.L.N.; Soares, C.R.F.S. Atributos físicos, químicos e biológicos do solo em ambientes de voçorocas no município de lavras—MG. *Rev. Bras. Cienc. Solo* **2011**, *35*, 567–577.
41. Embrapa. *Sistema Brasileiro de Classificação de Solos*, 3rd ed.; Embrapa: Brasília, Brazil, 2013.

42. Baver, L.D.; Gardner, W.H.; Gardner, W.R. *Soil Physics*, 5th ed.; John Wiley & Sons: New York, NY, USA, 1972.
43. Gee, G.W.; Bauder, J.W. Particle-size analysis. In *Methods of Soil Analysis*; Klute, A., Ed.; American Society of Agronomy: Madison, WI, USA, 1986; pp. 383–412.
44. Mclean, E.O.; Hedleson, M.R.; Bartlett, R.J.; Holowaychuk, D. Aluminium in soils: I. Extraction methods and magnitud clays in Ohio soils. *Soil Sci. Soc. Am. Proc.* **1958**, *22*, 382–387.
45. Mehlich, A. Determination of P, Ca, Mg, K, Na and NH_4. In *North Carolina Soil Testing Division*; University of North Carolina: Raleigh, USA, 1953; p. 195.
46. Shoemaker, H.E.; McLean, E.O.; Pratt, P.F. Buffer methods for determining the lime requirement of soils with appreciable amounts of extractable aluminum. *Soil Sci. Soc. Am. Proc.* **1961**, *25*, 274–277.
47. Embrapa. *Manual de Análises Químicas de Solos, Plantas e Fertilizantes*, 1st ed.; Embrapa Solos: Rio de Janeiro, Brazil, 1999.
48. Araujo, M.A.; Pedroso, A.V.; Amaral, D.C.; Zinn, Y.L. Paragênese mineral de solos desenvolvidos de diferentes litologias na região sul de Minas Gerais. *Rev. Bras. Cienc. Solo* **2014**, *38*, 11–25.
49. Kämpf, N.; Schwertmann, U. The 5 M NaOH concentration treatment for iron oxides in solis. *Clays Clay Miner.* **1982**, *40*, 401–408.
50. Moore, I.D.; Gessler, P.E.; Nielsen, G.A.; Peterson, G.A. Soil attribute prediction using terrain analysis. *Soil Sci. Soc. Am. J.* **1993**, *57*, 443–452.
51. Behrens, T.; Zhu, A.-X.; Schmidt, K.; Scholten, T. Multi-scale digital terrain analysis and feature selection for digital soil mapping. *Geoderma* **2010**, *155*, 175–185.
52. Brown, R.A.; McDaniel, P.; Gessler, P.E. Terrain attribute modeling of volcanic ash distributions in Northern Idaho. *Soil Sci. Soc. Am. J.* **2012**, *76*, 179–187.
53. Cavazzi, S.; Corstanje, R.; Mayr, T.; Hannam, J.; Fealy, R. Are fine resolution digital elevation models always the best choice in digital soil mapping? *Geoderma* **2013**, *195–196*, 111–121.
54. Adhikari, K.; Minasny, B.; Greve, M.B.; Greve, M.H. Constructing a soil class map of Denmark based on the FAO legend using digital techniques. *Geoderma* **2014**, *214–215*, 101–113.
55. Mosleh, Z.; Salehi, M.H.; Jafari, A.; Borujeni, I.E.; Mehnatkesh, A. The effectiveness of digital soil mapping to predict soil properties over low-relief areas. *Environ. Monit. Assess.* **2016**, *188*, 195.
56. Conrad, O.; Bechtel, B.; Bock, M.; Dietrich, H.; Fischer, E.; Gerlitz, L.; Wehberg, J.; Wichmann, V.; Böhner, J. System for automated geoscientific analyses (SAGA) v. 2.1.4. *Geosci. Model Dev.* **2015**, *8*, 1991–2007.
57. Jasiewicz, J.; Stepinski, T.F. Geomorphons—A pattern recognition approach to classification and mapping of landforms. *Geomorphology* **2013**, *182*, 147–156.
58. Cambule, A.H.; Rossiter, D.G.; Stoorvogel, J.J. A methodology for digital soil mapping in poorly-accessible areas. *Geoderma* **2013**, *192*, 341–353.
59. Silva, S.H.G.; de Menezes, M.D.; Owens, P.R.; Curi, N. Retrieving pedologist's mental model from existing soil map and comparing data mining tools for

refining a larger area map under similar environmental conditions in Southeastern Brazil. *Geoderma* **2016**, *267*, 65–77.

60. Teske, R.; Giasson, E.; Bagatini, T. Comparação do uso de modelos digitais de elevação em mapeamento digital de solos em Dois Irmãos, RS, Brasil. *Rev. Bras. Ciênc. Solo* **2014**, *38*, 1367–1376.
61. Ashtekar, J.M.; Owens, P.R. Remembering knowledge: An expert knowledge based approach to digital soil mapping. *Soil Horiz.* **2013**, *54*, 1–6.
62. Ashtekar, J.M.; Owens, P.R.; Brown, R.A.; Winzeler, H.E.; Dorantes, M.; Libohova, Z.; Dasilva, M.; Castro, A. Digital mapping of soil properties and associated uncertainties in the Llanos Orientales, South America. In *GlobalSoilMap*; Arrouays, D., McKenzie, N., Hempel, J., Forges, A.R., McBratney, A.B., Eds.; CRC Press: Boca Raton, USA, 2014; pp. 367–372.
63. De Menezes, M.D.; Silva, S.H.G.; de Mello, C.R.; Owens, P.R.; Curi, N. Solum depth spatial prediction comparing conventional with knowledge-based digital soil mapping approaches. *Sci. Agric.* **2014**, *71*, 316–323.
64. Shi, X.; Long, R.; Dekett, R.; Philippe, J. Integrating different types of knowledge for digital soil mapping. *Soil Sci. Soc. Am. J.* **2009**, *73*, 1682–1692.
65. Zhu, A.X.; Hudson, B.; Burt, J.; Lubich, K.; Simonson, D. Soil mapping using GIS, expert knowledge, and fuzzy logic. *Soil Sci. Soc. Am. J.* **2001**, *65*, 1463.
66. Landis, J.R.; Koch, G.G. The measurement of observer agreement for categorical data. *Biometrics* **1977**, *33*, 159–174.
67. Hou, X.; He, Y.; Jones, B.T. Recent advances in portable X-ray fluorescence spectrometry. *Appl. Spectrosc. Rev.* **2004**, *39*, 1–25.
68. Beven, K.J.; Kirkby, M.J. A physically based, variable contributing area model of basin hydrology/un modèle à base physique de zone d'appel variable de l'hydrologie du bassin versant. *Hydrol. Sci. Bull.* **1979**, *24*, 43–69.
69. Pierangeli, M.A.P.; Guilherme, L.R.G.; Curi, N.; Silva, M.L.N.; Oliveira, L.R.; Lima, J.M. Teor total e capacidade máxima de adsorção de chumbo em Latossolos Brasileiros. *Rev. Bras. Ciênc. Solo* **2001**, *25*, 279–288.
70. Triantafilis, J.; Lesch, S.M. Mapping clay content variation using electromagnetic induction techniques. *Comput. Electron. Agric.* **2005**, *46*, 203–237.
71. Waiser, T.H.; Morgan, C.L.S.; Brown, D.J.; Hallmark, C.T. In situ characterization of soil clay content with visible near-infrared diffuse reflectance spectroscopy. *Soil Sci. Soc. Am. J.* **2007**, doi:10.2136/sssaj2006.0211.
72. Viscarra Rossel, R.A.; Cattle, S.R.; Ortega, A.; Fouad, Y. In situ measurements of soil colour, mineral composition and clay content by vis-NIR spectroscopy. *Geoderma* **2009**, *150*, 253–266.
73. Curi, N.; Franzmeier, D.P. Effect of parent rocks on chemical and mineralogical properties of some Oxisols in Brazil. *Soil Sci. Soc. Am. J.* **1987**, *51*, 153–158.
74. Silva, A.R.; Souza Junior, I.G.; da Costa, A.C.S. Suscetibilidade magnética do horizonte b de solos do estado do Paraná. *Rev. Bras. Cienc. Solo* **2010**, *34*, 329–337.
75. Schwertmann, U.; Taylor, R.M. Iron oxides. In *Minerals in Soil Environments*; Dixon, J.B., Weed, S.B., Eds.; Soil Science Society America: Madison, WI, USA, 1989; pp. 379–438.

76. Dos Reis Barrios, M.; Marques Junior, J.; Panosso, A.R.; Siqueira, D.S.; la Scala Junior, N. Magnetic susceptibility to identify landscape segments on a detailed scale in th eRegion of Jaboticabal, Sao Paulo, Brazil. *Braz. J. Soil Sci.* **2012**, *36*, 1073–1082.
77. Da Costa, A.C.S.; Bigham, J.M.; Rhoton, F.E.; Traina, S.J. Quanitfication and characterizatin of maghemite in soils derived from volcanic rocks in Southern Brazil. *Clays Clay Miner.* **1999**, *47*, 466–473.
78. Dearing, J. *Environmental Magnetic Susceptibility*, 2nd ed.; Chi Publishing: Kenilworth, England, 1999.
79. UFV-CETEC-UFLA-FEAM *Mapa de Solos do Estado de Minas Gerais: Legenda Expandida*; FEAM: Belo Horizonte, Brazil, 2010.
80. Silva, B.M.; Santos, W.J.R.; Marques, J.J. *Levantamento Detalhado dos Solos da Fazenda Muquém/UFLA, Lavras —MG.*; Editora UFLA: Lavras, Brazil, 2014.
81. Minasny, B.; McBratney, A.B. Incorporating taxonomic distance into spatial prediction and digital mapping of soil classes. *Geoderma* **2007**, *142*, 285–293.
82. Trangmar, B.B.; Yost, R.S.; Uehara, G. Application of geostatistics to spatial of soil properties. *Adv. Agron.* **1985**, *38*, 45–94.
83. IBGE. *Manual Técnico de Pedologia*, 3rd ed.; IBGE: Rio de Janeiro, Brazil, 2015.
84. Brevik, E.C.; Miller, B.A. The use of soil surveys to aid in geologic mapping with an emphasis on the eastern and midwestern united states. *Soil Horiz.* **2015**, doi:10.2136/sh15-01-0001.
85. Curi, N.; Franzmeier, D.P. Toposequence of oxisols from the central Plateau of Brazil1. *Soil Sci. Soc. Am. J.* **1984**, *48*, 341–346.
86. Resende, M.; Curi, N.; Rezende, S.B.; Corrêa, G.F.; Ker, J.C. *Pedologia: Base Para Distinção de Ambientes*, 6th ed.; Editora UFLA: Lavras, Brazil, 2014.
87. Schaetzl, R.J.; Anderson, S. *Soil: Genesis and Geomorphology*, 1st ed.; Cambridge University Press: New York, NY, USA, 2005.
88. Kabata-Pendias, A. *Trace Elements in Soils and Plants*, 4th ed.; Taylor and Francis Group: Boca Raton, FL, USA, 2010.
89. Heuvelink, G.B.M.; Webster, R. Modelling soil variation: Past, present, and future. *Geoderma* **2001**, *100*, 269–301.
90. Arrouays, D.; Grundy, M.G.; Hartemink, A.E.; Hempel, J.W.; Heuvelink, G.B.M.; Hong, S.Y.; Lagacherie, P.; Lelyk, G.; McBratney, A.B.; McKenzie, N.J.; et al. GlobalSoilMap: Toward a fine-resolution global grid of soil properties. *Advances in Agronomy* **2014**, 125, 93–134.
91. Hengl, T.; Heuvelink, G.B.M.; Kempen, B.; Leenaars, J.G.B.; Walsh, M.G.; Shepherd, K.D.; Sila, A.; MacMillan, R.A.; Mendes de Jesus, J.; Tamene, L.; et al. Mapping soil properties of Africa at 250 m resolution: Random forests significantly improve current predictions. *PLoS ONE* **2015**, *10*, e0125814.
92. Hengl, T.; de Jesus, J.M.; MacMillan, R.A.; Batjes, N.H.; Heuvelink, G.B.M.; Ribeiro, E.; Samuel-Rosa, A.; Kempen, B.; Leenaars, J.G.B.; Walsh, M.G.; et al. SoilGrids1km—Global soil information based on automated mapping. *PLoS ONE* **2014**, *9*, e105992.